# Testing and Development of Regulatory Requirements for Steel Plate Concrete Structures

Prepared by

Brian Terranova
Ph.D. Candidate
Department of Civil, Structural and Environmental Engineering
University at Buffalo

and

Andrew Whittaker, Ph.D., S.E.
Professor and MCEER Director
Department of Civil, Structural and Environmental Engineering
University at Buffalo

Prepared for

Canadian Nuclear Safety Commission
Ottawa, Canada

October 2016

# TABLE OF CONTENTS

# TABLE OF FIGURES

# LIST OF TABLES

# 1. INTRODUCTION

## 1.1 Introduction

This report summarizes work on the project "Testing and Development of Regulatory Requirements for Steel Plate Concrete (SC) Structures" that was funded by the Canadian Nuclear Safety Commission (CNSC) and awarded to the University at Buffalo (UB). Purdue University was a subcontractor to UB.

The project included physical and numerical simulations of the response of SC wall piers subjected to simultaneous in-plane and out-of-plane loadings. The physical simulations were performed in the Bowen Laboratory at Purdue University under the direction of Professor Amit Varma, with assistance from Purdue graduate student Mr. Saahas Bhardwaj. The data reduction and numerical simulations reported here were performed at the University at Buffalo by the authors of this report. The conclusions drawn are those of the authors of this report.

The project was organized around tasks as summarized in Table 1-1 below, extracted from the project proposal. Progress reports were issued at milestones agreed to by CNSC and UB. Information from those reports are integrated into this final report.

Table 1-1: List of tasks and draft schedule of work

| Task | Description | Quarter | | | | | | | | | | | |
|------|-------------|---|---|---|---|---|---|---|---|---|----|----|----|
|      |             | 1 | 2 | 3 | 4 | 5 | 6 | 7 | 8 | 9 | 10 | 11 | 12 |
| 4.1 | Literature review | | | | | | | | | | | | |
| 4.2 | Refine testing program | | | | | | | | | | | | |
| 4.3 | Develop analytical tools | | | | | | | | | | | | |
| 4.4 | Execute testing program | | | | | | | | | | | | |
| 4.5 | Calibrate analytical tools | | | | | | | | | | | | |
| 4.6 | Develop CNSC guidance | | | | | | | | | | | | |

The literature review was performed at the beginning of the project to inform the future testing and numerical analysis. The testing program was refined in Task 4.2 in consultation with the CNSC. The physical simulations (Task 4.4 above) are described in this report. The analytical

tools were updated in Task 4.3 using the results of numerical analysis performed by Epackachi et al. (2014b; 2015) on the in-plane behavior of SC wall piers. Those models were used as the starting point for the numerical analysis exercise of Task 4.5.

## 1.2 Organization of this Report

This report is organized into five chapters.

Chapter 2 presents the physicals test of the SC walls, which were performed at Purdue University in collaboration with project partners Professor Amit Varma and Saahas Bhardwaj. The test fixture, instrumentation, loading protocol, and results of the experiments are described.

Chapter 3 discusses modeling of the CNSC experiments in LS-DYNA. The results of the simulated CNSC experiments are presented and validated to the degree possible with experimental data.

Chapter 4 discusses the parametric studies conducted to investigate the effects of OOP loading on the IP behavior of SC walls. The results of these studies are used to provide technical guidance to CNSC for the assessment of SC wall piers subjected to combined in-plane and out-of-plane loading.

Chapter 5 presents a summary of the project and the conclusions drawn by the authors of this report. A list of references follows Chapter 5.

## 1.3 Acknowledgments

The CNSC funded much of the work described in this report, including the execution of the experiments in the Bowen Laboratory at Purdue University. Much of the test fixture design and construction, and the specimen construction and testing, were performed under the leadership of Professor Amit Varma at Purdue University. Purdue graduate student Mr. Saahas Bhardwaj worked closely with Professor Varma on the experimental tasks. We acknowledge the financial support of CNSC and thank Professor Varma and Mr. Saahas Bhardwaj for their critical contributions to the test program.

Any data, opinions, findings, conclusions or recommendations expressed in this report are those of the authors, unless specifically noted otherwise, and do not necessarily reflect those of

MCEER, the State of New York, the CNSC, Purdue University, Professor Amit Varma or Mr. Saahas Bhardwaj.

# 2. PHYSICAL TESTING OF SC WALL PIERS

## 2.1 Introduction

This section of the report presents details and results of the physical tests on the SC wall piers conducted at Purdue University. The test matrix and test fixture are discussed in Section 2.2. Instrumentation of the test specimens is presented in Section 2.3. Results and discussion of the tests of CNSC1, CNSC2, and CNSC3 are presented in Sections 2.4, 2.5, 2.6, respectively.

## 2.2 Test Matrix and Test Fixture

The matrix of tests is presented in Table 2-1, wherein $f_c'$ is concrete compressive strength and $A_c$ is the plan area of the infill concrete. This matrix was reviewed and accepted by CNSC in 2014. The specimens are labeled CNSC1, -2 and -3. Each specimen was 12 in. thick, which includes the two 3/16-inch steel faceplates. The resultant faceplate reinforcement ratio (total area of faceplates divided by total area of wall) is 0.031, which is significant by comparison with reinforced concrete shear walls. The faceplates were constructed with ASTM Grade A36 steel, with a minimum specified yield strength of 36 ksi and a minimum specified tensile strength of 58 ksi. Based on tension coupon tests, the yield strength and tensile strength of the steel faceplate material were 47 ksi and 80 ksi, respectively.

Table 2-1: CNSC test matrix

| Specimen | Height (in.) | Length (in.) | Tie spacing (in.) | Stud spacing (in.) | Target out-of-plane force |
|----------|------|------|------|------|------|
| CNSC0 | 36 | 60 | 12 | 4 | N.A. |
| CNSC1 | 36 | 60 | 12 | 3 | $2\sqrt{f_c'}A_c$ |
| CNSC2 | 36 | 60 | 6 | 3 | Cracking |
| CNSC3 | 36 | 60 | 12 | 3 | Cracking |

Each specimen had an aspect (height-to-length) ratio of 0.6. An additional (control) specimen was constructed and tested in advance of CNSC1: tagged as CNSC0 in Table 2-1. The concrete compressive strength of the infill concrete and faceplate yield strength of CNSC0 were 5,800 psi and 57 ksi, respectively. The aspect ratio and reinforcement ratio of CNSC0 were 0.6 and 0.031 (a 12 in. thick wall with two 3/16-inch steel faceplates), respectively. Additional information on CNSC0 is presented in Kurt et al. (2015).

The shear studs and tie bars were fabricated from carbon steel with nominal yield and ultimate stress of 50 and 75 ksi, respectively. The 3/8 inch diameter tie bars were spaced at a distance equal to the wall thickness (=12 in.) in CNSC0, CNSC1, and CNSC3 and one-half the wall thickness (= 6 in.) in CNSC2. The spacing of the shear studs (connectors) is presented in Table 2-1. The faceplate slenderness ratio ($= s_s / t_p$, where $s_s$ is the spacing of the connectors [shear studs and cross ties], and $t_p$ is the faceplate thickness) was 16 for CNSC1, CNSC2 and CNSC3, and 21 for CNSC0, noting that the limiting value specified in Supplement No. 1 to AISC N690s1 (AISC, 2015) for steel with yield strength of 36 ksi is 28.

Figure 2-1 is a cross-section through the connection of a faceplate to the baseplate. This detail, which was developed by Purdue University to enable re-use of a foundation for testing SC walls, effectively strengthens the faceplate at its connection to the baseplate and forces buckling, fracture and tearing of the faceplate away from the baseplate.
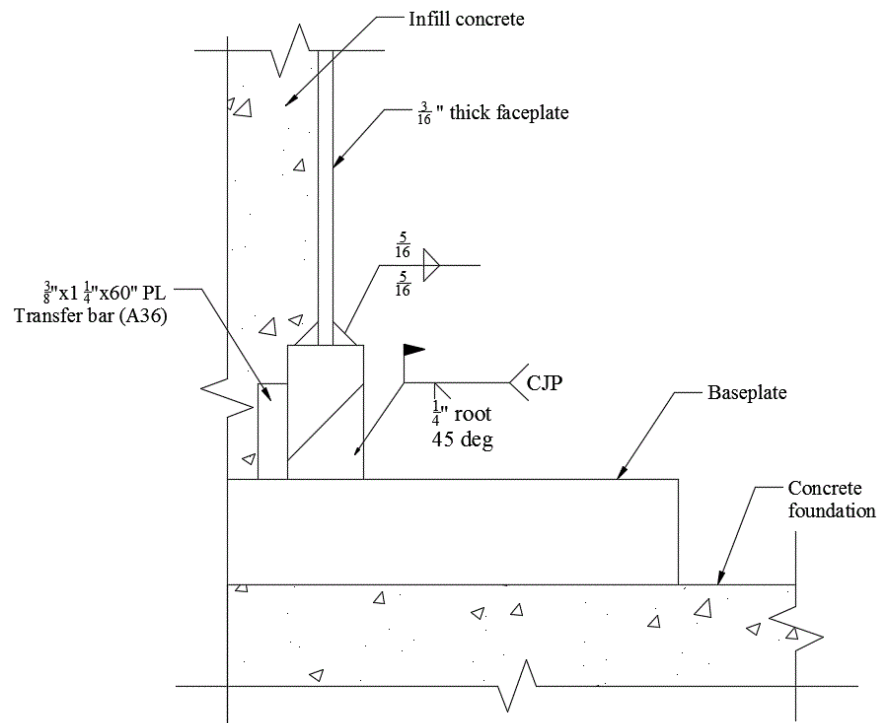


Figure 2-1: Faceplate-to-baseplate connection (courtesy of Purdue University)

Each wall was founded on a large re-usable foundation designed and constructed by Purdue University. The connection of the foundation to the wall was designed to develop the capacity of the faceplates, with the goal of forcing inelastic action into the walls above the foundation.

5

The last column in Table 2-1 identifies the target out-of-plane (OOP) force to be imposed prior to in-plane loading. An out-of-plane load was not applied to the control specimen, CNSC0. The amplitude of the out-of-plane (OOP) loadings for CNSC1, CNSC2 and CNSC3 were tied to equations derived in the early 1960s for shear resistance of plain concrete beams reinforced for flexure only. The concrete contribution to shear strength of $2\sqrt{f_c'}A_c$ is traditionally used for reinforced concrete design in the United States, although it has limited technical basis. (Wight (2015) shows that this empirical equation is unconservative for low longitudinal reinforcement ratios and conservative for high reinforcement ratios: for shallow specimens subjected to monotonic loading to failure in the absence of co-existing in-plane loadings. The effect of section depth (= wall thickness in this case), for which an increase in depth results in a decrease in shear strength of plain concrete, could not be investigated given the specimen dimensions studied here.) Cracking denotes imposing an OOP loading sufficient to introduce a diagonal crack in the concrete, which was estimated for preliminary calculations using equation 22.5.5.1 in ACI 318-14 (2014). The OOP loading was imposed statically and not cycled during the IP loading to failure.

A photograph of the test fixture and a 3D rendering of the fixture are shown in Figure 2-2a and Figure 2-2b, respectively. The OOP setup consisted of one 660-kip dual action actuator and beams to apply the OOP load to the specimen. The OOP load was applied 18 inches above the foundation, and the resulting ratio of shear span-to-depth was 1.5. In-plane loading was imposed on the specimen via loading beams and two 660-kip dual action actuators. The actuator clevises were detailed to accommodate the rotations associated with the IP and OOP loadings.

## 2.3 Instrumentation of the Test Specimens

Traditional transducers were used to monitor the response of each test specimen: strain gages, strain rosettes, string potentiometers, and linear variable differential transducers (LVDTs).

The locations of strain gages on the inner face, outer East face, and outer West face, near the base of the wall for CNSC1 and CNSC3 are identified in Figure 2-3a, Figure 2-3b, and Figure 2-3c, respectively. Strain rosettes on the exterior faces of the plates were used to estimate shear strain. Figure 2-3 shows the locations of the tie bars and shear studs near the base of the wall; a legend is presented in Figure 2-3a. Companion information for CNSC2 is presented in Figure 2-4. The scale in these figures can be determined by the distance between the shear studs: 3

inches. The solid black shaded zone identifies the baseplate; the hatched zone identifies the depth of the welded connection joining the faceplate to the baseplate.

The locations of the string potentiometers used to measure the in-plane and out-of-plane movement of a specimen are presented in Figure 2-5a and Figure 2-5b, respectively.

Three inclinometers were mounted on a specimen to measure rotation; two for in-plane movement (CM2, CM3) and one for out-of-plane movement (CM1). The locations of the inclinometers are identified in Figure 2-5.

Eight LVDTs were attached to a specimen: four to measure in-plane movement of the foundation block with respect to the strong floor, and four to measure vertical movement of the base plate with respect to the foundation block.
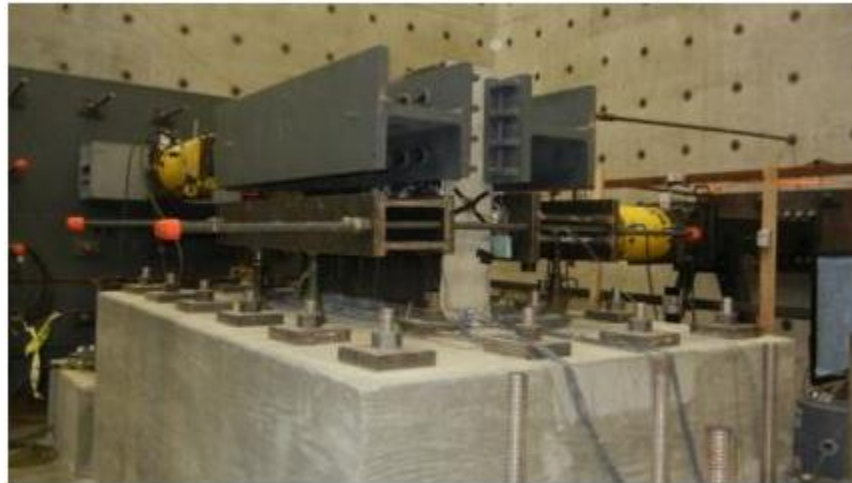
a) photograph of the text fixture
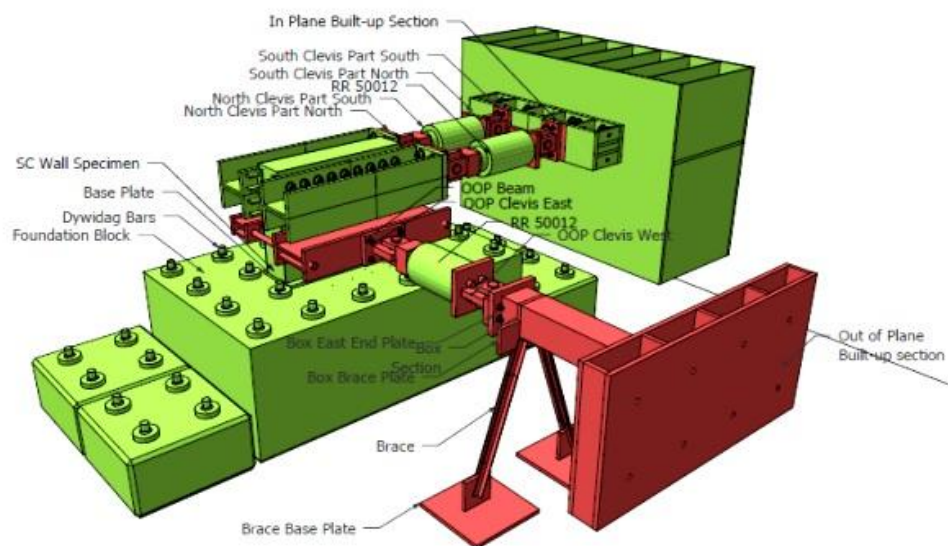


b) 3D rendering of the test fixture
Figure 2-2: CNSC test setup (courtesy of Purdue University)

(a) Typical faceplate, inner face



(b) East faceplate, outer face



(c) West faceplate, outer face
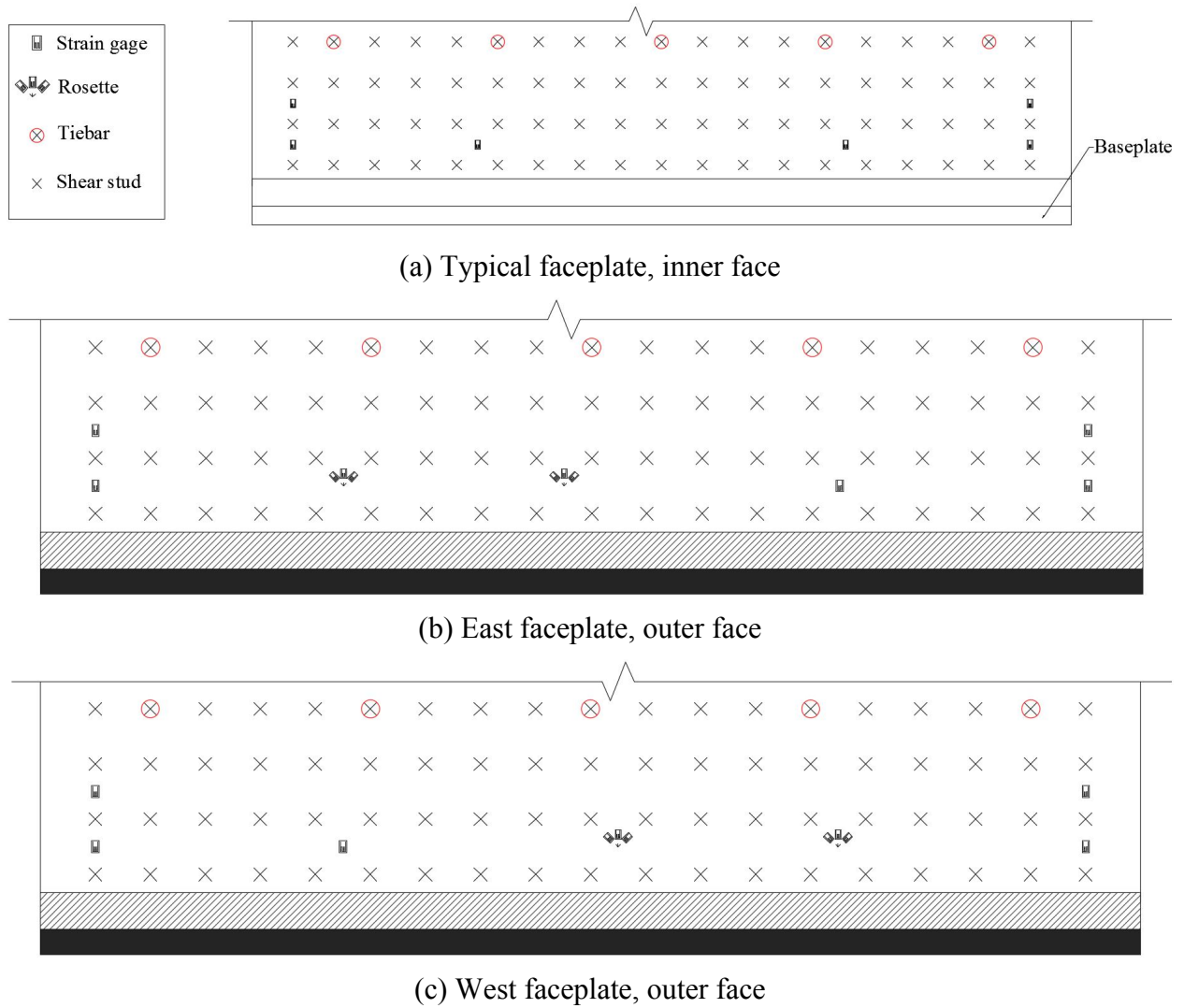
Figure 2-3: Layout of strain gages, tie bars, and shear studs, CNSC1, CNSC3
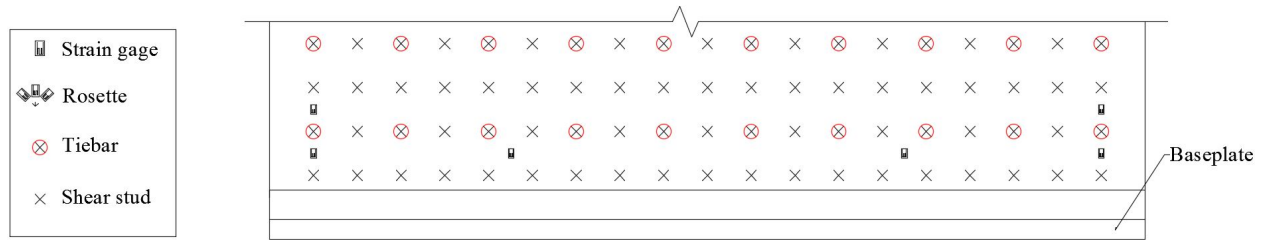
(a) Typical faceplate, inner face
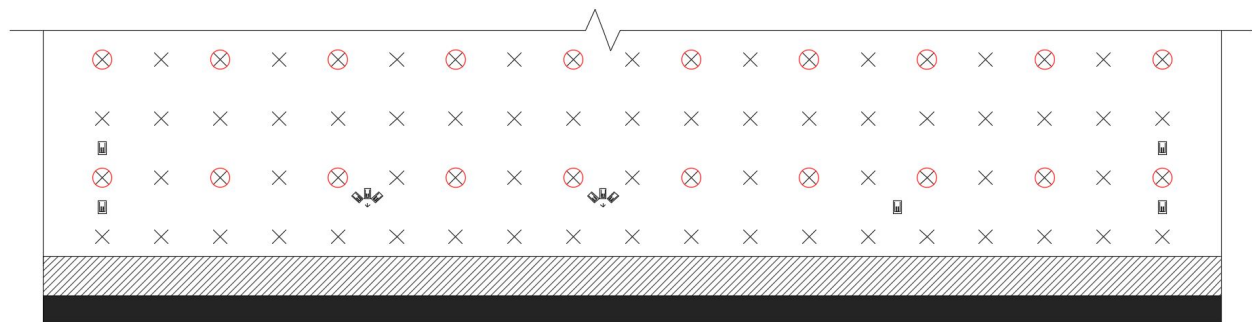


(b) East faceplate, outer face
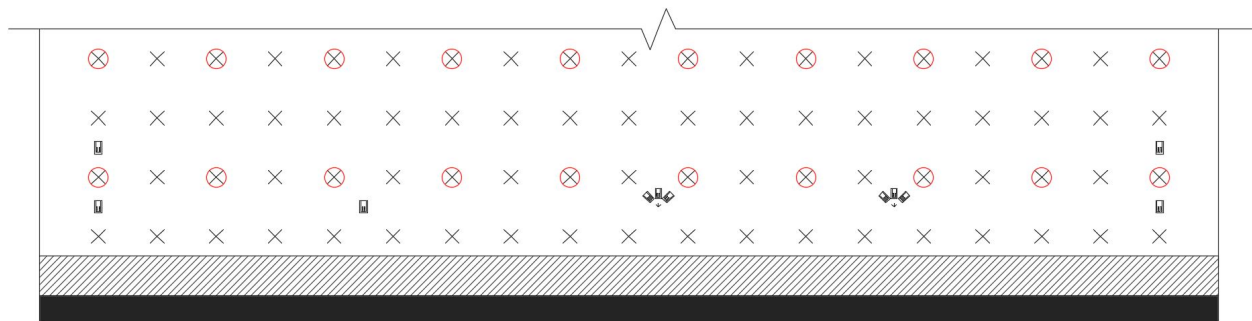


(c) West faceplate, outer face

Figure 2-4: Layout of strain gages, tie bars, and shear studs, CNSC2
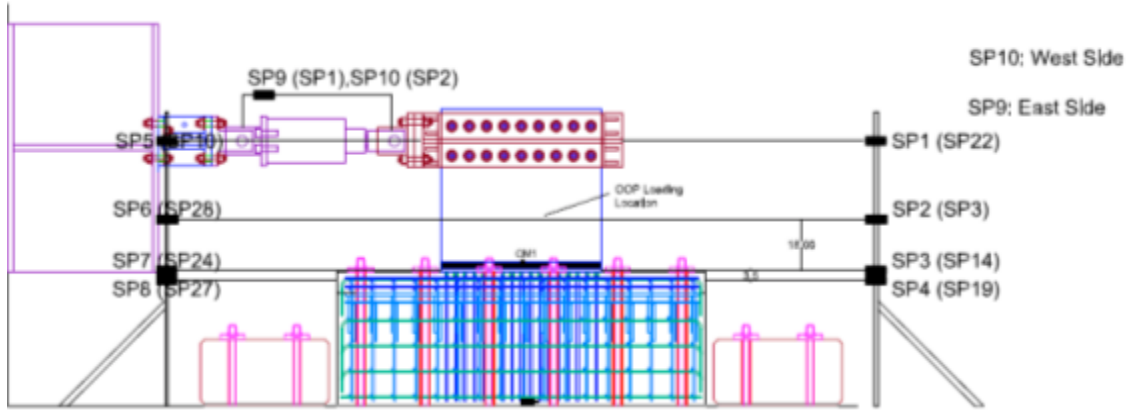
a) in-plane
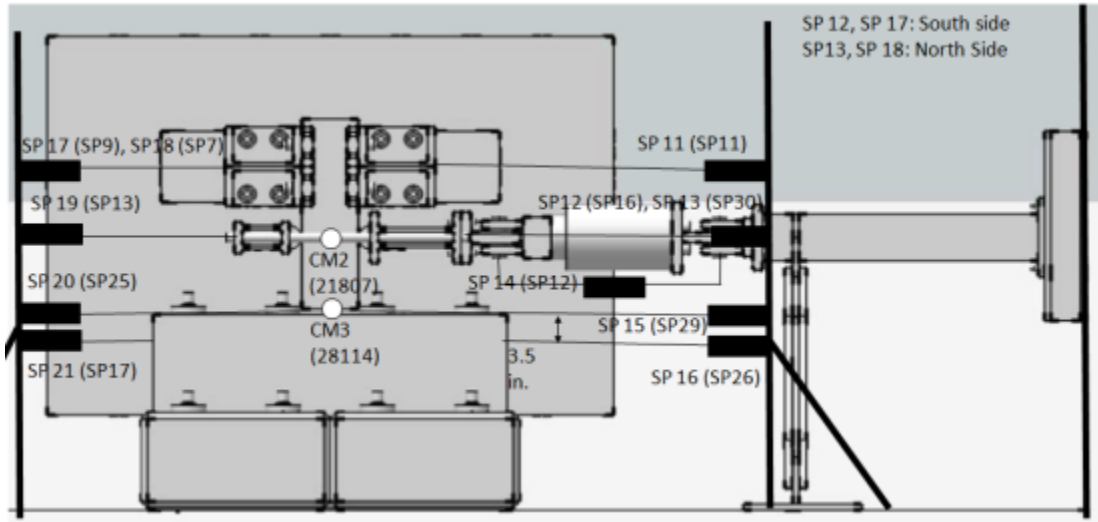


b) out-of-plane

Figure 2-5: Locations of string potentiometers (courtesy of Purdue University)

## 2.4 CNSC1 Test Protocol, Results, and Discussion

### 2.4.1 CNSC1 Test Protocol

Specimen CNSC1 was tested between 06/01/15 and 06/04/15. The concrete compressive strength on the first day of testing was 7700 psi, as determined by cylinder breaks. The specimen was initially subjected to four cycles of OOP loading, at magnitudes of 30, 60, 90, and 120 kips, respectively, to verify the test setup was functioning as intended. The OOP load was then maintained at a constant value of 120 kips $(=1.96\sqrt{f_c'}A_c)$[1] and incremental cyclic IP loading imposed. The loading protocol for CNSC1 is presented in Table 2-2, where $P_y$ and $\Delta_y$ are the

---

[1] The concrete area is the product of the length of the pier (60 in.) and the thickness of the concrete (11.625 in.).

yield load (=650 kips) and yield displacement of the specimen, respectively, calculated by pre-test analysis. The cycles are fully reversed loading, namely, one cycle is a push half cycle followed by a pull half cycle.

Table 2-2: Loading protocol for CNSC1

| Cycle | IP loading | Control | OOP loading |
|-------|-----------|---------|-------------|
| 1-2 | $0.25\,P_y$ | Force | |
| 3-4 | $0.50\,P_y$ | Force | |
| 5-6 | $0.75\,P_y$ | Force | |
| 7-8 | $1.0\,P_y$ | Displacement | 120 kips |
| 9-10 | $1.5\,\Delta_y$ | Displacement | |
| 11-12 | $2.1\,\Delta_y$ | Displacement | |
| 13 | $3.0\,\Delta_y$ | Displacement | |

### 2.4.2 CNSC1 Test Results

The OOP cyclic force-displacement relationship for CNSC2 is presented in Figure 2-6, where the OOP displacement was measured at the top of the wall, at the level where IP loading was applied later, as an average of the SP displacements at the ends of the wall. Data from OOP cycles at loads of 30 and 90 kips were lost and are not reported here. The IP cyclic force-displacement relationship for CNSC1 is presented in Figure 2-7. The post-yield displacement cycles (9 to 13) are presented in Figure 2-8. The loss of IP capacity with increasing cycles can be identified using the data presented in Table 2-3. Significant reductions in IP resistance were observed at large displacements. The IP displacement is the relative horizontal displacement between the level of the IP loading and the bottom of the wall (or top of footing).

The IP load-displacement relationship and backbone curve are presented in Figure 2-9. Points A, B, C, and D in the figure represent the onset of concrete cracking, yielding of steel faceplates, buckling of steel faceplates, and concrete crushing, respectively. The test was terminated at the displacement ✕ shown on the plot. The sequence of damage to CNSC1 is presented in Table 2-4. Concrete cracking at the open ends of the wall, steel faceplate yielding, steel face plate buckling, and concrete crushing in the SC wall occurred at drift ratios of 0.23%, 0.38%, 0.70%, and 1.0%,

respectively, and these points were identified by visual inspection (i.e., cracking and crushing of concrete, faceplate buckling) and review of strain gage data (faceplate yielding).
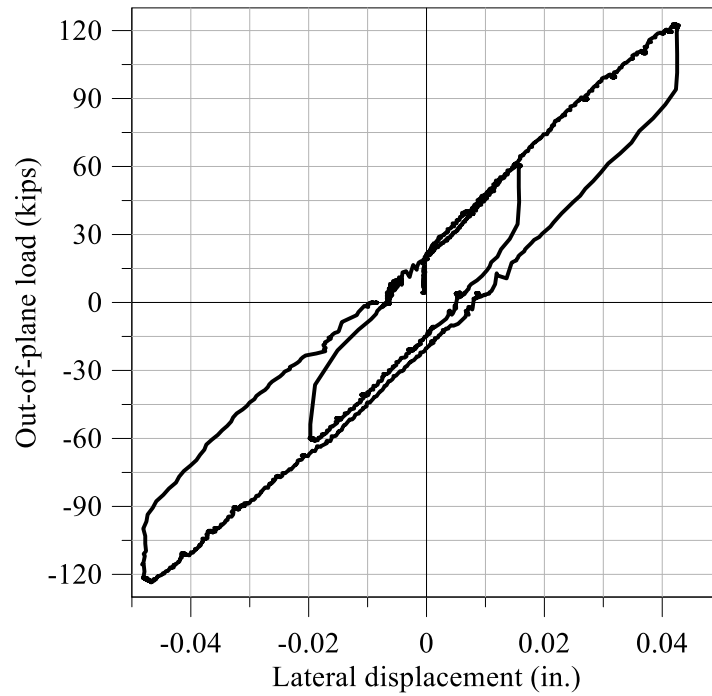
Figure 2-6: Out-of-plane force-displacement relationship, CNSC1
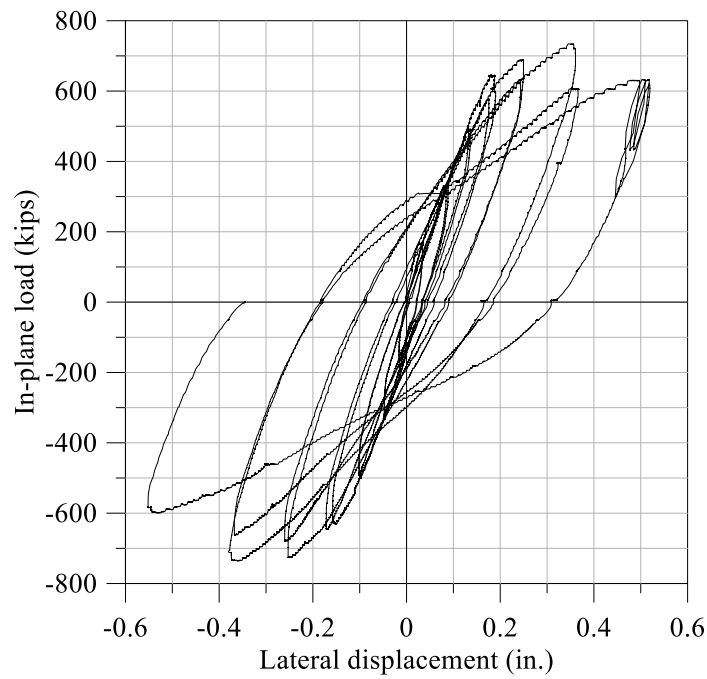
Figure 2-7: In-plane force-displacement relationship, CNSC1

13
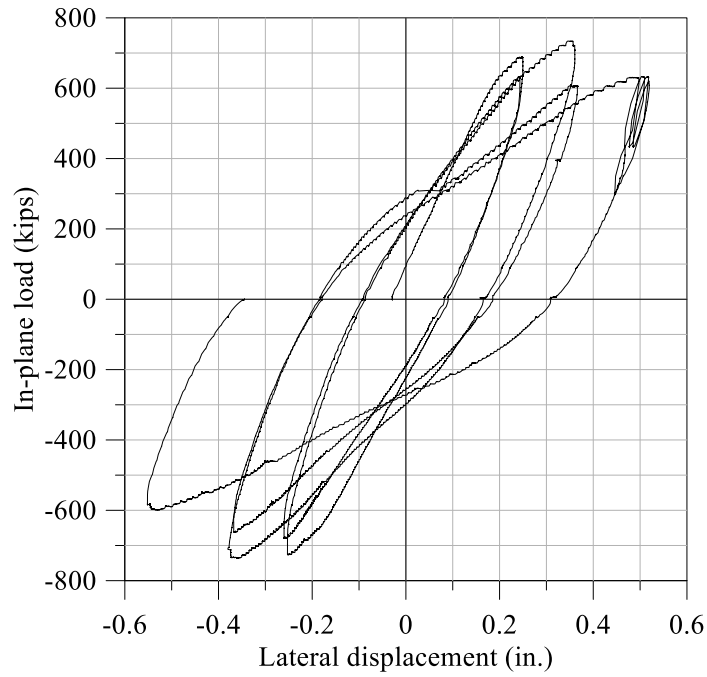
Figure 2-8: In-plane force-displacement relationship for post-yield cycles, CNSC1
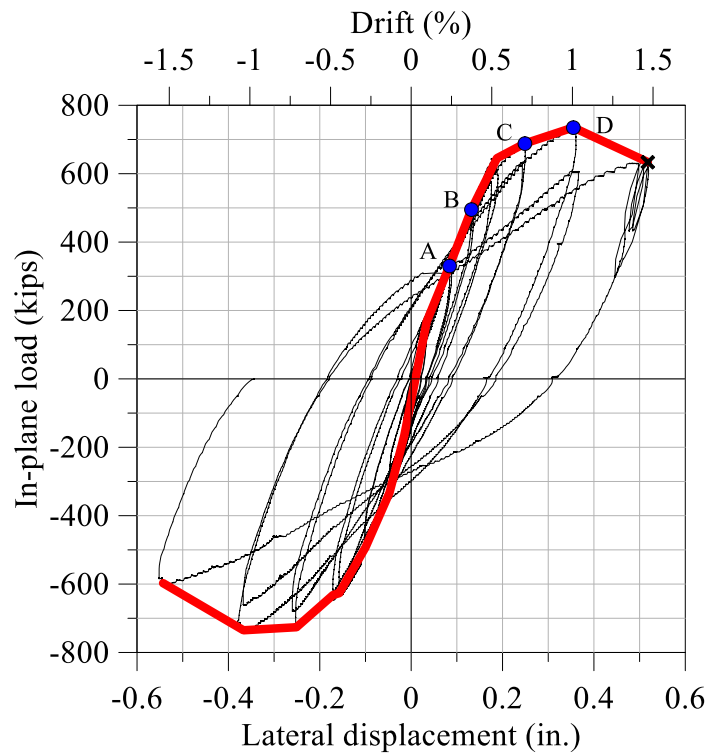


Figure 2-9: In-plane force-displacement relationship and backbone curve, CNSC1

14

Table 2-3: Loss of IP shear capacity, CNSC1

| Cycle | IP resistance at IP displacement (kips) | | | | | | | |
| | $\Delta_y$ | | $1.5\,\Delta_y$ | | $2.1\,\Delta_y$ | | $3\,\Delta_y$ | |
| | Push | Pull | Push | Pull | Push | Pull | Push | Pull |
|---|---|---|---|---|---|---|---|---|
| 7 | 630 | 625 | - | - | - | - | - | - |
| 8 | 575 | 645 | - | - | - | - | - | - |
| 9 | 570 | 632 | 687 | 726 | - | - | - | - |
| 10 | 515 | 532 | 630 | 675 | - | - | - | - |
| 11 | 500 | 518 | 630 | 610 | 730 | 735 | - | - |
| 12 | 400 | 432 | 496 | 552 | 606 | 661 | - | - |
| 13 | 375 | 376 | 456 | 445 | 544 | 515 | 630 | 600 |

Key results are presented in Table 2-5. The initial stiffness of the SC wall, calculated at a drift ratio less than 0.02%, is presented in the first column for the push and pull directions. The values of load and drift ratio at the onset of steel plate yielding are presented in columns two and three. The fourth and fifth column present the load and drift ratio at the onset of steel faceplate buckling. The peak loads and their corresponding drift ratios for the push and pull directions are presented in columns six and seven. The maximum drift ratios for the experiment and their corresponding loads in the push and pull directions are presented in columns eight and nine. Note that the maximum drift ratio does not correspond to failure of the CNSC1.

Table 2-4: Sequence of damage, CNSC1

| Cycle | Drift ratio (%) Push/Pull | Damage/Observations |
|---|---|---|
| 3 | 0.23/0.13 | Cracks on the North and South faces of the wall; specimen twisting |
| 5 | 0.38/0.28 | Yielding of steel faceplates, diagonal cracking at the base of the South wall; new cracks on the North face of the wall |
| 6 | 0.38/0.28 | New cracks; residual OOP drift |
| 7 | 0.51/0.45 | Large residual strains develop in the steel faceplates, initial separation of the faceplates from the infill concrete; new cracks formed |
| 9 | 0.70/0.70 | Buckling of the steel faceplate in the northwest and southwest corners of the wall; diagonal cracking on the South face; new diagonal cracks on the South face of the wall |
| 10 | 0.70/0.70 | Severe buckling of the steel faceplate in the northwest corner of the wall; buckling of the steel faceplate in the southeast corner of the wall; new diagonal cracks on the South face |
| 11 | 1.00/1.01 | Propagation of faceplate buckling from the southeast corner towards the mid-length of the wall; extensive cracking on the South face |
| 12 | 1.00/1.01 | Concrete crushing and spalling at the toes of the wall (North and South faces) |
| 13 | 1.43/1.52 | Propagation of faceplate buckling from the Northeast corner towards the mid-length of the wall |

Table 2-5: Summary results for CNSC1

| Initial stiffness (kip/in.) | Onset of steel plate yielding | | Onset of steel plate buckling | | Peak load | | Maximum drift | |
|---|---|---|---|---|---|---|---|---|
| Push/Pull | Load (kips) | Drift (%) | Load (kips) | Drift (%) | Load (kips) Push/Pull | Drift (%) Push/Pull | Load (kips) Push/Pull | Drift (%) Push/Pull |
| 5139/4966 | 493 | 0.38 | 689 | 0.70 | 735/735 | 0.99/1.01 | 634/597 | 1.44/1.51 |

The accumulated damage to the wall pier on its South and North faces from cycles 1 through 12 is shown in Figure 2-10 and Figure 2-11, respectively. The text on the red fill in the figures identifies the forces at which the related cracks formed. Damage to the South and North faces of CNSC1 after cycle 13 are presented in Figure 2-12 and Figure 2-13, respectively. Local buckling of the steel faceplates and concrete cracking and spalling are clearly visible. The wall twisted in the latter stages of the test and there was considerable OOP residual drift.
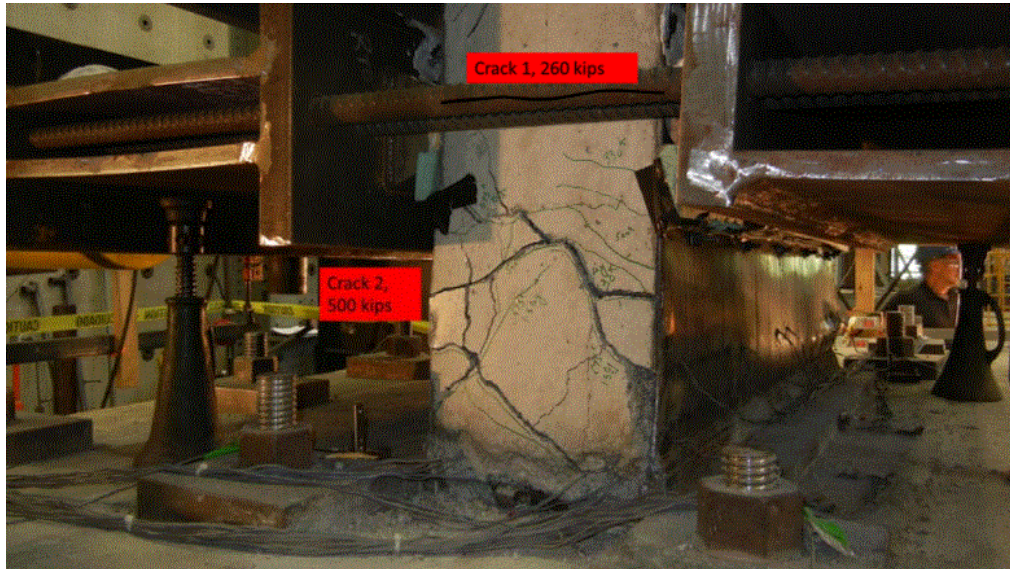
Figure 2-10: Accumulated damage on South face, cycles 1-12, CNSC1
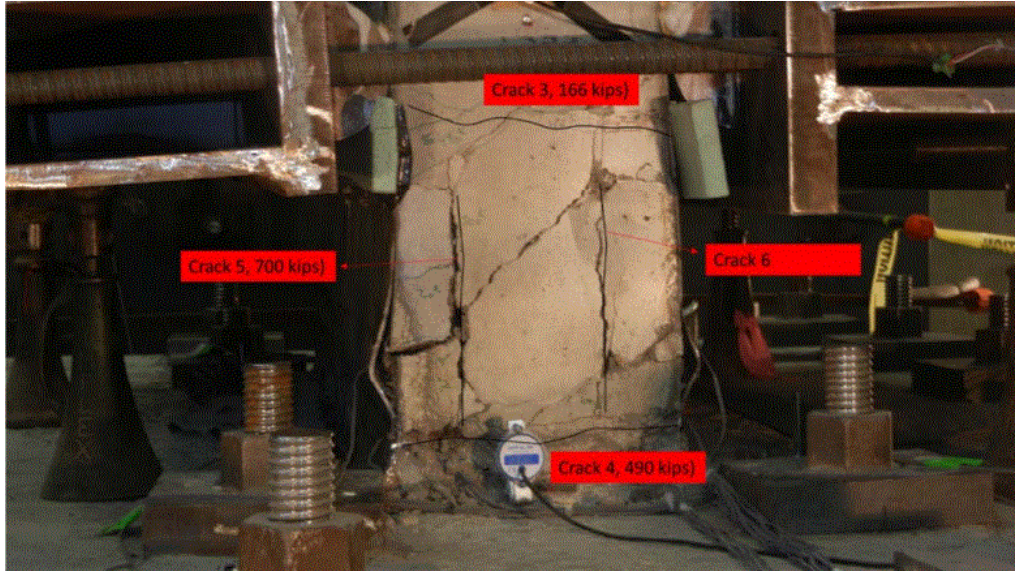


Figure 2-11: Accumulated damage on the North face, cycles 1-12, CNSC1

Figure 2-12: Damage on South face of CNSC1 after cycle 13



Figure 2-13: Damage on North face of CNSC1 after cycle 13

The cumulative energy dissipation in CNSC1 is presented in Figure 2-14. The energy dissipated in each cycle ($EDC$) is presented in Table 2-6. Equivalent viscous damping ($EVD$) data are presented in Figure 2-15 and Table 2-7, where $EVD$ is computed using Equation (2-1) (Chopra, 2011).

$$EVD = \frac{1}{4\pi} \frac{EDC}{E_{So}}$$
(2-1)

where $EDC$ is the energy dissipated per cycle (area under the force-displacement relationship) and $E_{So}$ is the strain energy (defined as $ku_o^2/2$, where $k$ is the secant stiffness to maximum displacement $u_o$).

Table 2-6: Energy dissipated per cycle, CNSC1

| Cycle | 5 | 6 | 7 | 8 | 9 | 10 | 11 | 12 | 13 |
|---|---|---|---|---|---|---|---|---|---|
| $EDC$ (kip-in) | 34.4 | 28.5 | 74.5 | 64.4 | 159 | 154 | 315 | 292 | 476 |
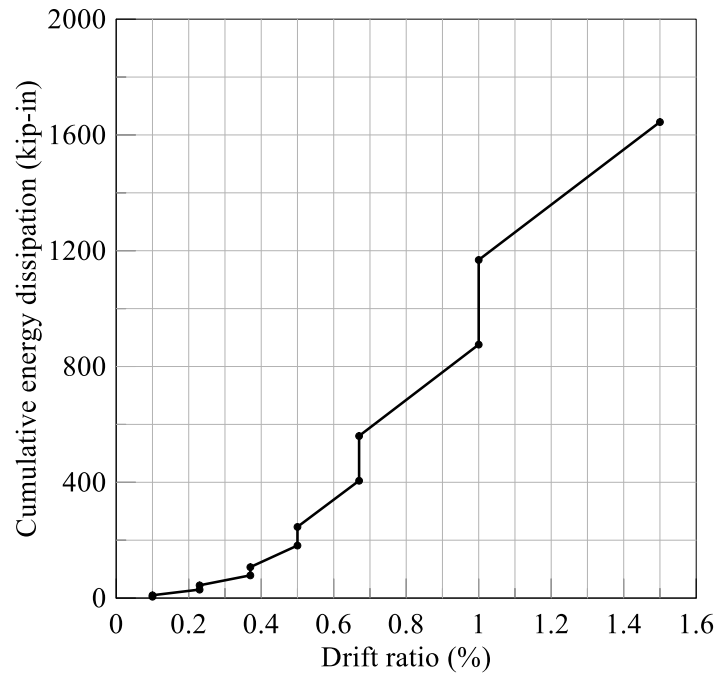


Figure 2-14: Cumulative energy dissipation, CNSC1
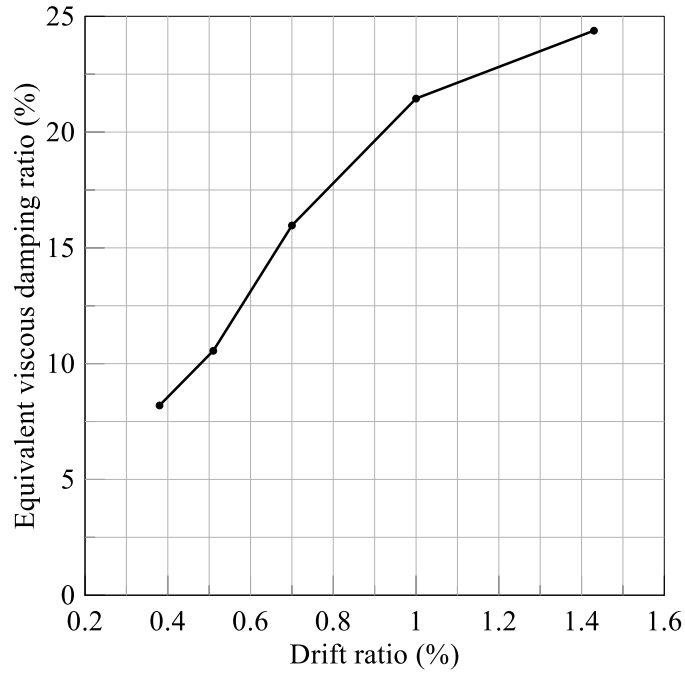
Figure 2-15: Equivalent viscous damping ratio, CNSC1

Table 2-7: Equivalent viscous damping, CNSC1

| Drift ratio (%) | 0.38 | 0.51 | 0.70 | 1.00 | 1.43 |
|---|---|---|---|---|---|
| *EVD* (%) | 8.2 | 10.6 | 16.0 | 21.4 | 24.4 |

### 2.4.3 Behaviors of CNSC1 and CNSC0

Figure 2-16 presents the in-plane force-displacement responses of the control specimen (CNSC0) and CNSC1. The uniaxial compressive strengths of the concrete for CNSC0 and CNSC1 were 5800 psi and 7700 psi, respectively. The yield strengths of the steel faceplates (slenderness ratios) in CNSC0 and CNSC1 were 57 ksi (21) and 47 ksi (16), respectively. These differences in material strengths and slenderness ratios make a direct comparison of the responses of the CNSC0 and CNSC1 impossible because both the steel faceplates and infill concrete contribute to the in-plane strength of SC wall piers. Both specimens were pushed to a drift ratio (lateral displacement divided by the distance between the point of in-plane loading) of approximately 1.5%. The control specimen failed due to cyclic yielding of the steel faceplates, leading to fracture of the base metal close to the weld (Kurt et al., 2015). The test of CNSC1 was terminated after cyclic yielding of the steel faceplates, leading to compression failure and spalling of infill concrete.

20
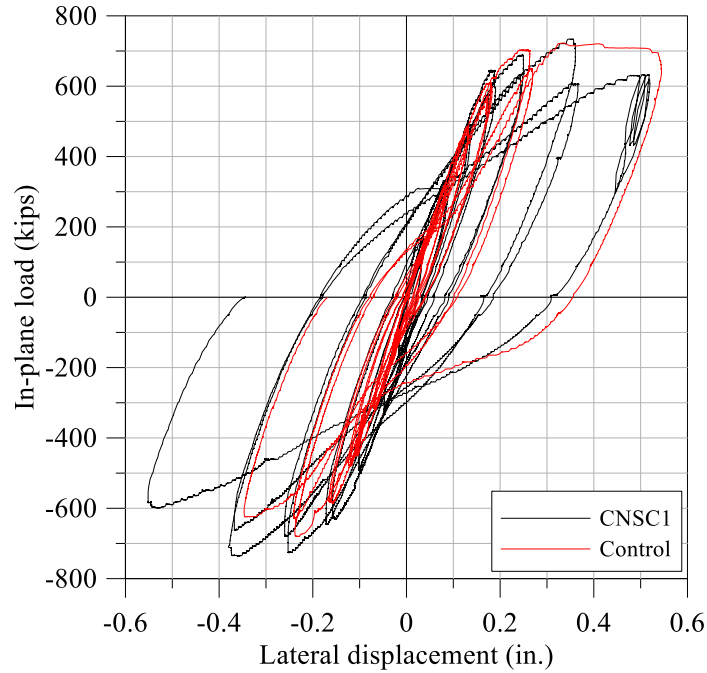
Figure 2-16: In-plane force-displacement responses of CNSC0 and CNSC1

## 2.5 CNSC2 Test Protocol, Results, and Discussion

### 2.5.1 CNSC2 Test Protocol

Specimen CNSC2 was tested on 11/11/15 and 11/12/15. The concrete compressive strength on the first day of testing was 5300 psi. The specimen was initially subjected to five cycles of OOP loading, at magnitudes of 30, 60, 90, 120 and 240 kips, respectively, to verify the test setup was functioning as intended, and to crack the wall due to OOP shear. Cracking of the specimen due to OOP load was first observed at 220 kips. The OOP load was then maintained at 240 kips (= $4.73\sqrt{f_c'}A_c = 1.2*(2\sqrt{f_c'}A_c + A_s f_y d / s)$, where $f_c'$ is concrete compressive strength, $A_c$ is plan area of infill concrete, $A_s$, $f_y$, and $s$ are the area, tensile yield strength, and spacing of the shear reinforcement, respectively, and $d$ is the effective depth of the cross section) and then incremental cyclic IP loading imposed. The loading protocol for CNSC2 is presented in Table 2-8, where $P_y$ and $\Delta_y$ are the yield load (=504 kips) and yield displacement (=0.19 in.) of the specimen, respectively, calculated by pre-test analysis considering in-plane and out-of-plane loading. The cycles were fully reversed: a push half cycle followed by a pull half cycle.

21

Table 2-8: Loading protocol for CNSC2

| Cycle | IP loading | Control | OOP loading |
|-------|-----------|---------|-------------|
| 1-2 | $0.25\,P_y$ | Force | |
| 3-4 | $0.50\,P_y$ | Force | |
| 5-6 | $0.75\,P_y$ | Force | |
| 7-8 | $1.00\,P_y$ | Displacement | 240 kips |
| 9-10 | $1.50\,\Delta_y$ | Displacement | |
| 11-12 | $2.00\,\Delta_y$ | Displacement | |
| 13 | $3.00\,\Delta_y$ | Displacement | |

### 2.5.2 CNSC2 Test Results

The OOP cyclic force-displacement relationship for CNSC2 is presented in Figure 2-17, where the OOP displacement was measured at the top of the wall, at the level where the IP loading was later applied. Cracking was first observed at an OOP load of approximately 220 kips. The cyclic loading of the wall in the OOP direction resulted in diagonal cracks on its exposed North and South faces as presented in Figure 2-18. The long diagonal crack on the North face was produced by OOP loading before the application of IP loads. The short diagonal cracks on the South face near the base of the wall resulted from OOP loading; the longer diagonal crack propagating from the point of application of the OOP load formed after the first IP cycle of loading.
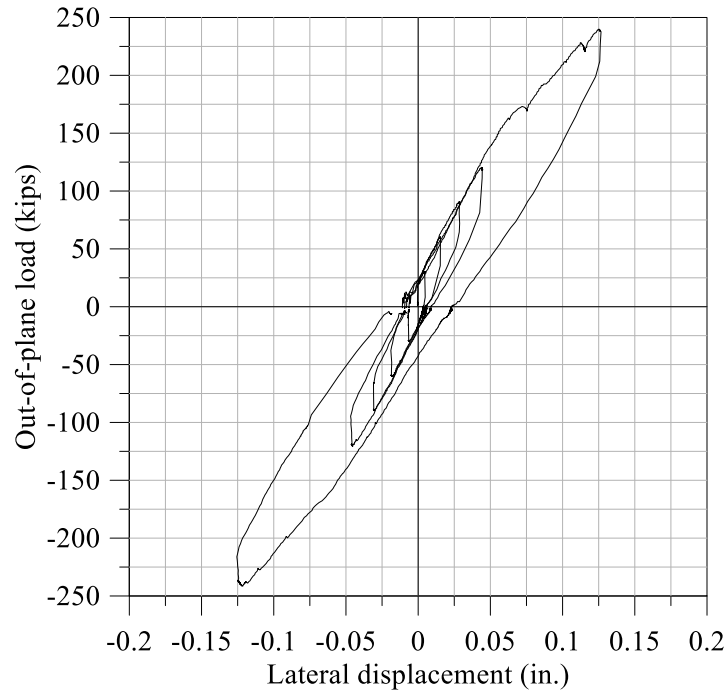
Figure 2-17: Out-of-plane force-displacement relationship, CNSC2



| (a) North face | (b) South face |

Figure 2-18: Diagonal cracking caused by OOP loading, CNSC2

The IP cyclic force-displacement relationship for CNSC2 is presented in Figure 2-19. The post-yield displacement cycles (9 to 13) are presented in Figure 2-20. The loss of IP capacity with increasing cycles can be identified using the data presented in Table 2-9. Data from cycle 10 was lost. Significant reductions in IP resistance were observed at large displacements.
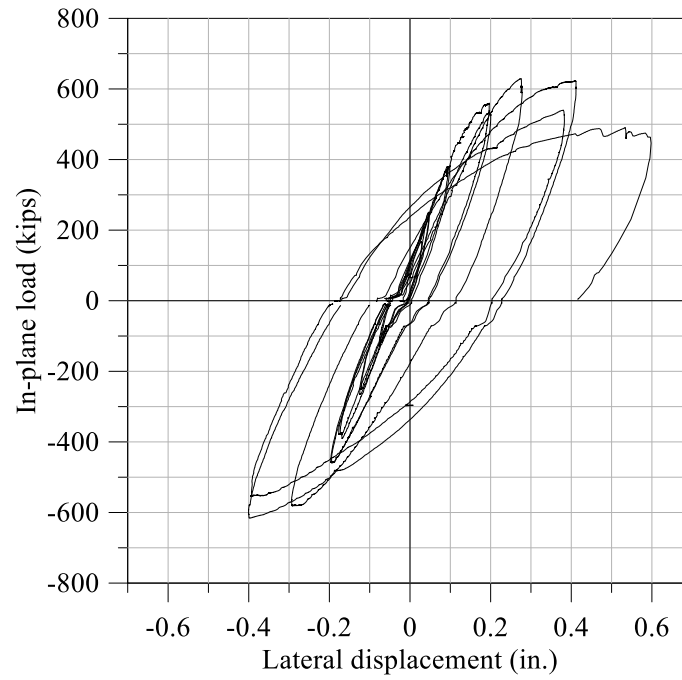
Figure 2-19: In-plane force-displacement relationship, CNSC2
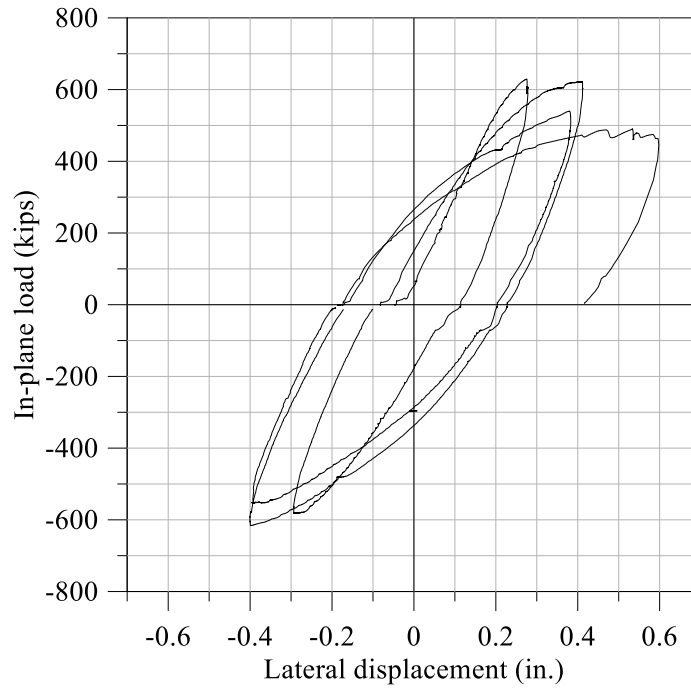


Figure 2-20: In-plane force-displacement relationship for post yield cycles, CNSC2

24

Table 2-9: Loss of IP capacity, CNSC2

| Cycle | IP resistance at IP displacement (kips) | | | | | | | |
|---|---|---|---|---|---|---|---|---|
| | $\Delta_y$ | | $1.5\Delta_y$ | | $2.0\Delta_y$ | | $3\Delta_y$ | |
| | Push | Pull | Push | Pull | Push | Pull | Push | Pull |
| 7 | 558 | 458 | - | - | - | - | - | - |
| 8 | 530 | 457 | - | - | - | - | - | - |
| 9 | 536 | 493 | 630 | 580 | - | - | - | - |
| 10 | - | - | - | - | - | - | - | - |
| 11 | 471 | 496 | 568 | 565 | 623 | 616 | - | - |
| 12 | 430 | 455 | 493 | 510 | 539 | 551 | - | - |
| 13 | 387 | - | 435 | - | 466 | - | 463 | - |

The IP load-displacement relationship and backbone curve are presented in Figure 2-21; the hysteresis loops are offset approximately 0.03 inch from the origin due to twisting of the SC wall pier caused by the applied OOP load. Points A, B, C, and D in the figure represent the onset of concrete cracking under IP loading, yielding of steel faceplates, buckling of steel faceplates, and concrete crushing, respectively. The test was terminated at the displacement ✕ shown on the plot. The sequence of damage to CNSC2 is presented in Table 2-10. Concrete cracking under IP loading, steel faceplate yielding, steel face plate buckling, and concrete crushing in the SC wall occurred at drift ratios of 0.15%, 0.37%, 0.76%[2], and 1.14%, respectively. The tie bar on the North end of the wall ruptured in cycle 13; the approximate point of its rupture on the IP force-displacement relationship is identified in Figure 2-21 by point E.

---

[2] Steel faceplate buckling occurred in cycle 10; the drift in cycle 9 is presented here and used in Figure 2-21.
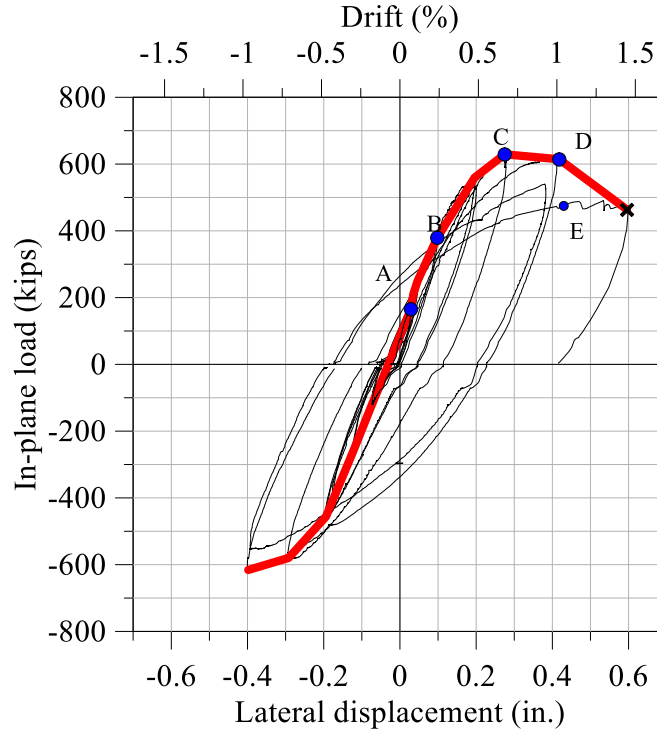
Figure 2-21: In-plane force-displacement relationship and backbone curve, CNSC2

Key results are presented in Table 2-11. The initial stiffness of the SC wall, calculated at a drift ratio less than 0.02%, is presented in the first column for the push and pull directions. The values of load and drift ratio at the onset of steel plate yielding are presented in columns two and three. The fourth and fifth column present the load and drift ratio at the onset of steel faceplate buckling. The peak loads and their corresponding drift ratios for the push and pull directions are presented in columns six and seven. The maximum drift ratios for the experiment and their corresponding loads in the push and pull directions are presented in columns eight and nine. The maximum drift ratio does not correspond to failure (loss of gravity load resistance) of CNSC2.

The accumulated damage to the wall pier on the South and North faces from cycles 1 through 12 is shown in Figure 2-22. The damage to the South and North faces of CNSC2 after cycle 13 is presented in Figure 2-23. Local buckling of the steel faceplates and concrete cracking and spalling are clearly visible. The wall twisted in the latter stages of the test and there was considerable OOP residual drift. A tie bar ruptured on the North end of the wall in cycle 13, as described previously and shown in Figure 2-24.

Table 2-10: Sequence of damage, CNSC2

| Cycle | Drift ratio (%) Push/Pull | Damage/Observations |
|---|---|---|
| OOP 240 kips | - | Diagonal crack on the North face propagating from the point of application of OOP load; short diagonal cracks near the base of the wall on the South face |
| 1 | 0.15/0.15 | Diagonal crack on the South face propagating from the point of application of OOP load |
| 2 | 0.17/0.15 | Propagation of cracks on the South face; new diagonal cracks on the North face at the top and bottom of the wall |
| 3 | 0.23/0.24 | New diagonal cracks on North and South face at the point of OOP loading |
| 4 | 0.23/0.24 | Specimen twisting |
| 5 | 0.37/0.39 | Yielding of the steel faceplate on the West (tension) side of the wall; new cracking observed on the North and South faces of the wall |
| 6 | 0.35/0.38 | New cracks form on the South face of the wall at the point of OOP loading |
| 7 | 0.54/0.55 | Yielding of the steel faceplate on the East (compression) side of the wall; additional cracking on the South face at top and bottom of wall and IP loading location |
| 8 | 0.56/0.55 | Additional cracking observed on South wall at IP loading location; OOP residual displacement approximately 0.4 inch |
| 9 | 0.76/0.81 | Drifting of wall in OOP direction; difficult to maintain OOP load; cracks propagate on South and North faces |
| 10 | - / -[1] | Buckling of steel faceplate in the northwest, southeast and southwest corners of the wall; OOP residual displacement approximately 0.8 inch |
| 11 | 1.14/1.11 | Buckling of steel faceplate in the Northeast corner of the wall; cracks propagating; concrete crushing and spalling at the toes of the wall; OOP and IP residual drifts are 1.6 and 0.17 inch, respectively |
| 12 | 1.06/1.08[2] | Extensive cracking on the South and North faces of the wall; additional spalling of concrete; shear studs visible on the South face of the wall; severe buckling of face plates in the North and South East corners of the wall; propagation of faceplate buckling towards the mid point of the wall |
| 13 | 1.7/ - | Tie bar rupture on the North side of the wall |

1. The data from cycle 10 was not recovered from the test; description based on visual observation.
2. The drift ratios of cycle 12 are slightly smaller than cycle 11 due to uncertainty in the stability of the wall during this cycle.

Table 2-11: Summary results for CNSC2

| Initial stiffness (kip/in.) | Onset of steel plate yielding | | Onset of steel plate buckling | | Peak load | | Maximum drift | |
|---|---|---|---|---|---|---|---|---|
| Push/Pull | Load (kips) | Drift (%) | Load (kips) | Drift (%) | Load (kips) Push/Pull | Drift (%) Push/Pull | Load (kips) Push/Pull | Drift (%) Push/Pull |
| 2658/3051 | 380 | 0.37 | 629 | 0.76 | 629/616 | 0.76/1.11[1] | 464/616 | 1.70/1.11[2] |

1. Peak load in the push (pull) direction occurred in cycle 9 (11)
2. Maximum drift occurred in cycle 13 (11) for the push (pull) direction; drifts in cycle 12 are slightly smaller due to concerns regarding the stability of the wall; pull cycle 13 not conducted



(a) South face



(b) North face

Figure 2-22: Accumulated damage, cycles 1-12, CNSC2



(a) South face



(b) North face

Figure 2-23: Damage to CNSC2 after cycle 13

Figure 2-24: Tie bar rupture at North end of wall, CNSC2

The cumulative energy dissipation in CNSC2 is presented in Figure 2-25. The energy dissipated in each cycle (EDC) is presented in Table 2-12. Equivalent viscous damping ($EVD$) data are presented in Figure 2-26 and Table 2-13, where $EVD$ is calculated per Equation (2-1).
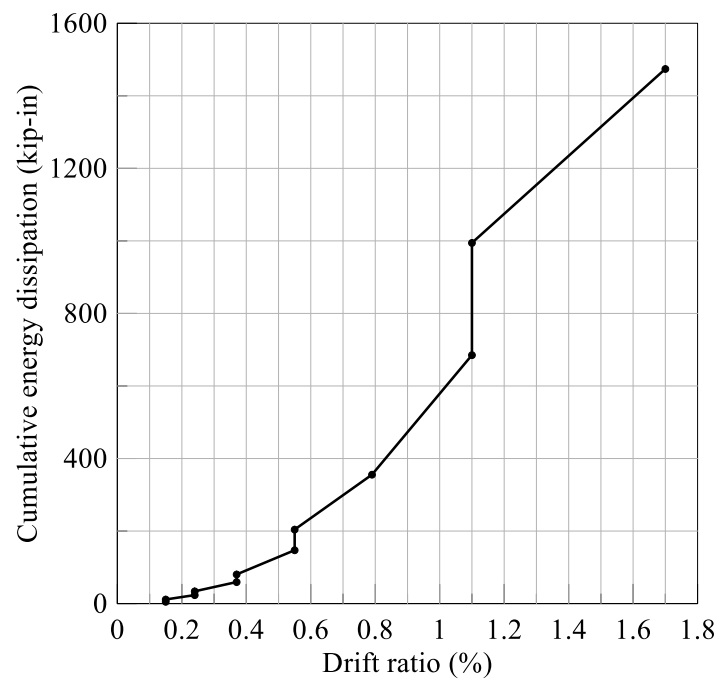


Figure 2-25: Cumulative energy dissipation, CNSC2

Table 2-12: Energy dissipated per cycle, CNSC2

| Cycle | 5 | 6 | 7 | 8 | 9 | 10 | 11 | 12 | 13 |
|---|---|---|---|---|---|---|---|---|---|
| *EDC* (kip-in) | 25.5 | 21.0 | 66.7 | 57.0 | 151 | - | 330 | 309 | 480 |
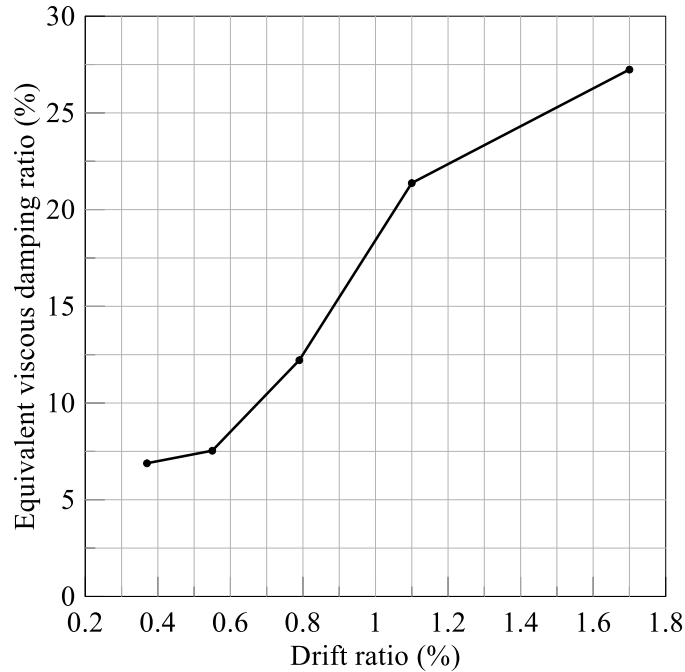


Figure 2-26: Equivalent viscous damping ratio, CNSC2

Table 2-13: Equivalent viscous damping, CNSC2

| Drift ratio (%) | 0.37 | 0.55 | 0.79 | 1.10 | 1.70 |
|---|---|---|---|---|---|
| *EVD* (%) | 6.9 | 7.5 | 12.2 | 21.4 | 27.2 |

### *2.5.3 Behaviors of CNSC2 and CNSC0*

Figure 2-27 presents the in-plane force-displacement responses of CNSC0 and CNSC2. The uniaxial compressive strengths of the concrete (slenderness ratio) for CNSC0 and CNSC2 were 5800 psi (21) and 5300 psi (16), respectively. The faceplate yield strengths of CNSC0 and CNSC2 were 57 ksi and 47 ksi, respectively. These differences in faceplate slenderness and material strengths make it difficult to quantify the effects of the OOP load on the IP response by comparing specimen responses. The control specimen and CNSC2 were pushed to a drift ratio of 1.5% and 1.7%, respectively. CNSC0 failed due to cyclic yielding of the steel faceplates, leading to fracture of the base metal close to the weld (Kurt et al., 2015). The test of CNSC2 was

terminated after cyclic yielding of the steel faceplates leading to spalling of the infill concrete and tie bar rupture.
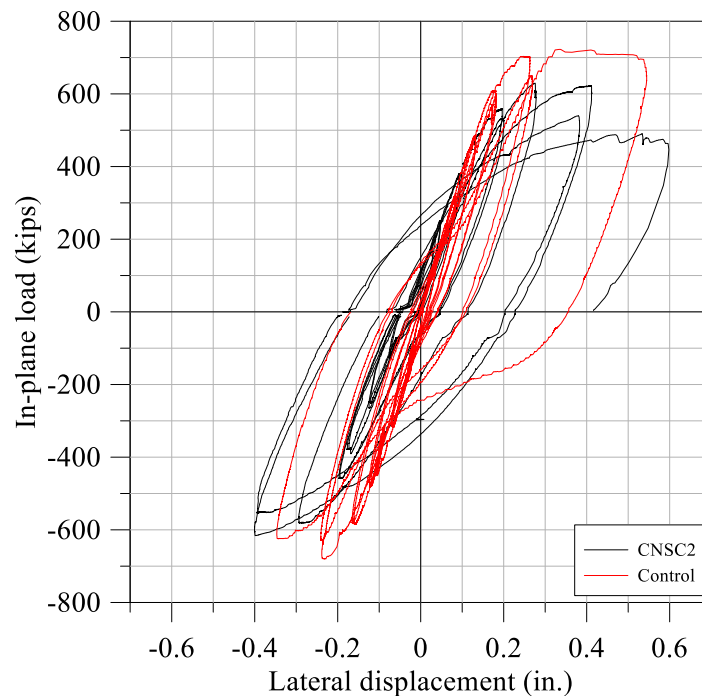


Figure 2-27: In-plane force-displacement responses of CNSC0 and CNSC2

## 2.6 CNSC3 Test Protocol, Results, and Discussion

### 2.6.1 CNSC3 Test Protocol

Specimen CNSC3 was tested on 02/09/16 and 02/10/16. The concrete compressive strength on the first day of testing was 5,300 psi. Cracks formed on the exposed North and South faces of the wall (see Figure 2-28) due to the post-tensioning of the beams to the specimen (see Figure 2-2) for the application of OOP loads. The specimen was subjected to five cycles of OOP loading, at magnitudes of 50, 100, 150, 200 and 250 kips, respectively, to verify the test setup was functioning as intended, and to crack the infill concrete due to OOP shear. The OOP load was then maintained at 250 kips ($=4.92\sqrt{f'_c}A_c$) and incremental cyclic IP loading imposed. The loading protocol for CNSC3 is presented in Table 2-14, where $P_y$ and $\Delta_y$ are the in-plane yield load (=505 kips) and yield displacement (=0.175 in.) of the specimen, respectively, calculated by pre-test analysis.

<table>
(a) North face        (b) South face
</table>

(a) North face                      (b) South face

Figure 2-28: Initial cracking of specimen before OOP load application, CNSC3

Table 2-14: Loading protocol for CNSC3

| Cycle | IP loading[1] | Control | OOP loading |
|-------|---------------|---------|-------------|
| 1-2 | $0.25\,P_y$ | Force | |
| 3-4 | $0.50\,P_y$ | Force | |
| 5-6 | $0.75\,P_y$ | Force | 250 kips |
| 7-8 | $1.00\,P_y$ | Displacement | |

1. $P_y$ is the estimated in-plane yield strength

## 2.6.2 CNSC3 Test Results

The OOP cyclic force-displacement relationship for CNSC3 is presented in Figure 2-29, where the OOP displacement was measured at the top of the wall, at the level where the IP loading was later applied. The OOP cyclic loading resulted in diagonal cracks in both the push and pull directions, on the exposed North and South faces of the wall, as presented in Figure 2-30. The cracks propagated diagonally downwards from the level of application of the OOP load.

The IP cyclic force-displacement relationship for CNSC3 is presented in Figure 2-31. Significant reductions in IP resistance were observed in cycle 8. The significant drop in the in-plane load in

cycle 8, at a displacement of 0.18 inch, resulted from the operator trying to avoid overshooting the target displacement.
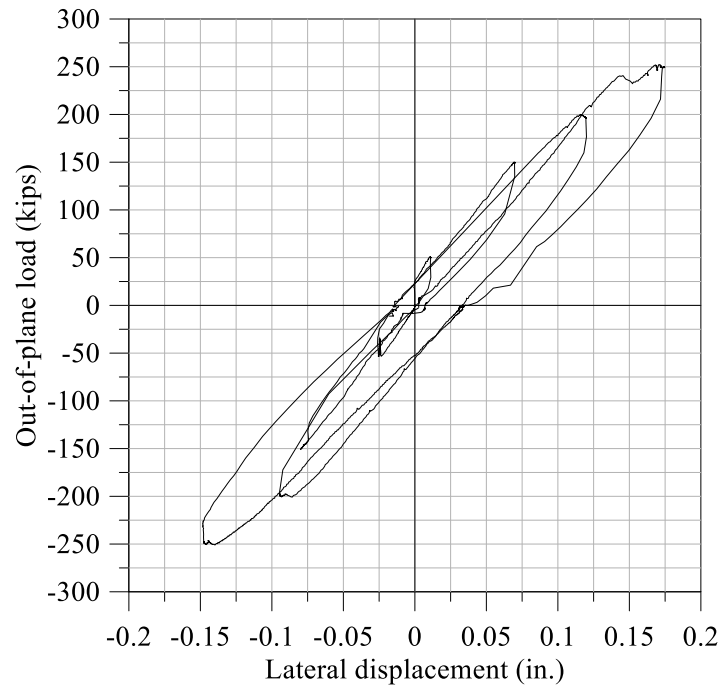


Figure 2-29: Out-of-plane force-displacement relationship, CNSC3



|  (a) North face | (b) South face |

Figure 2-30: Additional diagonal cracking caused by OOP loading, CNSC3
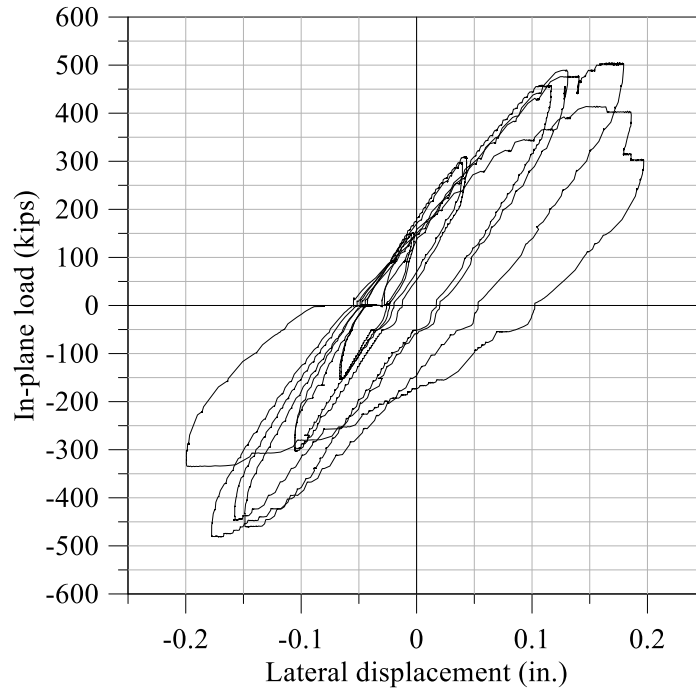
Figure 2-31: In-plane force-displacement relationship, CNSC3

The IP load-displacement relationship and backbone curve are presented together in Figure 2-32; the hysteresis loops are offset from the origin by approximately 0.035 inch due to twisting of the SC wall pier caused by the applied OOP load. Points A, B, C, and D in the figure represent the onset of concrete cracking under IP loading, yielding of steel faceplates, buckling of steel faceplates, and concrete crushing, respectively. The test was terminated at the displacement ✕ shown on the plot (displayed at point D). The sequence of damage to CNSC3 is presented in Table 2-15. Concrete cracking under IP loading, steel faceplate yielding, steel face plate buckling, and concrete crushing in the SC wall occurred at drift ratios of 0.09%, 0.19%, 0.50%, and 0.56%, respectively.

Key results are presented in Table 2-16. The initial stiffness of the SC wall, calculated at a drift ratio less than 0.02%, is presented in the first column for the push and pull directions. The values of load and drift ratio at the onset of steel plate yielding are presented in columns two and three. The fourth and fifth column present the load and drift ratio at the onset of steel faceplate buckling. The peak loads and their corresponding drift ratios for the push and pull directions are presented in columns six and seven. The maximum drift ratios for the experiment and their

34

corresponding loads in the push and pull directions are presented in columns eight and nine. The maximum drift ratio does not correspond to gravity load failure of CNSC3.

Table 2-15: Sequence of damage, CNSC3

| Cycle | Drift ratio (%) Push/Pull | Damage/Observations |
|---|---|---|
| Pre-test | -/- | Diagonal cracks on the North and South faces propagating from the point of application of OOP load on the East face to the base plate on the West face; diagonal cracks on the North face propagating from the West face: cracks above the point of OOP load application; small diagonal cracks on the South face located mid-depth of the cross section and above point of OOP load application |
| OOP 100 kips | - | Short diagonal cracks on the North face propagating from the East face towards the base plate on the West face below the point of OOP load application; short diagonal cracks on the South face at the mid-depth of the cross section, propagating from East to West |
| OOP 150 kips | - | Diagonal cracks on the North face propagating from the point of OOP load application on the East face towards the base plate on the West face |
| OOP 200 kips | - | Diagonal cracks on the South face from the point of OOP load application to the mid-depth of the cross section from the East face towards the West face |
| OOP 250 kips | - | Diagonal cracks on the North face propagating from the point of OOP load application on the West face to the East face towards the base plate; short diagonal cracks on the South face propagating from the West face to the East face |
| 1 | 0.09/0.08 | Propagation of diagonal cracks on the North and South faces; new diagonal cracks on the South face |
| 2 | 0.08/0.09 | New diagonal cracks on the South face |
| 3 | 0.19/0.21 | Yielding of the steel faceplate on the West (tension) side of the wall; new diagonal cracks on the North face at the point of OOP loading |
| 4 | 0.20/0.21 | Propagation of diagonal cracks on the South face; new diagonal cracks on the North face near the base of the wall |
| 5 | 0.35/0.36 | New horizontal cracks located at the mid-depth of the cross section on the South face |
| 6 | 0.39/0.41 | Significant growth of cracks on the North and South faces; yielding of the steel faceplate on the East (compression) side of the wall |
| 7 | 0.50/0.49 | Buckling of the steel faceplate in the northeast corner of the wall; significant opening of cracks on the North and South faces |
| 8 | 0.56/0.56 | Concrete crushing and spalling at the toes of the wall; significant movement of wall in the OOP direction; difficult to maintain OOP load; buckling of the East faceplate along the length of the wall, 2 inches above the baseplate; deformation of the steel faceplate at the point of OOP load application on the West face; OOP and IP residual drifts are 1.0 and 0.07 inch, respectively |
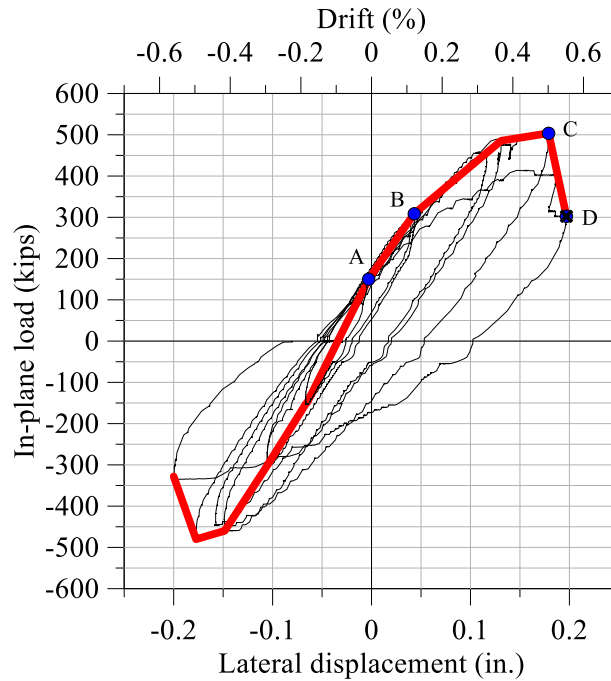
Figure 2-32: In-plane force-displacement relationship and backbone curve, CNSC3

The accumulated damage to the wall pier on the exposed South and North faces of the wall after cycle 8 is shown in Figure 2-33. Local buckling of the steel faceplates and concrete cracking and spalling are clearly visible. Figure 2-34 presents additional photographs of damage including faceplate buckling and OOP residual drift.

Table 2-16: Summary results for CNSC3

| Initial stiffness (kip/in.) | Onset of steel plate yielding | | Onset of steel plate buckling | | Peak load | | Maximum drift | |
|---|---|---|---|---|---|---|---|---|
| Push/Pull | Load (kips) | Drift (%) | Load (kips) | Drift (%) | Load (kips) Push/Pull | Drift (%) Push/Pull | Load (kips) Push/Pull | Drift (%) Push/Pull |
| 3500/3576 | 309 | 0.19 | 504 | 0.50 | 504/481 | 0.50/0.49 | 303/328 | 0.56/0.56 |

(a) South face                                    (b) North face

Figure 2-33: Accumulated damage after cycle 8, CNSC3





(a) Faceplate buckling                          (b) OOP residual drift

Figure 2-34: Additional photographs of damage after cycle 8, CNSC3

The cumulative energy dissipation in CNSC3 is presented in Figure 2-35. The energy dissipated in each cycle ($EDC$) is presented in Table 2-17. Equivalent viscous damping ($EVD$) data are presented in Figure 2-36 and Table 2-18, where $EVD$ is computed using Equation (2-1).
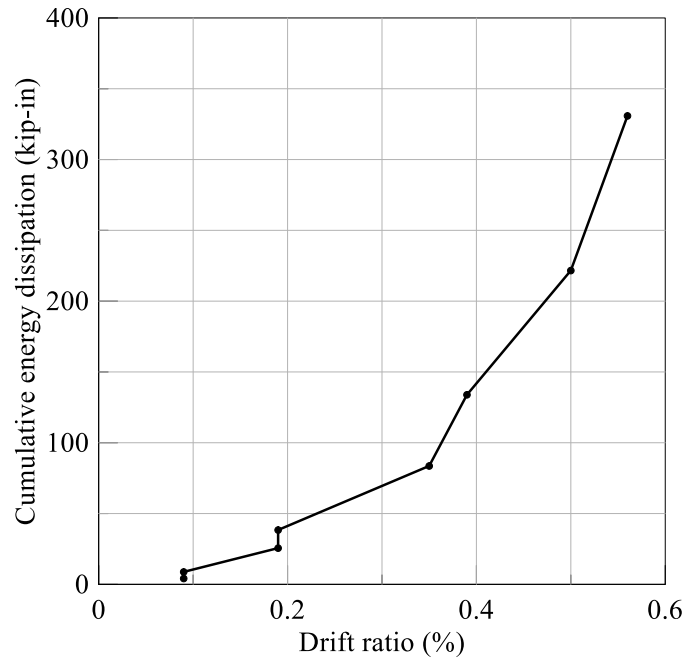
Figure 2-35: Cumulative energy dissipation, CNSC3

Table 2-17: Energy dissipated per cycle, CNSC3

| Cycle | 6 | 7 | 8 |
|---|---|---|---|
| *EDC* (kip-in) | 50.3 | 87.7 | 109 |
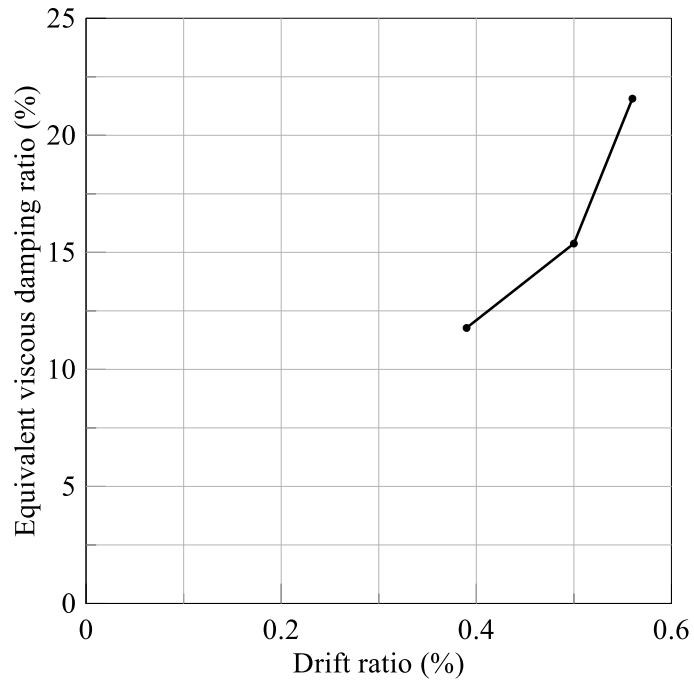


Figure 2-36: Equivalent viscous damping ratio, CNSC3

Table 2-18: Equivalent viscous damping, CNSC3

| Drift ratio (%) | 0.39 | 0.50 | 0.56 |
|---|---|---|---|
| *EVD* (%) | 11.8 | 15.4 | 21.6 |

### 2.6.3 Behaviors of CNSC3 and CNSC0

Figure 2-37 presents the in-plane force-displacement responses of CNSC0 and CNSC3. The uniaxial compressive strengths of the concrete (slenderness ratio) for CNSC0 and CNSC3 were 5800 psi (21) and 5300 psi (16), respectively. The faceplate yield strengths of CNSC0 and CNSC3 were 57 ksi and 47 ksi, respectively. The differences between CNSC0 and CNSC3 make it impossible to directly compare the experimental results. CNSC0 and CNSC3 were pushed to a drift ratio of 1.50% and 0.56%, respectively. CNSC0 failed due to cyclic yielding of the steel faceplates, leading to fracture of the base metal close to the weld. The test of CNSC3 was terminated after significant buckling of the steel faceplate on the Northeast corner of the wall and spalling of the infill concrete.
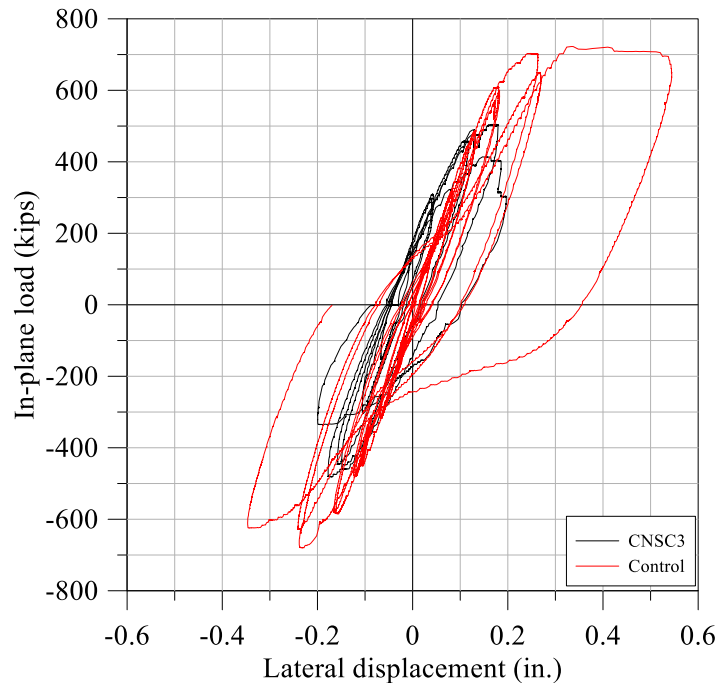


Figure 2-37: In-plane force-displacement responses of control specimen and CNSC3

# 3. NUMERICAL SIMULATION OF SC WALL PIERS

## 3.1 Introduction

This section of the report describes numerical simulations performed to support the physical tests of Section 2, namely, the simultaneous in-plane (IP) and out-of-plane (OOP) loading of SC wall piers. The simulations described here utilized, as a starting point, validated numerical models developed in LS-DYNA (LSTC, 2013) by Epackachi et al. (2014b, 2015) for calculating the IP response of SC wall piers. The validated model developed by Epackachi et al. for the IP response of SC walls used:

- The smeared crack Winfrith model for infill concrete, MAT085, using concrete material properties including the nominal compressive and tensile strengths, elastic modulus, Poisson's ratio of 0.18, specific fracture energy, and aggregate size. In the absence of experimental data, The specific fracture energy can be estimated for a given aggregate size using CEB (1990) in the absence of experimental data.

- The plastic-damage model for the steel faceplates, MAT081, using steel material properties including the nominal yield and ultimate strengths, elastic modulus, Poisson's ratio, and plastic strain thresholds corresponding to the beginning of the softening and rupture as established using coupon test results.

- Beam, shell, and solid elements to model connectors, steel faceplates, and infill concrete, respectively, and a mesh size of 1 in for the solids and shells

- Tie constraint to attach the studs and tie rods to the steel faceplates (and the baseplate if provided) and LAGRANGE-IN-SOLID constraint available in LS-DYNA to attach the connectors to the infill concrete elements.

The IP response of SC wall piers is dominated by the behavior of the steel faceplates. Given that the OOP response of an SC wall will be strongly influenced by the behavior of the concrete, it was prudent to first exercise the IP model described above using data from tests of singly reinforced concrete (RC) specimens that were not reinforced for shear. The RC beam simulations are presented in Section 3.2. Section 3.3 presents numerical simulations of the physical tests described in Section 2.

**3.2 RC Beam Simulations**

Data from tests of RC beams performed by Bresler et al. (1963) and Mphonde et al. (1985) were used to validate the Winfrith (MAT085) concrete model. The corresponding LS-DYNA simulations are summarized in Table 3-1, where $w$ is the width of the beam, $h$ is the height of the beam, $l$ is the length of the beam, $f_c'$ is the unconfined uniaxial compressive strength of concrete, $f_t'$ is the tensile strength of the concrete (taken as $0.1 f_c'$ unless specified in the experiment), $\rho$ is the longitudinal reinforcement ratio, $E$ is Young's modulus for concrete, calculated as as $E = 57000\sqrt{f_c'}$ per ACI 318-14 (ACI, 2014), $G$ is fracture energy calculated using Equation 2.1-7 or Table 2.1.4 of CEB-FIP Model Code (CEB-FIP, 1990), and $w$ is crack width, calculated as $w = 2G / f_t'$ per Figure 3 of Wittmann et al. (1988). Test 1 was performed by Bresler et al. and Tests 2 through 6 were performed by Mphonde et al. (1985). In these experiments, the shear span-to-depth ratio, $a / d$, was varied from 1.5 to 4 and the concrete compressive strength varied between 3200 and 10634 psi. The longitudinal reinforcement ratios in these beams are high, and especially so for specimens 2 through 6. Additional simulations were then performed for $a / d = 1.5$: the ratio chosen for the testing of the SC wall panels, as described in Section 2.

Table 3-1: Summary of LS-DYNA simulations of plain RC specimens

| Test | Beam dimensions $w \times h \times l$ (in) | $a/d$ | $f_c'$ (psi) | $f_t'$ (psi) | $\rho$ (%) | $E$ (psi) | $G$ (lb-in/in²) | $w$ (in) |
|---|---|---|---|---|---|---|---|---|
| 1 | 12.2 × 21.9 × 144 | 4 | 3,270 | 575 | 1.8 | 3.26E6 | 0.371 | 0.0013 |
| 2 | 6 × 13.25 × 96 | 3.6 | 3,273 | 327 | 3.4 | 3.26E6 | 0.371 | 0.0023 |
| 3 | 6 × 13.25 × 96 | 2.5 | 3,246 | 325 | 3.4 | 3.25E6 | 0.371 | 0.0023 |
| 4 | 6 × 13.25 × 96 | 1.5 | 3,637 | 364 | 3.4 | 3.44E6 | 0.399 | 0.0022 |
| 5 | 6 × 13.25 × 96 | 1.5 | 6,593 | 659 | 3.4 | 4.63E6 | 0.548 | 0.0017 |
| 6 | 6 × 13.25 × 96 | 1.5 | 10,364 | 1036 | 3.4 | 5.88E6 | 0.714 | 0.0014 |

Figure 3-1 describes the Bresler et al. experiment. The corresponding LS-DYNA model is presented in Figure 3-2. One-inch long beam elements were used to model the longitudinal reinforcement (4 #9 bars with a 1-inch cover, corresponding to a reinforcement ratio of 1.8%). Eight-node solid elements were used to model the concrete. The concrete was modeled with 1 × 1 × 1 in. elements. The rebar was embedded into the concrete using node sharing. The constant stress formulation (ELFORM=1 in LS-DYNA) and cross section integrated beam element (Hughes-Liu beam in LS-DYNA) were used for the solid and beam elements, respectively. The

Winfrith concrete model was used to model the concrete in the beam. The d3crack database was activated to visualize the crack pattern during loading. The PIECEWISE_LINEAR_PLASTICITY (MAT024) material model was used to model the Grade 60 reinforcement. The pin and roller boundary conditions were applied by constraining the displacements of three rows of nodes in the (Y and Z) and (Z) directions, respectively. A displacement was imposed at the center of the beam (1495 nodes) using a PRESCRIBED_MOTION_SET. Figure 3-3 shows the boundary conditions and the applied load.
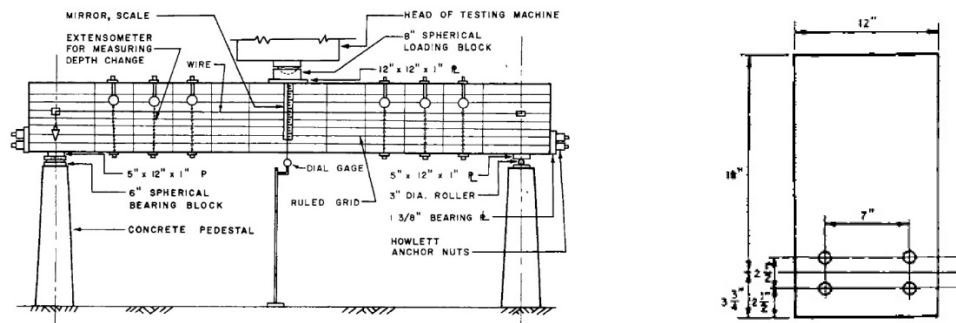


Figure 3-1: Experimental setup (Bresler et al., 1963)



(a) Isometric view                    (b) Cross section view (XZ plane)
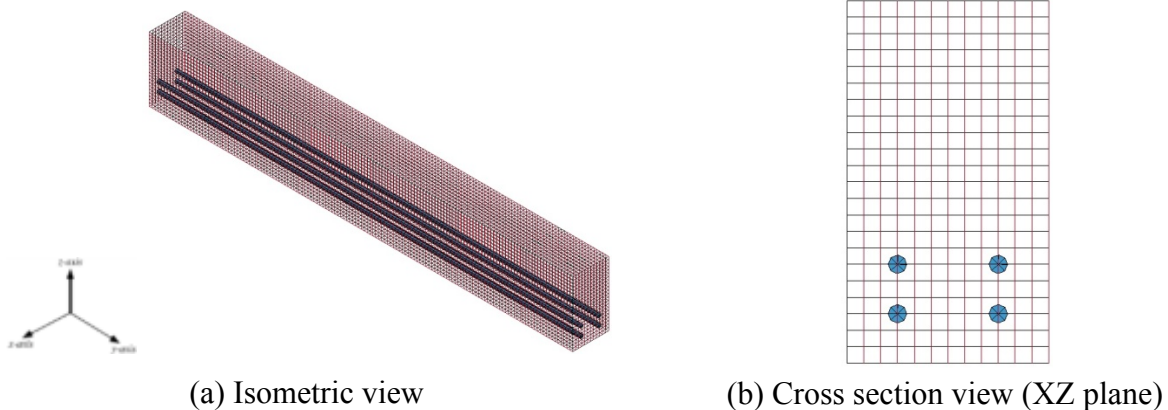
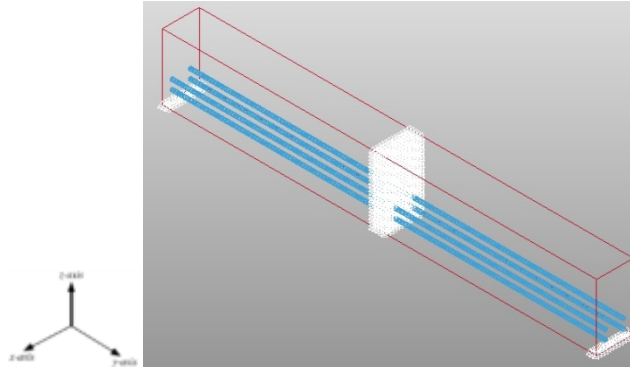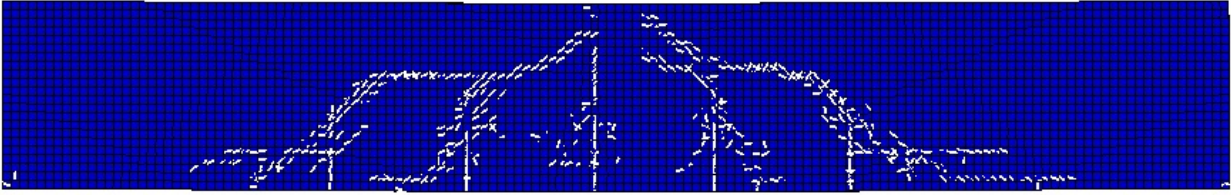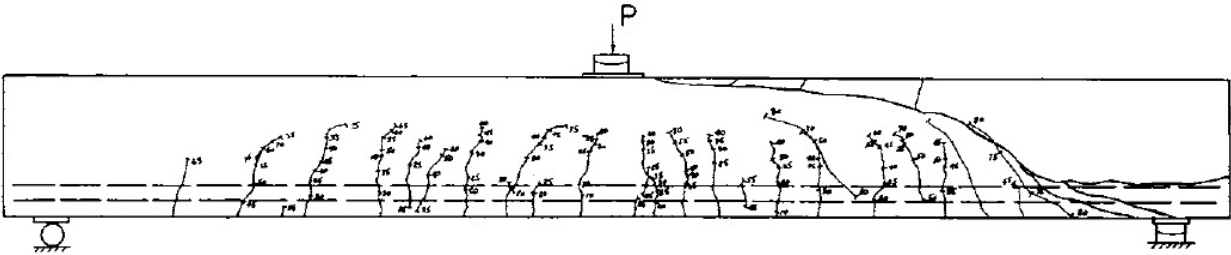Figure 3-2: LS-DYNA model of the Bresler et al. (1963) experiment

Figure 3-3: LS-DYNA loading and boundary conditions

Figure 3-4a and Figure 3-4b present the final crack pattern of the beam from the LS-DYNA simulation and the experiment, respectively. The crack pattern from the simulation is in reasonably good agreement with the experiments. Cracking at the support caused by slippage of the longitudinal reinforcement was not observed in the simulation because perfect bond was assumed. Figure 3-4c presents the force-displacement relationship at the center of the beam for the experiment and the simulation. The peak force observed in the simulation and experiment are 70 and 75 kips, respectively. The simulation is in good agreement with the experiment.

An illustration of the beam used in the Mphonde et al. (1985) experiments is presented in Figure 3-5. The input for the simulations is presented in Table 3-1 as Tests 2 through 6. The LS-DYNA model to simulate the Mphonde experiments is presented in Figure 3-6. One-inch beam elements were used to model the longitudinal reinforcement (3 #8 bars with a 1-inch cover corresponding to a reinforcement ratio of 3.36%). Eight-node solid elements were used to model the concrete. The concrete was modeled with $1 \times 1 \times 1$ in. elements. The rebar was embedded into the concrete using node sharing. The constant stress formulation (ELFORM=1 in LS-DYNA) and cross section integrated beam element (Hughes-Liu beam in LS-DYNA) were used for the solid and beam elements, respectively. The Winfrith concrete model was used to model the concrete in the beam. Material constants are presented in Table 3-1. The d3crack database was activated to visualize the crack pattern during loading. The PIECEWISE_LINEAR_PLASTICITY (MAT024) material model was used to model the Grade 60 reinforcement. The pin and roller boundary conditions were applied by constraining the displacements of one row of nodes in the (Y and Z) and (Z) directions, respectively. The location of the constraints was moved to simulate the different span lengths (i.e., 35.25, 58.75, and 84 in). A displacement was imposed at the center of the beam (505 nodes) using a PRESCRIBED_MOTION_SET.

(a) Simulation



(b) Experiment
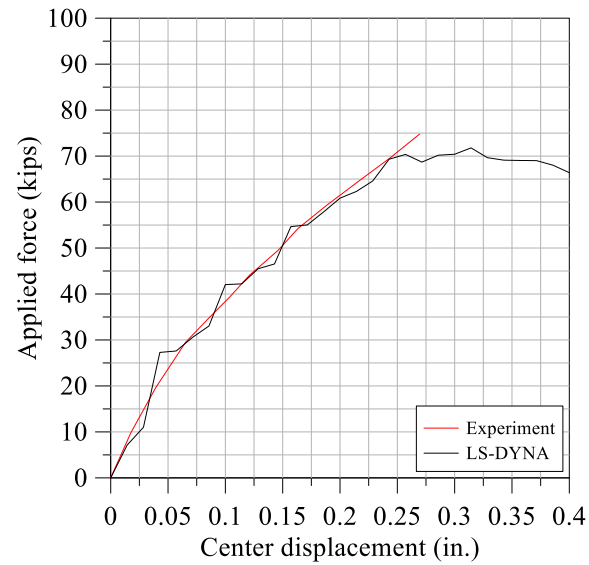


(c) Force-displacement relationships

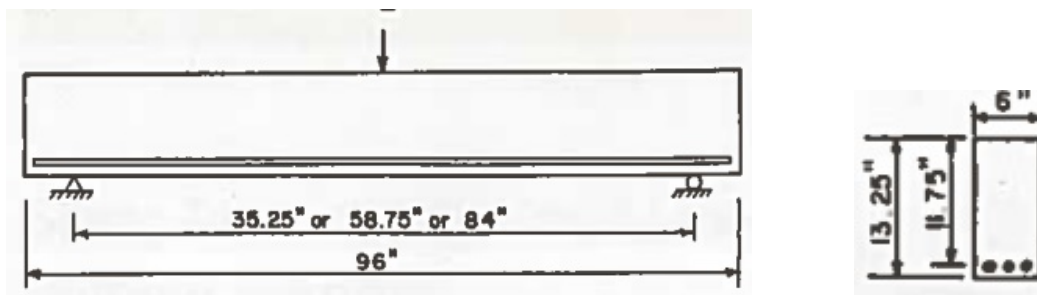Figure 3-4: Experimental (Bresler) and LS-DYNA results



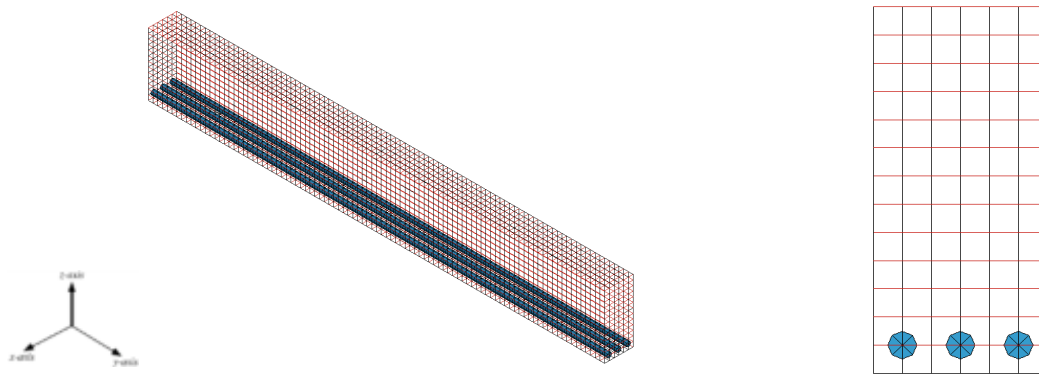Figure 3-5: Experimental setup (Mphonde et al., (1985))

Figure 3-6: LS-DYNA model of the Mphonde et al. (1985) experiment

Table 3-2 summarizes the simulations of the Mphonde experiments using average shear stress at maximum resistance, calculated here as peak load divided by the product of the section width and total depth. The simulations reasonably recover the maximum shear stress calculated from the experimental results for different values of $a/d$. Not shown here, because the experimental data are not available, is the post-peak shear force response, which will affect the IP behavior of SC walls. The Winfrith concrete model reasonably captures the OOP peak shear strength of plain reinforced concrete beams (i.e., no shear reinforcement) under *monotonic* loading, and is used hereafter to simulate the *cyclic* OOP and combined IP and OOP response of SC walls. Note that the normalized maximum shear stresses for Tests 2 through 6 are much greater than the value of 2.0 routinely used for the shear design of reinforced concrete beams and slabs in the United States for two reasons: 1) the longitudinal reinforcement ratios are high for all specimens (which increases monotonic shear capacity of plain reinforced concrete), and 2) the ratio of *a* to *d* is 1.5 for Tests 4, 5 and 6, which alters the shear-force-resisting mechanism from that of a slender beam to a deep beam (i.e., strut joining the point of load application to the point of reaction).

Table 3-2: Summary of RC beam simulation results

| Test | $a/d$ | Maximum shear stress (psi) | | Maximum shear stress normalized by $\sqrt{f_c'}$ | | Difference (%) |
|------|-------|------------|----------|------------|----------|----------------|
| | | Experiment | LS-DYNA | Experiment | LS-DYNA | |
| 2 | 3.6 | 183 | 198 | 3.19 | 3.46 | 8 |
| 3 | 2.5 | 220 | 302 | 3.86 | 5.30 | 37 |
| 4 | 1.5 | 328 | 379 | 5.44 | 6.28 | 16 |
| 5 | 1.5 | 881 | 974 | 10.85 | 12.0 | 11 |
| 6 | 1.5 | 1223 | 1371 | 11.86 | 13.3 | 12 |

## 3.3 Simulation of CNSC Experiments

A model of the CNSC experiments was built in LS-DYNA using the approach described in Section 3.1. The model, shown in Figure 3-7, is composed of infill concrete, baseplate, steel faceplates, tie rods, and shear studs. The foundation was not included in the model: the bottom nodes of the baseplate were fixed. The element types, sizes, and formulations, and material models used for each part of the model are summarized in Table 3-3.

In experiments CNSC1 and CNSC3, the tie bars were spaced at 12 inches on center along the height and length of the wall, with the first tie bar located 12 inches above the baseplate and 6 inches from the edge of the wall (see Figure 3-8); the tie bar is shown in yellow. In CNSC2, the tie bars were spaced at 6 inches on center along the height and length of the wall, with the first tie bar located 6 inches above the baseplate and 3 inches from the edge of the wall (see Figure 3-9). The shear studs on the faceplates were spaced at 3 inches on center along the height and length of the wall. The total wall thickness was 12 inches. The yield strength and tensile strengths of the steel faceplate material were 47 ksi and 80 ksi, respectively. The OOP loading was simulated by applying nodal forces to the steel and concrete elements at a height of 18 inches above the base of the wall. Once the wall was cycled OOP and the desired OOP load was reached, the OOP load was held constant, and the wall was then subjected to displacement-controlled cyclic IP loading at its top.

The follow subsections present results of the LS-DYNA simulations. Comparisons are made between the results of the experiments and the LS-DYNA simulations.
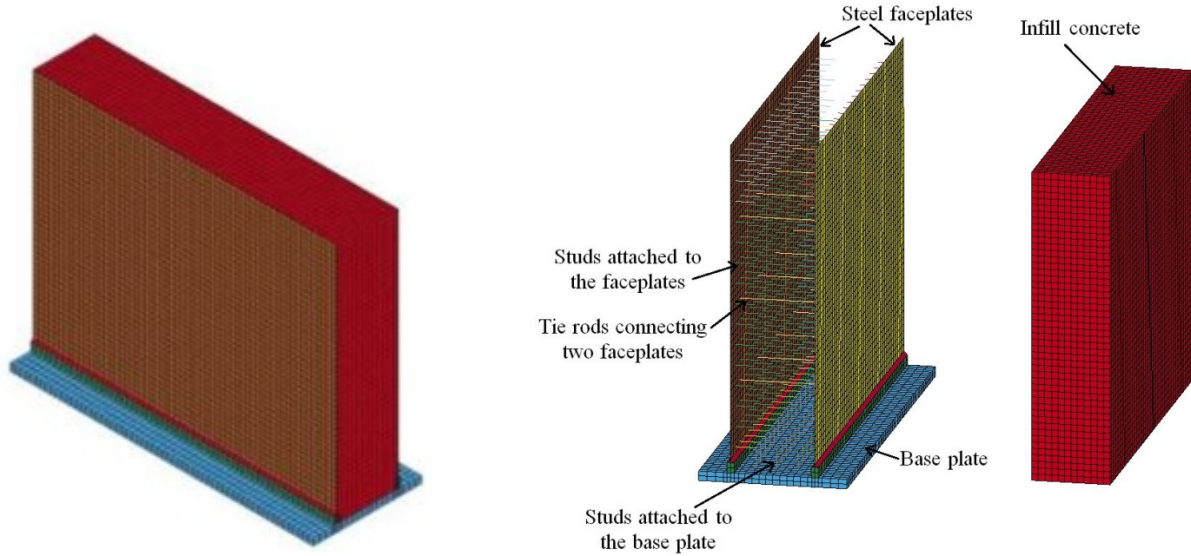
Figure 3-7: LS-DYNA model of CNSC experiments

Table 3-3: Summary of the LS-DYNA models of the CNSC specimens

| Part | Element | | | Material model |
|------|---------|---------|-------------|----------------|
| | Type | Size | Formulation | |
| Infill concrete | Solid | 1 × 1 × 1 in | Constant stress solid | Winfrith (MAT085) |
| Faceplate | Shell | 1 × 1 in | Belytschko-Tsay | Plasticity_with_Damage (MAT081) |
| Shear studs | Beam | 1 in | Hughes-Liu with cross section integration | Piecewise_Linear_Plasticity (MAT024) |
| Tie rods | Beam | 1 in | Hughes-Liu with cross section integration | Piecewise_Linear_Plasticity (MAT024) |
| Baseplate | Solid | 1 × 1 × 1 in | Constant stress solid | Elastic (MAT003) |
| Welds | Solid | 1 × 1 × 1 in | Constant stress solid | Elastic (MAT003) |
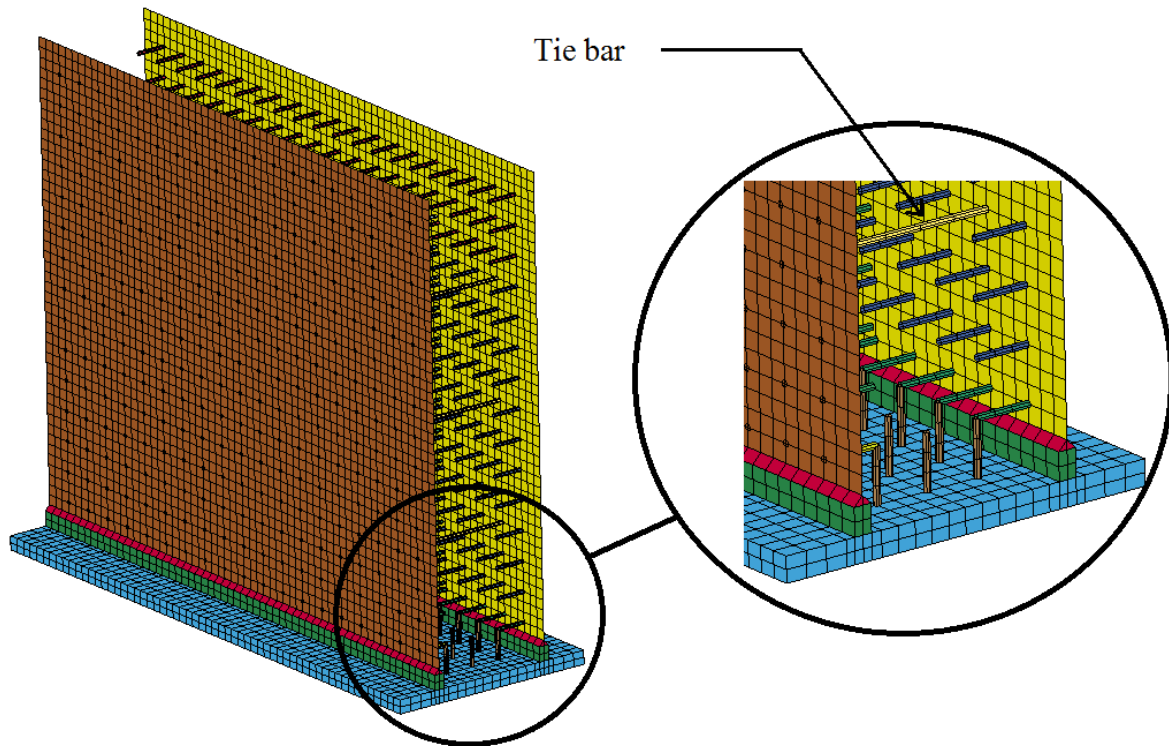
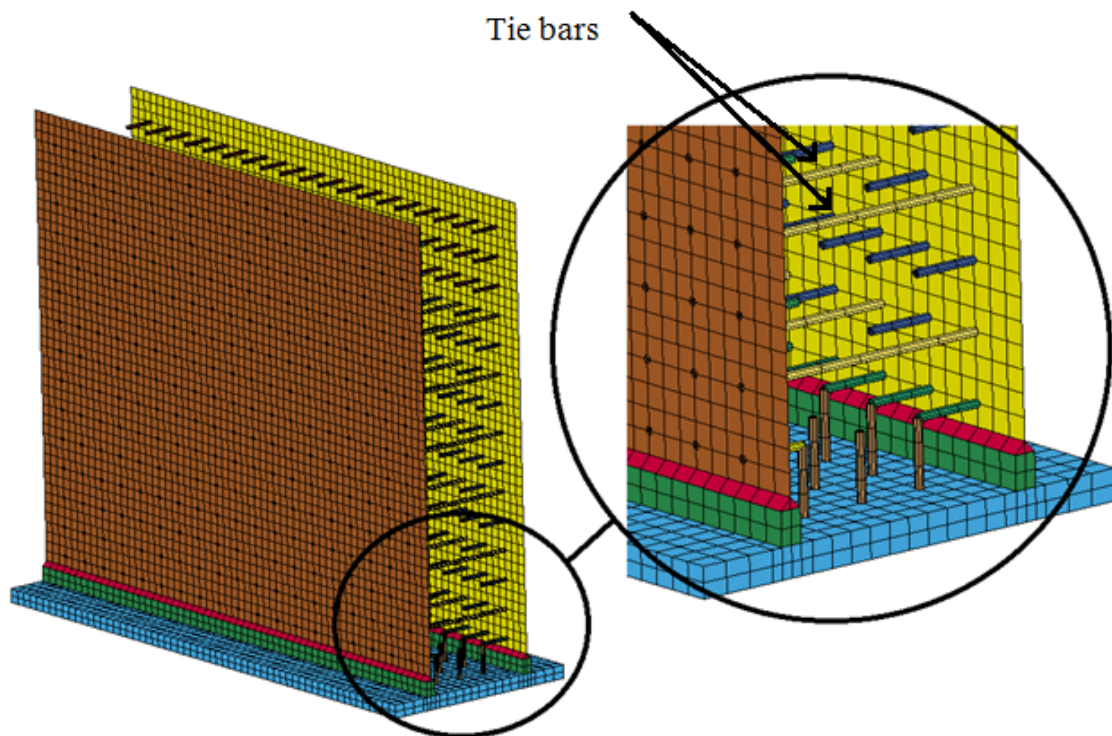Figure 3-8: CNSC1 and CNSC3 tie bar details



Figure 3-9: CNSC2 tie bar details

### 3.3.1 CNSC1 Simulations

The uniaxial compressive strength of the infill concrete in CNSC1 on the first day of physical testing was 7700 psi. CNSC1 was initially subjected to four cycles of OOP loading at magnitudes of 30, 60, 90 and 120 kips. The OOP load was maintained at a constant value of 120 kips and incremental cyclic IP loading was then imposed. The IP loading protocol in the simulation and experiment consisted of seven load steps with two cycles per load step and a maximum drift of 1.6%: see Table 2-2.

The OOP force-displacement relationship of the SC panel for the experiment and the simulation are shown in Figure 3-10. The stiffness of the SC panel in the numerical model is slightly greater than that observed in the experiment because the foundation (and its flexibility) was not modeled. A plan view of the wall pier and directions of applied IP and OOP load are presented in Figure 3-11. The configuration presented in Figure 3-11 shows the direction of applied OOP load during IP loading and is denoted as the push direction; the West and East faceplate is in tension and compression due to the OOP load, respectively. The distribution of vertical stress on the tension faceplate (West) at the instant before the IP cyclic loading was imposed for the experiment and the numerical model are presented in Figure 3-12; the stresses are plotted as a function of the distance along the length of the wall from point O (see Figure 3-11). Points P1, P2, P3, P4, and P5 (labeled in Figure 3-11 and Figure 3-12) correspond to distances of 3, 15, 30, 45, and 57 inches from point 0 at the bottom of the base plate. Points P1, P2, P3, P4, and P5 also correspond to locations of strain gages on the West face (shown in Figure 2-3c). The vertical stresses calculated from the numerical analysis are in reasonably good agreement with the values measured in the experiment. No yielding of the faceplates was observed during OOP loading in either the experiment or the simulation.
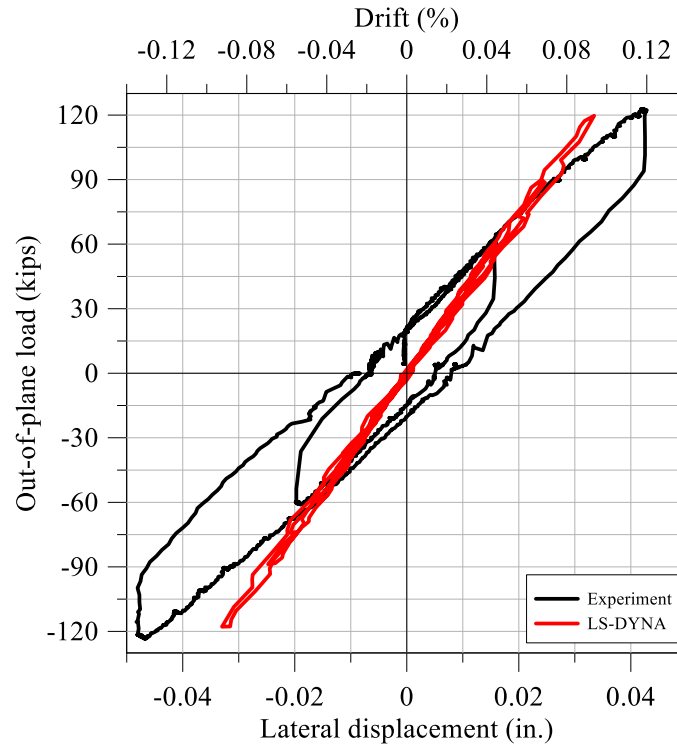
Figure 3-10: OOP force-displacement relationship, LS-DYNA and experiment, CNSC1
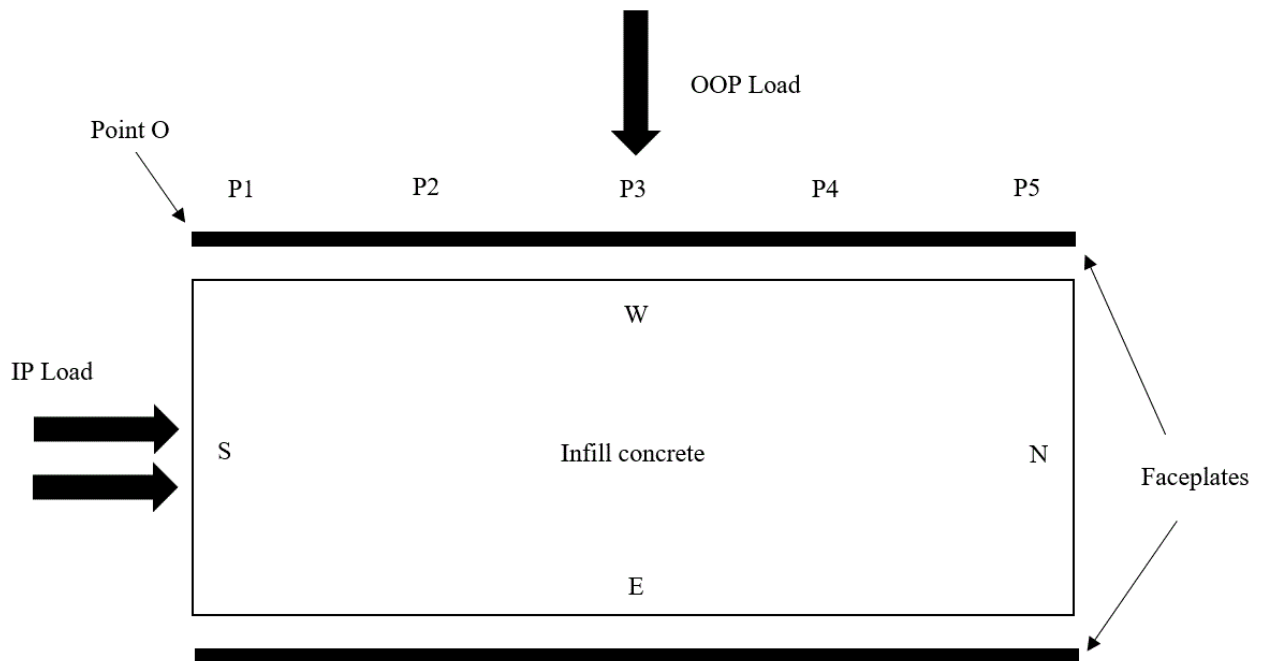


Figure 3-11: Plan view of wall pier and loading directions, push direction configuration
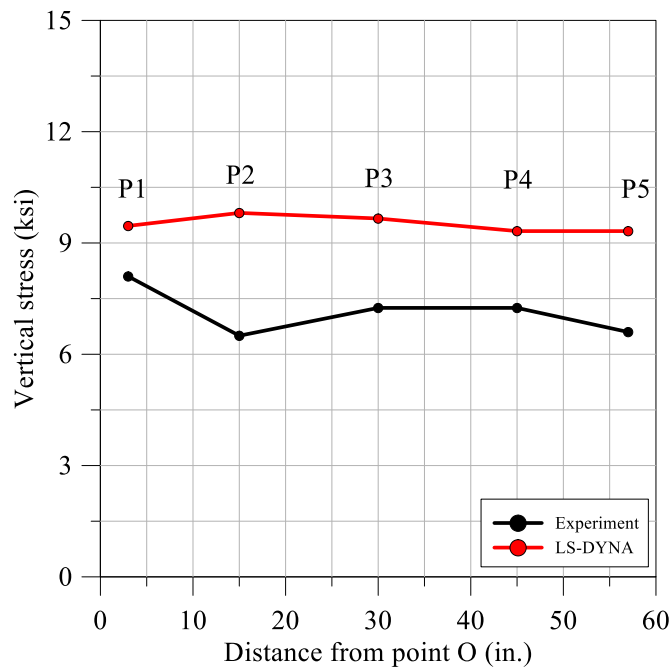
Figure 3-12: Distribution of vertical stresses on tension plate at instant before IP cyclic loading, CNSC1

The axial stresses in the tie bars at the instant before application of the IP loading is shown in Figure 3-13; the stresses are shown in units of psi. The greatest stresses are observed in the tie bars located below point of application of the OOP load, which is an expected outcome. The maximum axial stress due to the applied OOP load is 6.2 ksi: much less than the yield stress.

The IP force-displacement relationship of the SC panel for the simulation and the experiment are shown in Figure 3-14. The predictions of peak shear resistance, post-peak strength reductions, and rate of reloading/unloading stiffness for peak and post-peak IP strength cycles compared favorably with the test results; the initial IP stiffness of the numerical model is significantly larger than that of the experiment because the flexibility of the foundation was not considered in the numerical model.
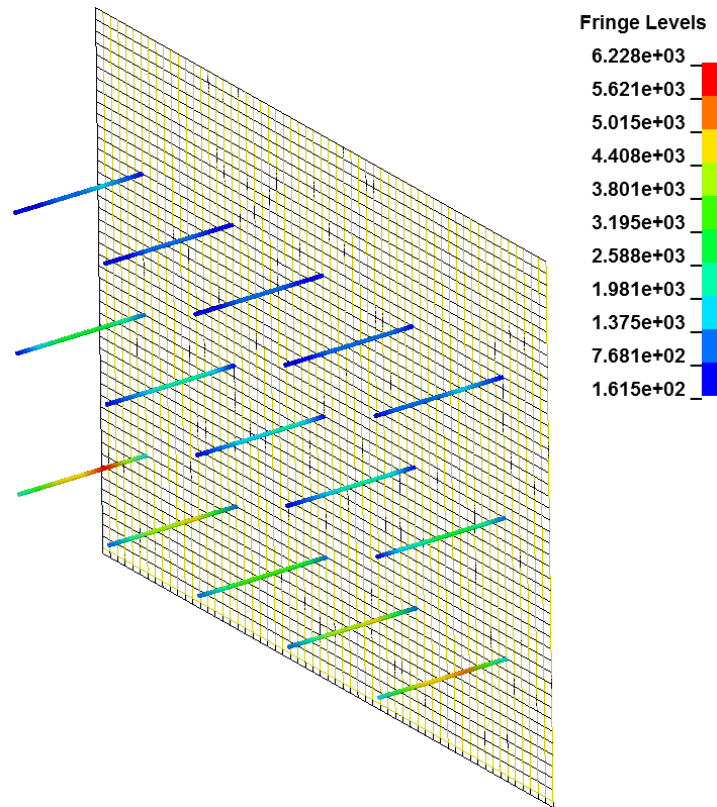
Figure 3-13: Distributions of axial stress in tie bars at instant before IP cyclic loading, CNSC1 (units of psi)
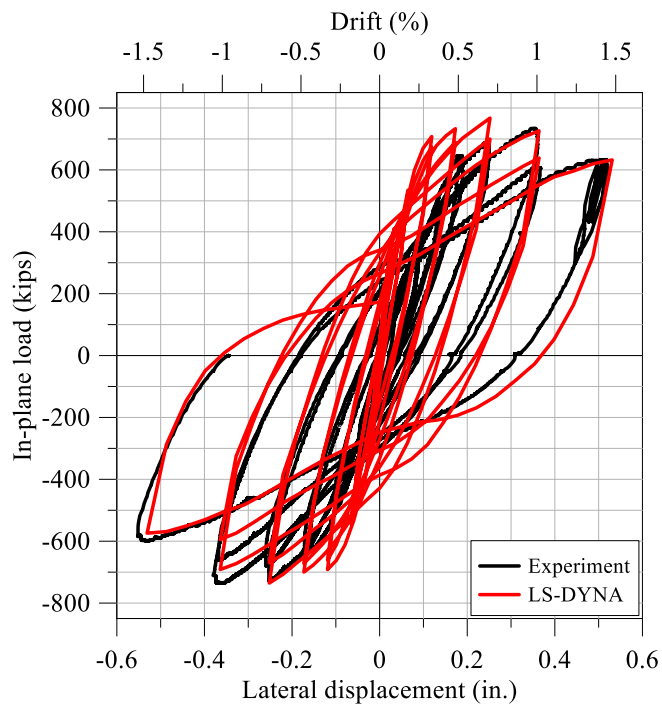


Figure 3-14: IP force-displacement relationship, LS-DYNA and experiment, CNSC1

The IP equivalent viscous damping, $EVD$, calculated using Equation (2-1) at different levels of story drift are presented in Figure 3-15 for both the numerical simulation and the experiment. The calculated damping ratios from the numerical simulation are slightly greater than from the experiment. The IP force-displacement relationships for cycles 8 and 9, which correspond to drift ratios of 0.5 and 0.7%, respectively, are shown in Figure 3-16a and Figure 3-16b, respectively. The numerical model slightly overshoots the peak force and its hysteresis loops are wider, leading to an overprediction of the dissipated energy. Because the secant stiffness to maximum displacement is similar for the numerical solution and the experiment, the overprediction of dissipated energy leads directly to an overprediction of $EVD$: see Figure 3-15. Figure 3-17 presents the observed and simulated local damage to CNSC1; cracking of the concrete and local buckling of the steel faceplates at the toes of the wall were observed in both the experiment and the numerical simulation. The numerical model cannot predict crushing (spalling) of infill concrete as observed in the experiment.
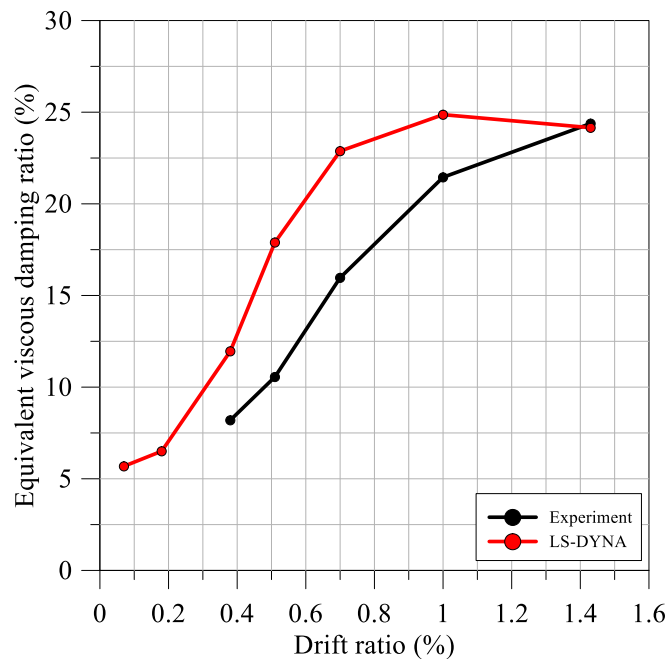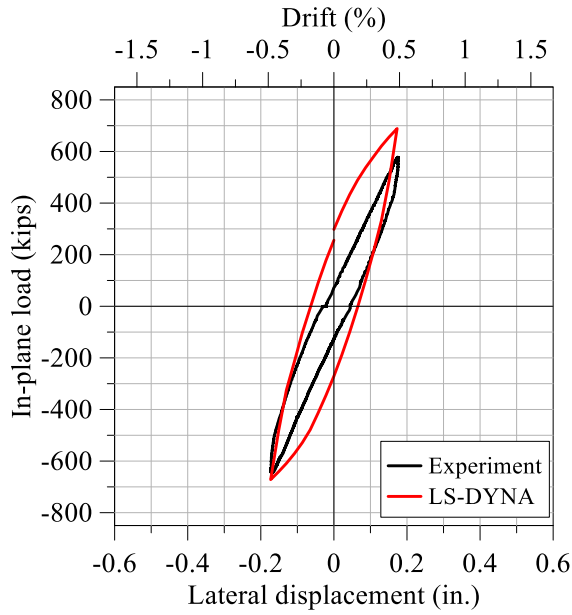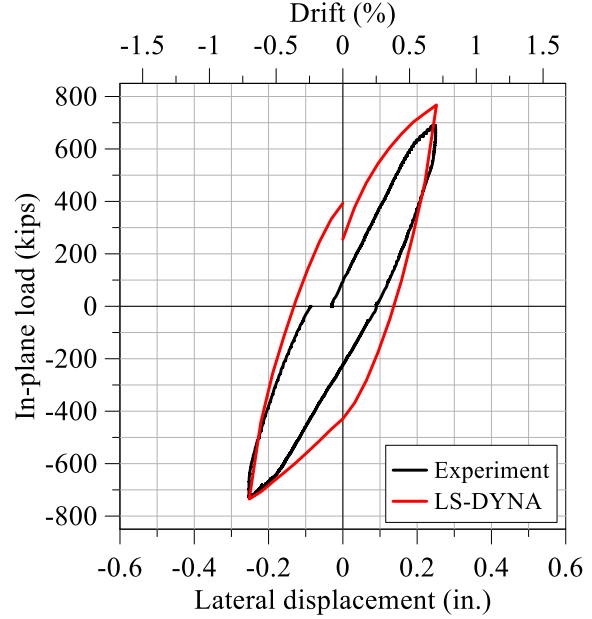


Figure 3-15: Equivalent viscous damping ratio, LS-DYNA and experiment, CNSC1

(a) Cycle 8, drift ratio = 0.5%                    (b) Cycle 9, drift ratio = 0.7%

Figure 3-16: Selected IP force-displacement relationships, LS-DYNA and experiment, CNSC1
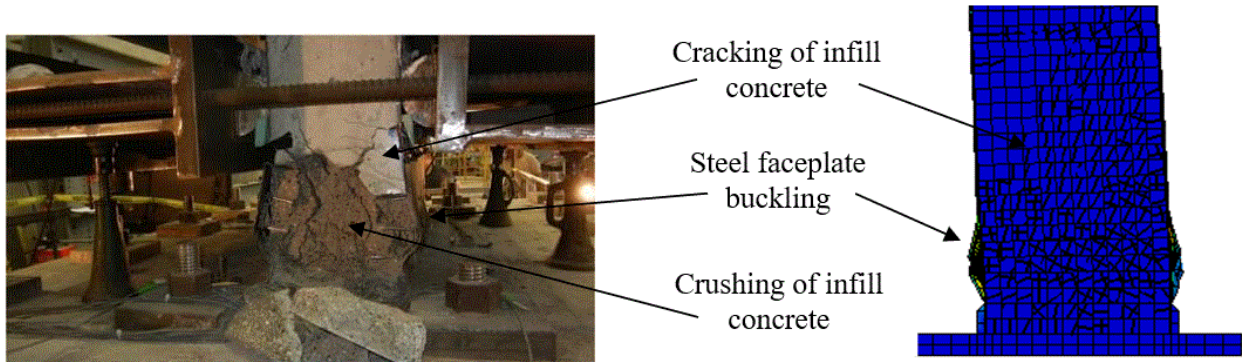


Figure 3-17: Observed and predicted damage to CNSC1

The LS-DYNA-predicted cyclic force-displacement relationships of the infill concrete and steel faceplates are presented in Figure 3-18a and Figure 3-18b, respectively. The IP shear forces in the infill concrete and steel faceplates were calculated at the baseplate using the SPLANE feature in LS-DYNA; the feature allows the user to perform cuts using section planes to aggregate forces. The total IP force-displacement relationship is also presented in Figure 3-18a and Figure 3-18b (in grey), to show the contribution of the infill concrete and steel faceplates to the overall resistance of the wall pier. The steel faceplates dominate the behavior of the SC wall pier in the

IP direction, which is an expected result. The pinched hysteresis loops for the infill concrete is associated with damage to the infill concrete (i.e., cracking), as observed in Figure 3-17a.

The LS-DYNA-predicted OOP force history of the infill concrete and the steel faceplates is presented in Figure 3-19. The SC wall pier was subjected to four cycles of OOP load at magnitudes of 30, 60, 90, and 120 kips before being held constant (at time=1.7 seconds in Figure 3-19) for the application of the IP loading. The infill concrete dominates the behavior of the SC wall pier in the OOP direction.



| (a) Infill concrete | (b) Steel faceplates |
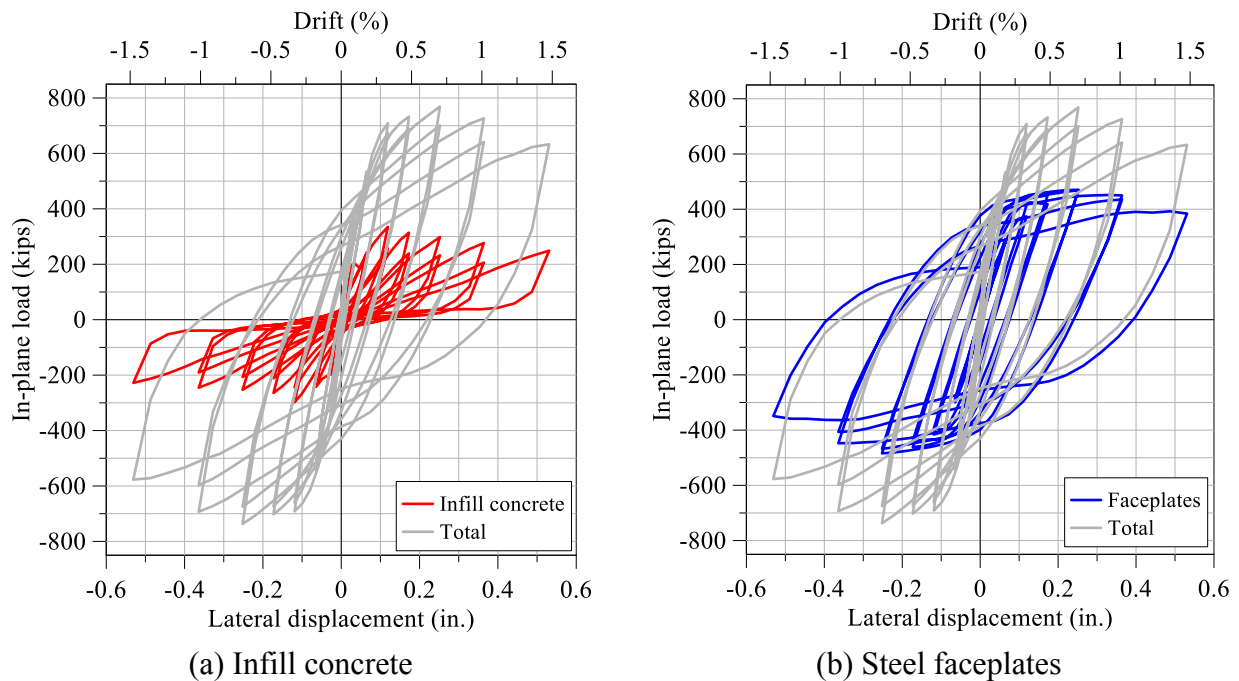
Figure 3-18: LS-DYNA-predicted IP cyclic force-displacement relationships, CNSC1

Figure 3-20 presents the IP force-displacement relationship for the experiment, and the LS-DYNA simulations with and without the applied OOP load. The initial stiffness, pinching, and rate of reloading/unloading of the numerical model are similar for the numerical model with and without the applied OOP load. The backbone curves for the force-displacement relationships presented in Figure 3-20 are presented in Figure 3-21. The differences in initial stiffness for the experiment and the numerical model are observed clearly using the backbone curves. The OOP load reduces the IP capacity of the LS-DYNA model by approximately 6%.
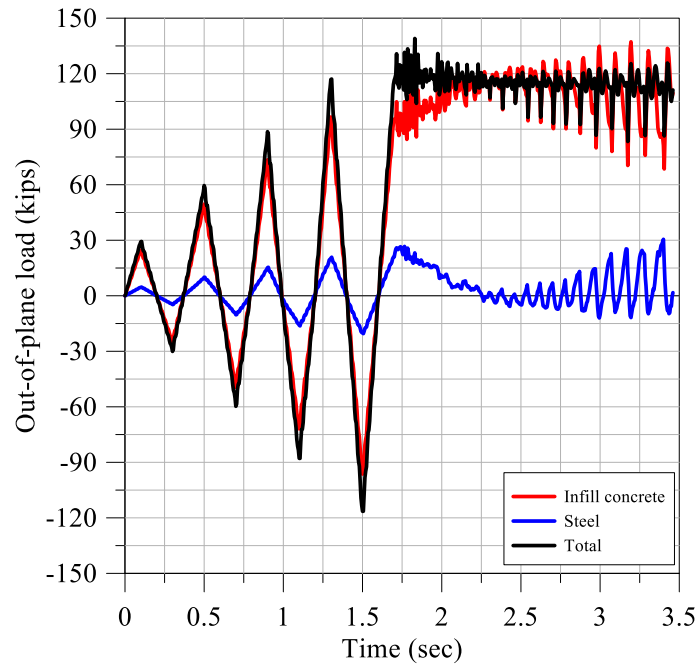
Figure 3-19: LS-DYNA-predicted components of the OOP cyclic force history, CNSC1
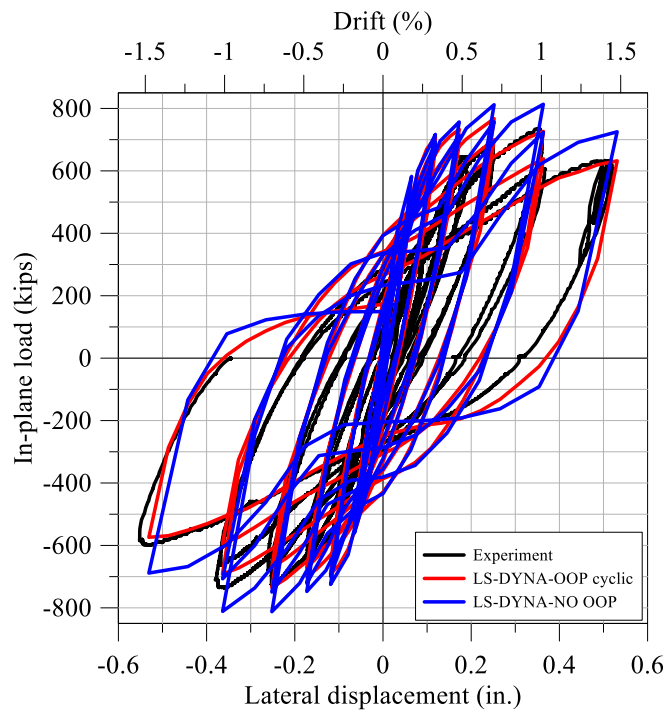


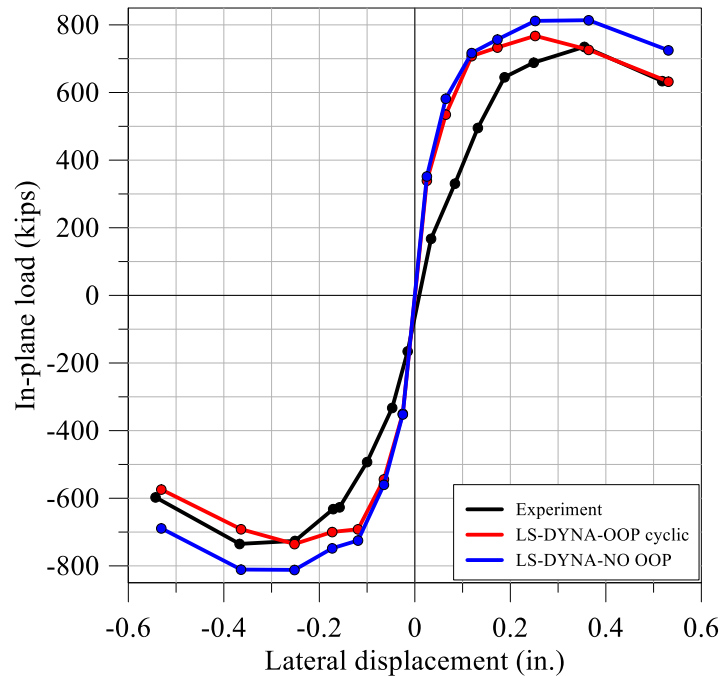Figure 3-20: IP force-displacement relationships, CNSC1

Figure 3-21: Backbone curves, CNSC1

### 3.3.2 CNSC2 Simulations

The uniaxial concrete compressive strength on the first day of testing was 5300 psi. The SC specimen was initially subjected to five cycles of OOP loading, at magnitudes of 30, 60, 90, 120, and 240 kips, respectively. In both the simulation and the experiment, the OOP load was then maintained at 240 kips and incremental cyclic IP loading was imposed. The loading protocol in the experiment and the simulation consisted of seven load steps with two cycles per load step and a maximum drift of 1.7%: see Table 2-8.

Figure 3-22 presents the OOP force-displacement relationship for the experiment and the simulation. The stiffness of the numerical model is in relatively good agreement with that of the experiment. The distributions of vertical stress on the tension faceplate (West side) in the push configuration at OOP loads of 60, 90, 120, and 240 kips are presented in Figure 3-23a, Figure 3-23b, Figure 3-23c , and Figure 3-23d, respectively; the stresses are plotted as a function of the distance along the length of the wall from point O (see Figure 3-11). The distances of 3, 15, 30, 45, and 57 inches from Point 0 correspond to points P1, P2, P3, P4, and P5, respectively. The predicted stresses are in relatively good agreement with the stresses measured in the experiment. The faceplates did not yield during cyclic OOP loading in either the experiment or the numerical simulation.
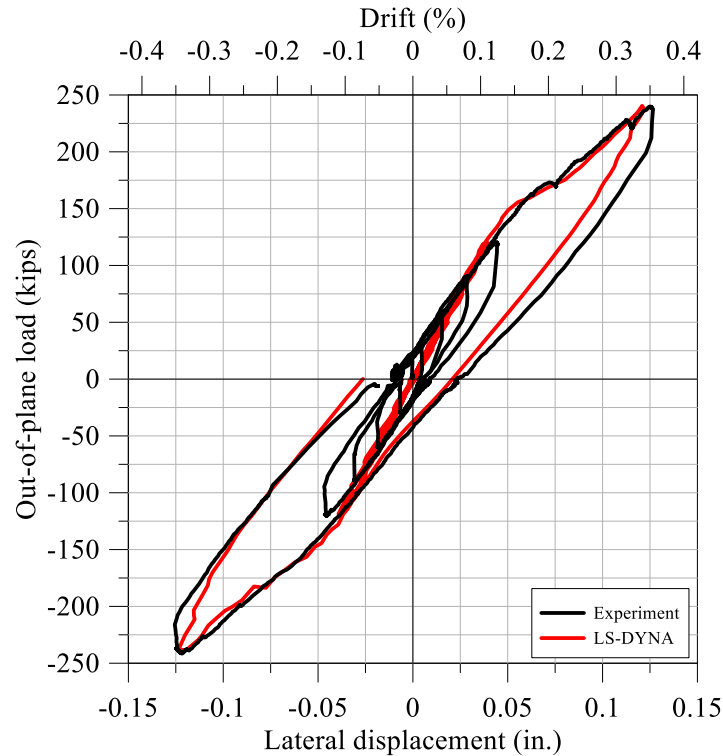
Figure 3-22: OOP force-displacement relationship, LS-DYNA and experiment, CNSC2

Figure 3-24 presents the distributions of axial stress in the tie bars at the instant before application of the IP load; the magnitude of the OOP load was 240 kips. The maximum axial stress was observed in the tie bars near the base of the wall: an expected result. The predicted maximum axial stress was 37 ksi, and less than the yield value.

The IP force-displacement relationship for the simulation and the experiment are presented in Figure 3-25. The numerical model predicted the peak shear resistance and rates of reloading/unloading with reasonable accuracy. The OOP load in cycles 12 and 13 of the experiment was not maintained at 240 kips: it gradually decreased as the IP capacity of the wall diminished. To account for this in the numerical simulation, the OOP load in the numerical model decayed linearly from 240 kips at the start of cycle 12 to a value of 0 kips at the end of cycle 13.
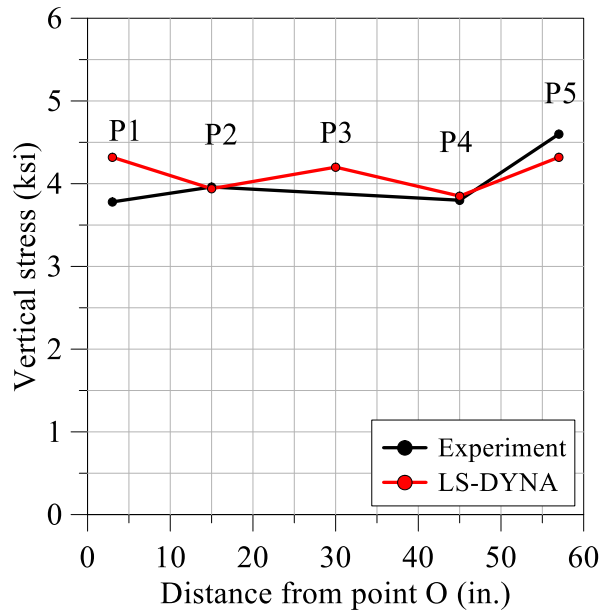
(a) OOP load = 60 kips
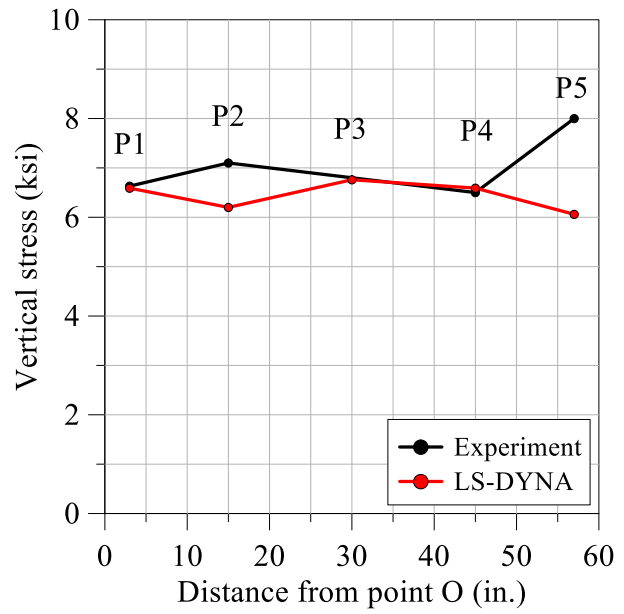
(b) OOP load = 90 kips
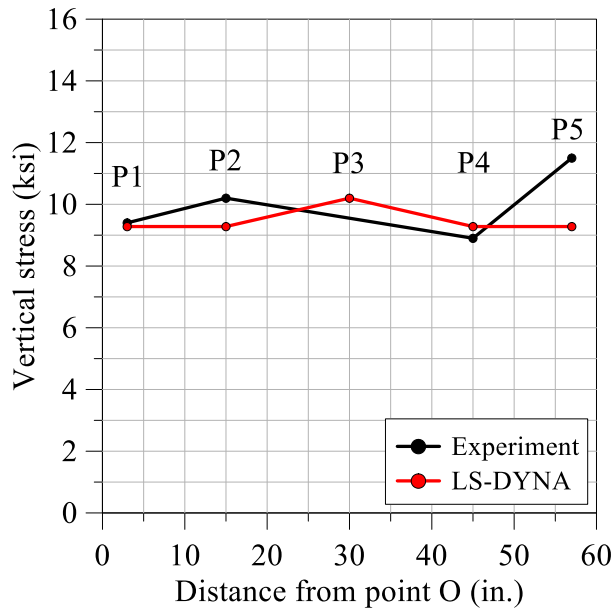
(c) OOP load = 120 kips
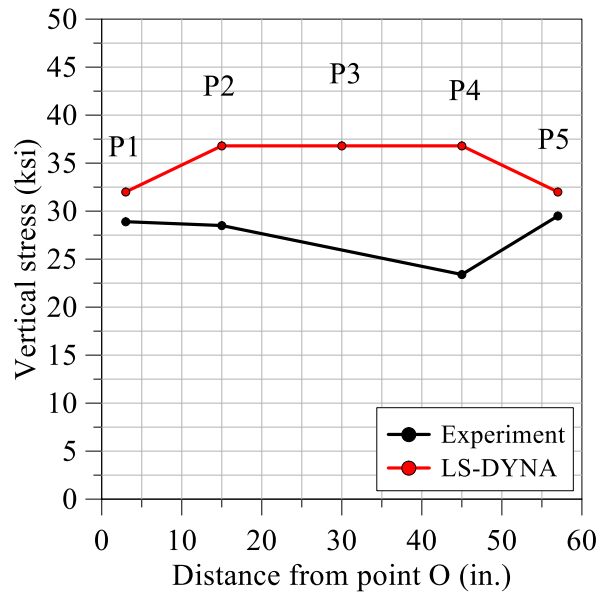
(d) OOP load = 240 kips

Figure 3-23: Distributions of vertical stress in the tension plate, CNSC2
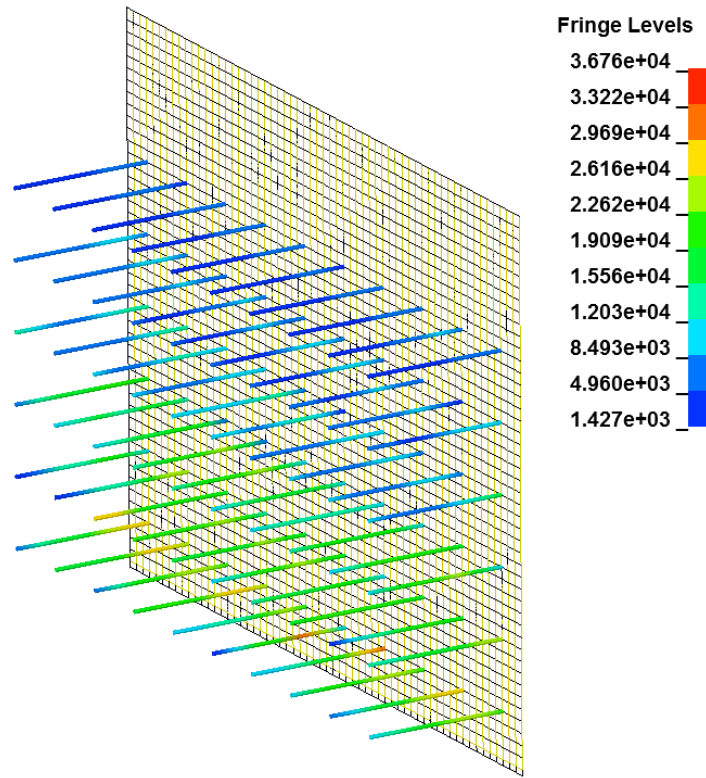
Figure 3-24: Distributions of axial stress in tie bars at instant before IP cyclic loading, CNSC2 (units of psi)
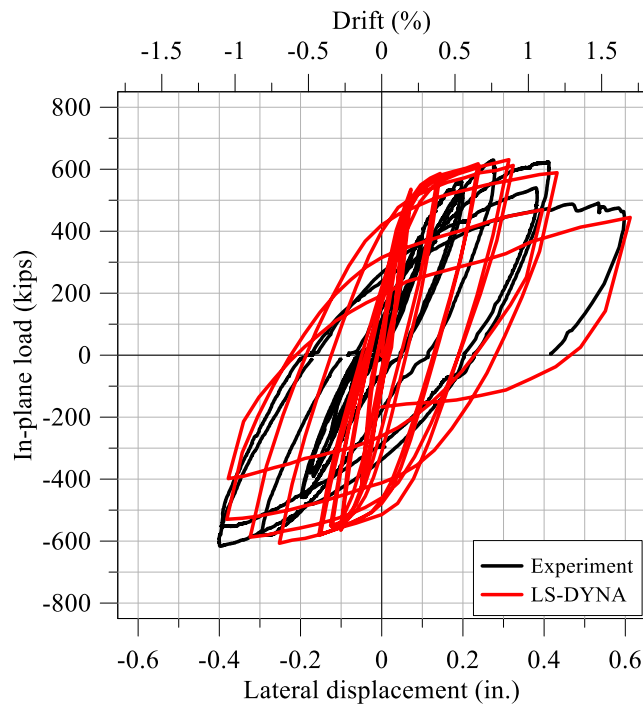


Figure 3-25: IP force-displacement relationship, LS-DYNA and experiment, CNSC2

The calculated equivalent viscous damping ratio, $EVD$, for the experiment and the numerical simulation are presented in Figure 3-26. The damping ratios predicted using the numerical model are significantly greater than those measured in the experiment. Figure 3-27a and Figure 3-27b present the IP force-displacement relationships for cycles 7 and 9, respectively; cycles 7 and 9 correspond to drift ratios of 0.55 and 0.79%, respectively. The numerical model overshoots the peak force measured in the experiment in Cycle 7 but the numerically predicted energy dissipation in these cycles are significantly wider than those calculated from the experiment, leading to greater values of $EVD$.

The measured and predicted damage to CNSC2 are shown in Figure 3-28. Local buckling of the steel faceplates and cracking of the concrete are seen in both the experiment and the simulation. Large concrete strains are predicted and crushing of concrete was observed at the toes of the wall.
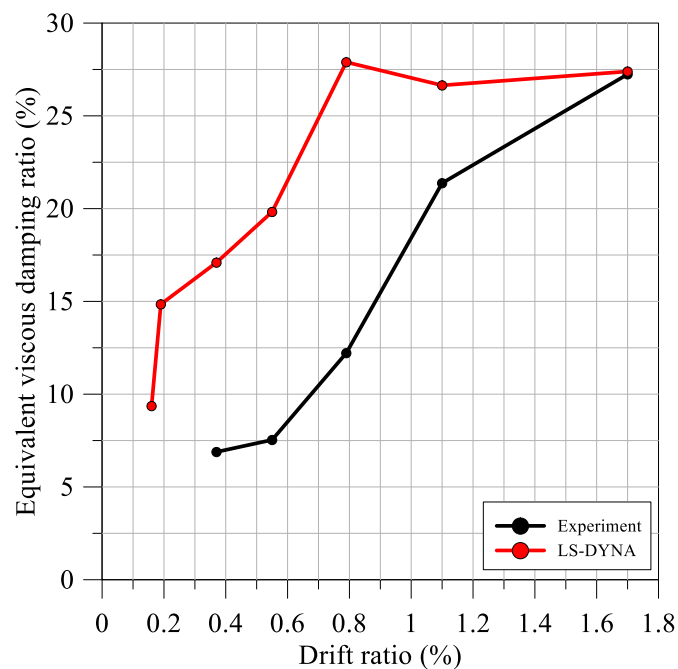


Figure 3-26: Equivalent viscous damping ratio, LS-DYNA and experiment, CNSC2
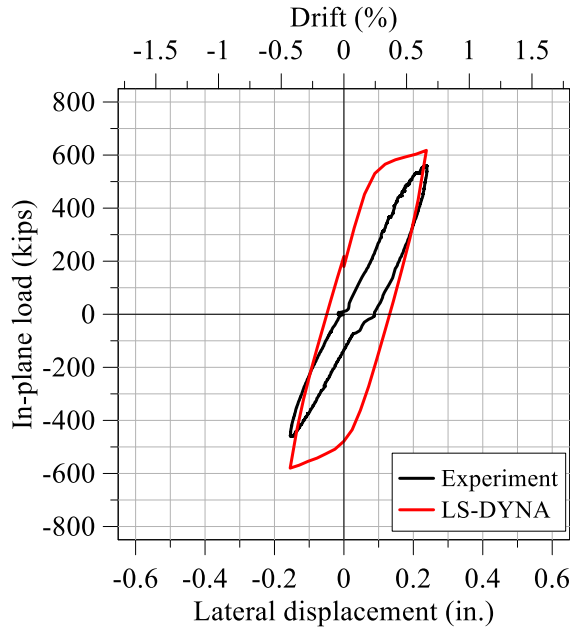
(a) Cycle 7, drift ratio = 0.55%    (b) Cycle 9, drift ratio = 0.79%
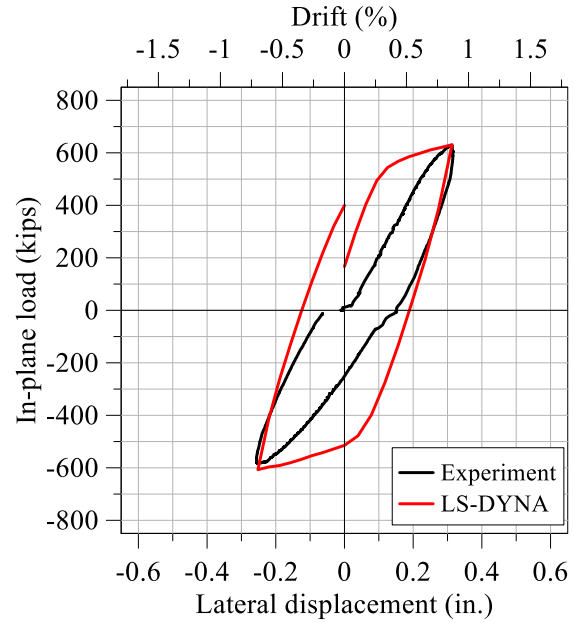
Figure 3-27: Selected IP force-displacement relationships, LS-DYNA and experiment, CNSC2
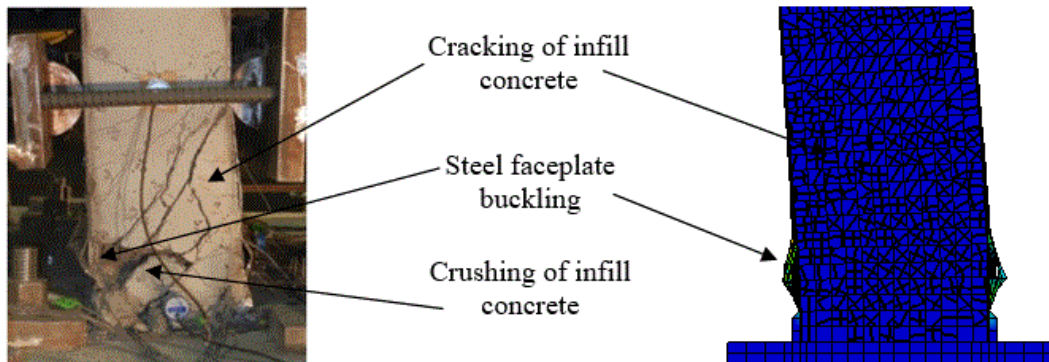


Figure 3-28: Observed and predicted damage to CNSC2

Figure 3-29a and Figure 3-29b show the LS-DYNA-predicted IP cyclic force-displacement relationships for the infill concrete and steel faceplates, respectively. The predicted IP force-displacement relationship of the pier is shown in grey to highlight the contribution of the infill concrete and steel faceplates to the total IP shear resistance. The steel faceplates dominate the behavior of the wall piers in the IP direction. The predicted hysteresis loops for the infill concrete and the steel faceplates are pinched, due to concrete cracking and faceplate buckling, respectively. The components of resistance in LS-DYNA-predicted OOP cyclic force history are presented in Figure 3-30; the total applied load is also displayed to highlight the contribution of

each component to the OOP shear resistance. The infill concrete dominates the behavior in the OOP direction: an expected result. The linear decay in the numerically applied OOP load in cycles 12 and 13, related to the relaxation of the OOP loading in the experiment, is shown in Figure 3-30.



(a) Infill concrete　　　　　　　　　　　(b) Steel faceplates
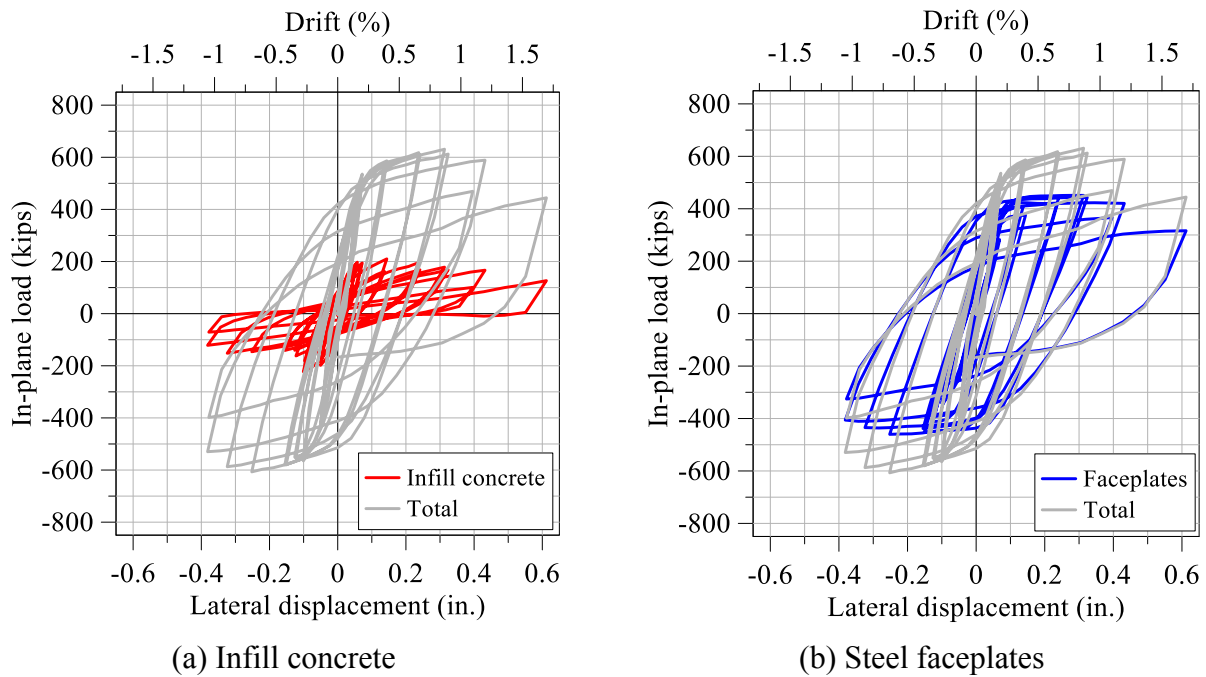
Figure 3-29: LS-DYNA-predicted IP cyclic force-displacement relationships, CNSC2
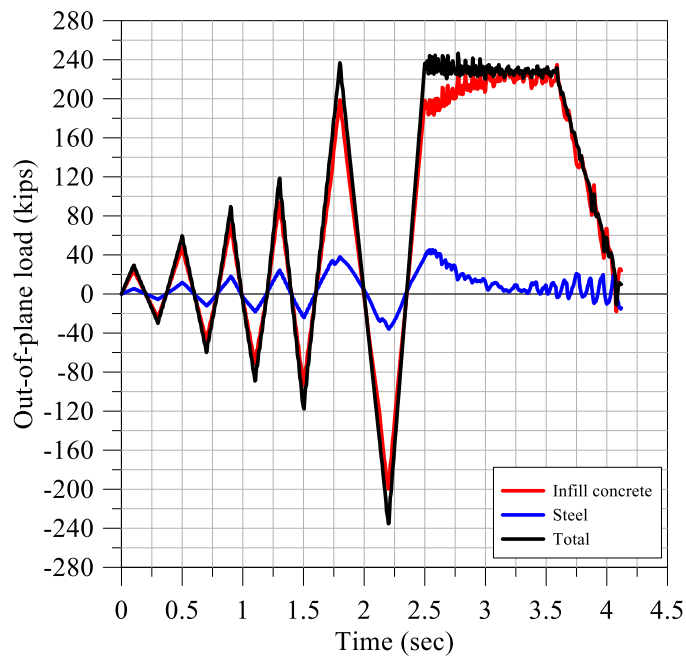


Figure 3-30: LS-DYNA-predicted components of the OOP cyclic force history, CNSC2

The IP force-displacement relationship for the experiment and the LS-DYNA simulations with and without applied OOP load are presented in Figure 3-31. The application of the OOP load significantly reduces the IP capacity of the wall piers, although the initial stiffness and rates of reloading/unloading are not significantly affected. The backbone curves for the cyclic loadings of Figure 3-31 are shown in Figure 3-32. The application of the OOP load to the LS-DYNA model reduced the IP capacity by 22%.
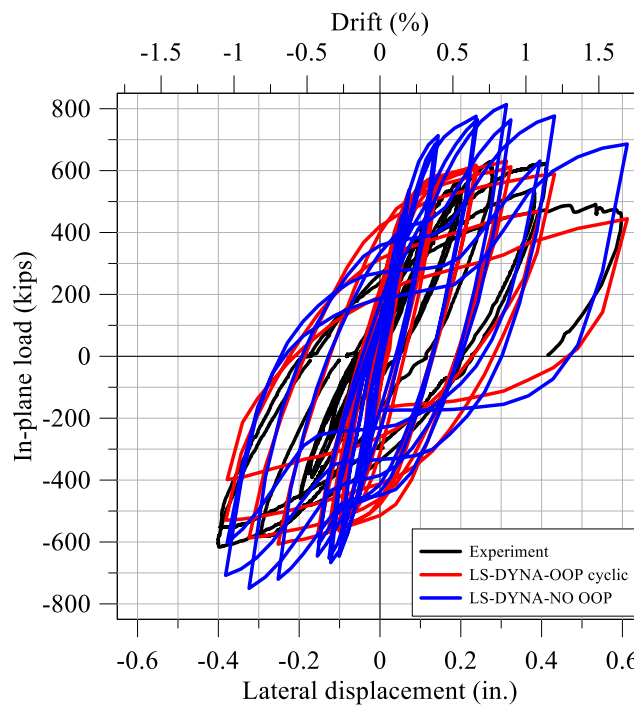


Figure 3-31: IP force-displacement relationships, CNSC2
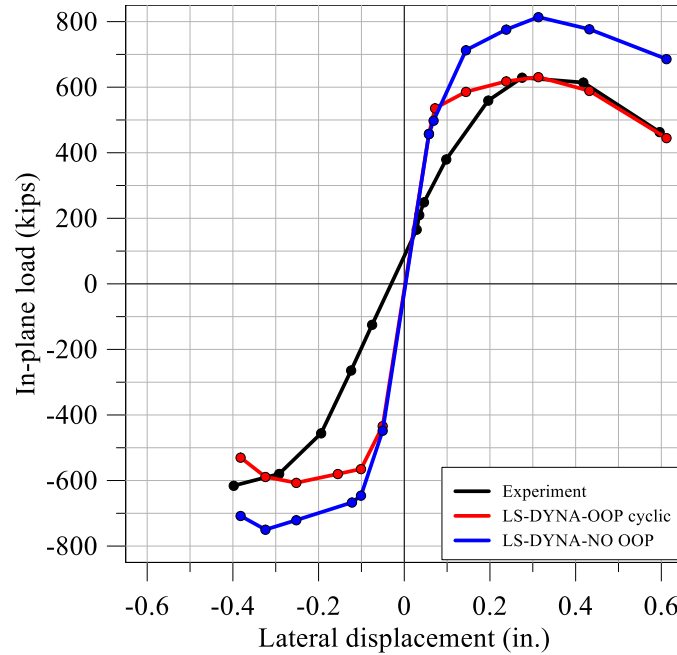
Figure 3-32: Backbone curves, CNSC2

### 3.3.3 CNSC3 Simulations

The uniaxial concrete compressive strength on the day of testing was 5300 psi. The specimen was initially subjected to five cycles of OOP loading, at magnitudes of 50, 100, 150, 200, and 250 kips, respectively, before IP cyclic loading was imposed. The loading protocol used for the experiment and the simulation consisted of seven load steps with two fully reversed cycles per load step and a maximum drift of 0.56%: see Table 2-14.

The OOP force-displacement relationship for the experiment and numerical model are presented in Figure 3-33. Similar to the simulations of CNSC1 and CNSC2, the numerical model is slightly stiffer for OOP loading than that measured in the experiment. The distributions of vertical stress on the West faceplate (see Figure 3-11) at OOP loads of 50, 150, 200, and 250 kips are presented in Figure 3-34a, Figure 3-34b, Figure 3-34c, and Figure 3-34d, respectively; the data from the cycle with an applied OOP load of 100 kips was lost. The location of points P1 through P5 on the tension faceplate are those described in Sections 3.3.1 and 3.3.2, for CNSC1 and CNSC2, respectively; the strain gage data at point P5 was not reliable and not plotted. The predicted and measured vertical stresses on the tension faceplate are in good agreement.

The distributions of axial stress in the tie bars at the instant before application of IP loading is shown in Figure 3-35; the stresses are shown in units of psi. The magnitude of applied load is 250 kips. The maximum axial stress is approximately 32 ksi, occurring in the bottom row of tie bars near the connection to the faceplate: smaller than the yield stress.
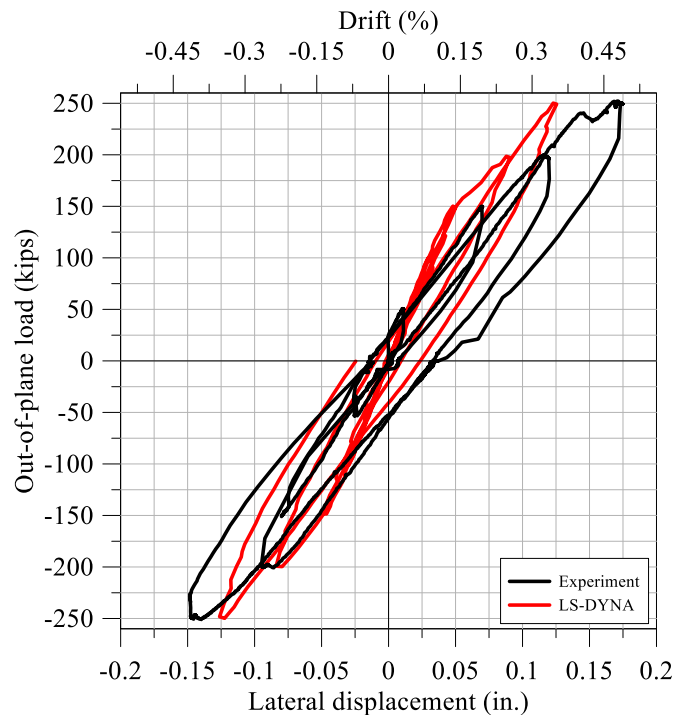


Figure 3-33: OOP force-displacement relationship, LS-DYNA and experiment, CNSC3

The simulated and measured IP force-displacement relationships for CNSC3 are presented in Figure 3-36; the numerical model over predicted the peak IP capacity by 12% and did not predict the loss of IP capacity observed in the experiment. In the experiment, failure of CNSC3 was triggered by significant buckling of the steel faceplate at the Northeast corner of the wall and spalling of the infill concrete. The damage to the infill concrete was not predicted using the Winfrith concrete model, which assumes elastic-perfectly plastic behavior in compression. The numerical model predicted buckling of the East steel faceplate and concrete cracking on the North and South faces (seen in Figure 3-37). The Winfrith model enabled the development of large compressive strains in the infill concrete, but not damage in the form of spalling, for which erosion strains (a numerical workaround) would have to be specified. A new material model would be needed to capture this loss of strength at large compressive strains.
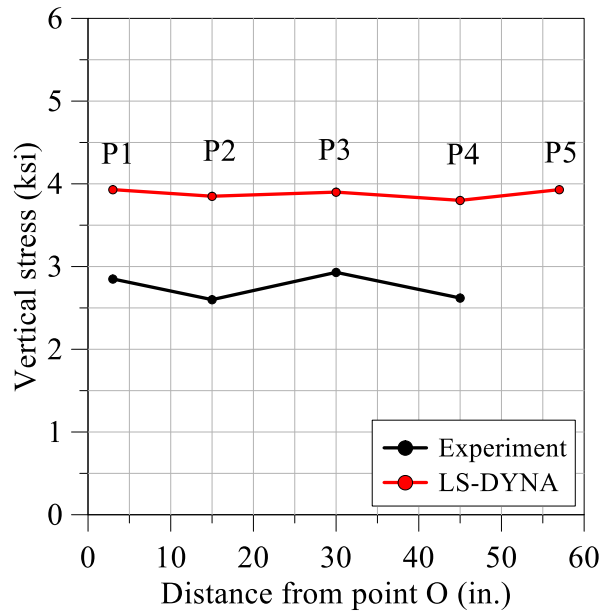
(a) OOP load = 50 kips
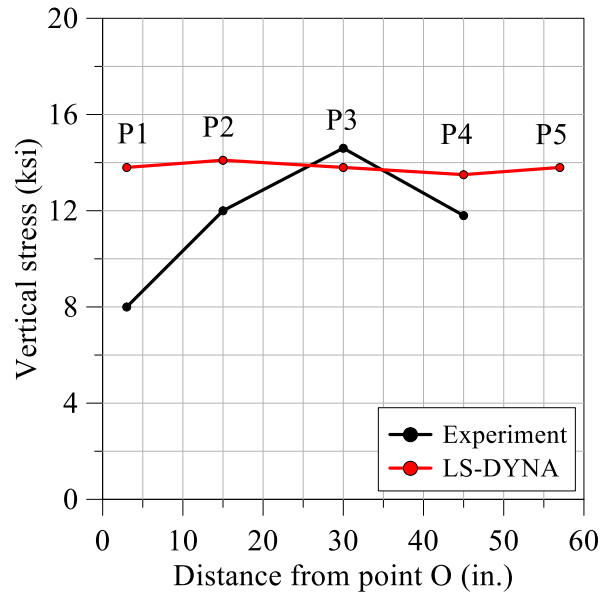
(b) OOP load = 150 kips
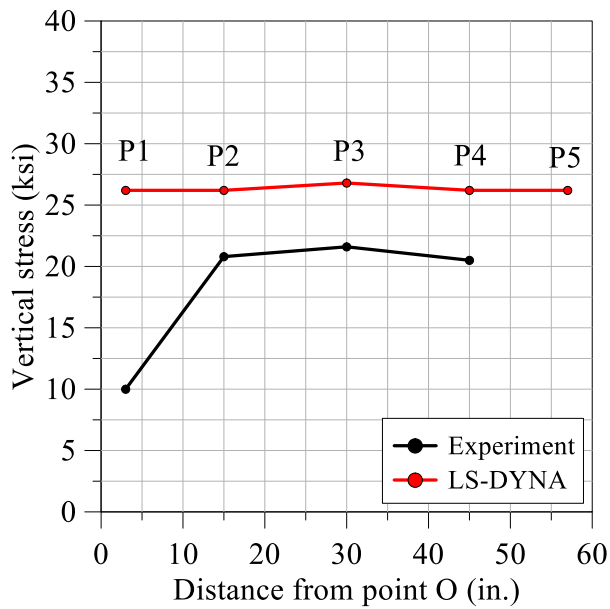
(c) OOP load = 200 kips
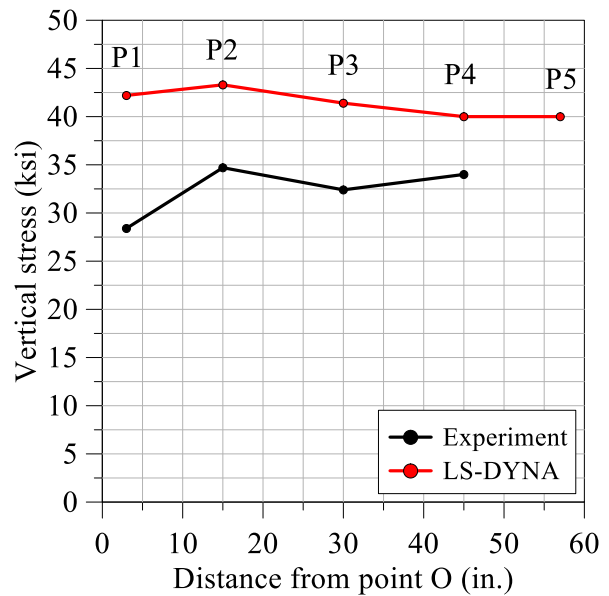
(d) OOP load = 250 kips

Figure 3-34: Distributions of vertical stress in the tension plate, CNSC3
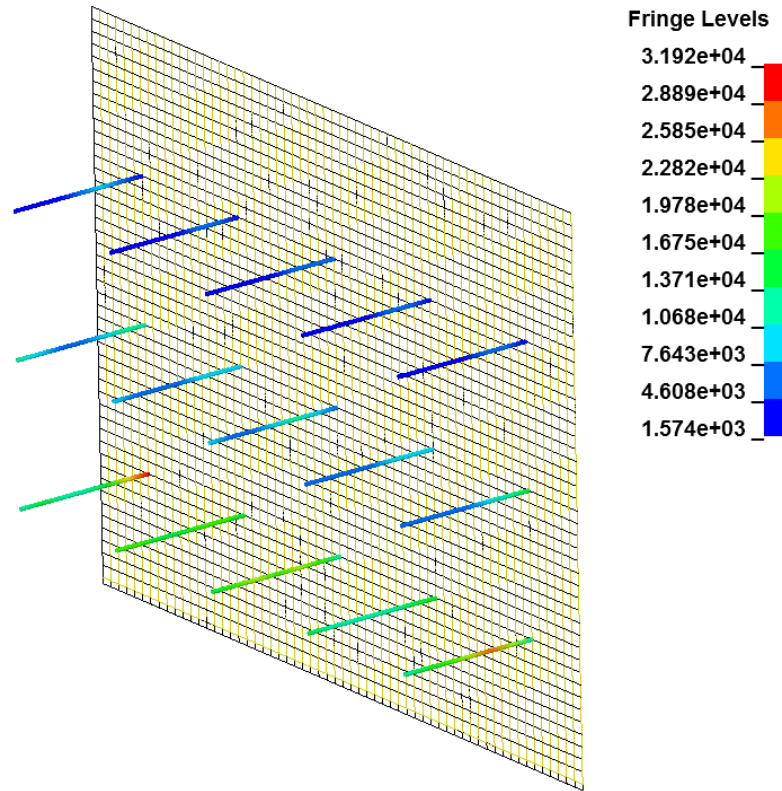
Figure 3-35: Distributions of axial stress in tie bars at instant before IP cyclic loading, CNSC3 (units of psi)
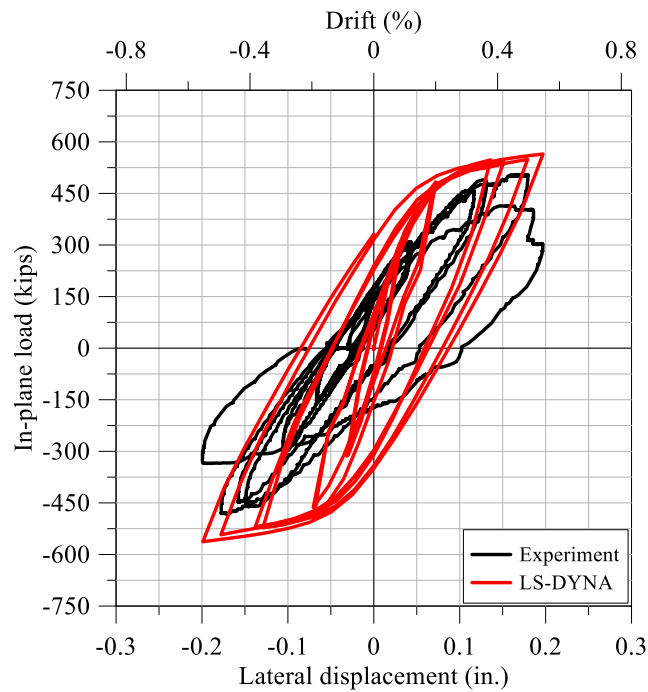


Figure 3-36: IP force-displacement relationship, LS-DYNA and experiment, CNSC3
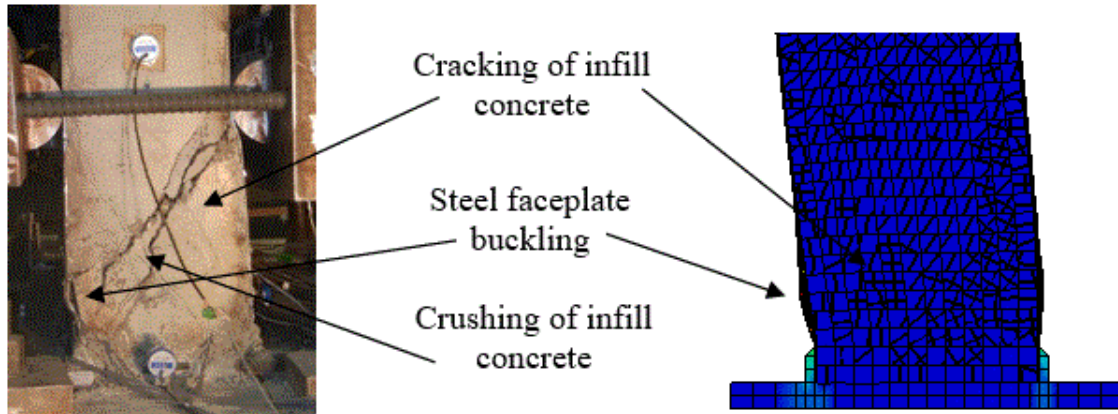
Figure 3-37: Observed and predicted damage to CNSC3

The equivalent viscous damping ratios, $EVD$, for the experiment and the numerical simulation are presented in Figure 3-38; the predicted values of damping are greater than those back-calculated from the experimental data because the energy dissipated per loop are greater. The IP force-displacement relationships for cycles 6 and 7, which correspond to drift ratios of 0.39% and 0.51%, are presented in Figure 3-39a and Figure 3-39b, respectively.

The predicted and measured equivalent viscous damping ratios are in relatively good agreement at a drift ratio of 0.56% (seen in Figure 3-38). The measured and predicted IP force-displacement relationships for cycle 8, corresponding to a drift ratio of 0.56%, are presented in Figure 3-40. The damping ratios are similar because the energy dissipated per cycle and strain energy are both proportionally greater in the experiment.
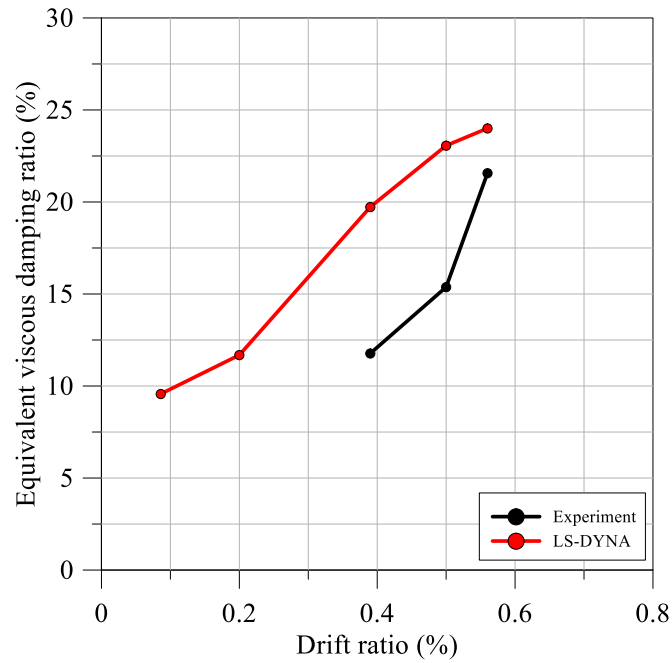
Figure 3-38: Equivalent viscous damping ratio, LS-DYNA and experiment, CNSC3



(a) Cycle 6, drift ratio = 0.39%

(b) Cycle 7, drift ratio = 0.51%
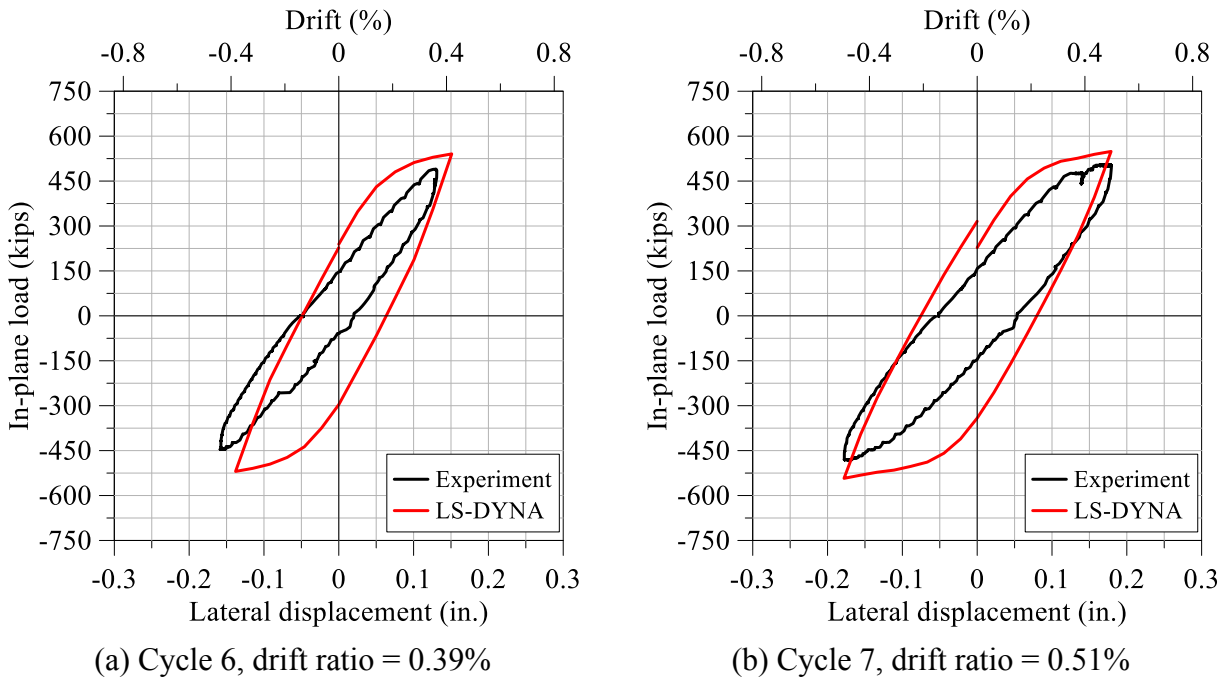
Figure 3-39: Selected IP force-displacement relationships, LS-DYNA and experiment, CNSC3
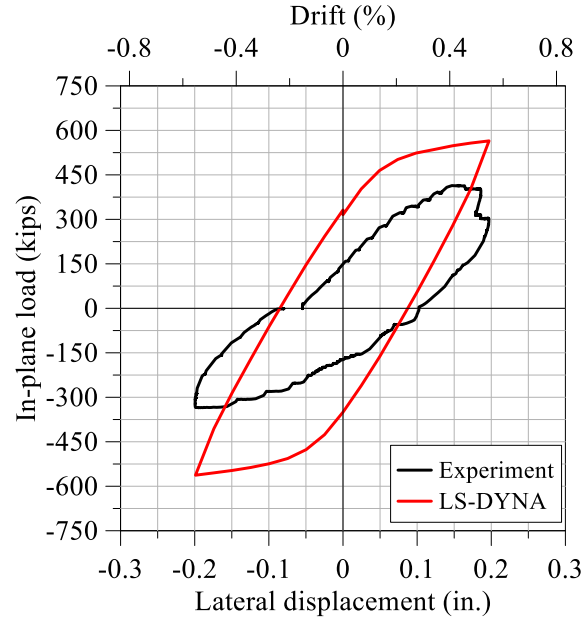
Figure 3-40: IP force-displacement relationship, cycle 8, drift ratio = 0.56%, LS-DYNA and experiment, CNSC3

Figure 3-41a and Figure 3-41b show the LS-DYNA-predicted IP cyclic force-displacement relationship of the infill concrete and steel faceplates, respectively. The predicted IP force-displacement relationship of the pier is shown in grey to highlight the contribution of the infill concrete and steel faceplates to the total IP shear resistance. Pinching of the hysteresis loops for the concrete and the steel faceplates in the simulations is minimal. The LS-DYNA-predicted OOP cyclic force history is presented in Figure 3-42; the infill concrete dominated the OOP behavior of the SC walls, as expected.

Figure 3-43 shows the IP force-displacement relationship for the experiment, and the LS-DYNA simulations with and without the applied OOP load. The corresponding backbone curves are presented in Figure 3-44. The application of OOP load reduces the IP capacity of the numerical model by 22%.
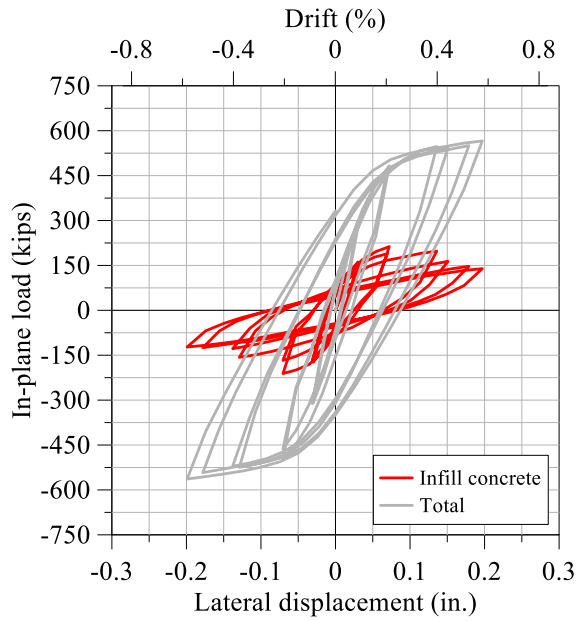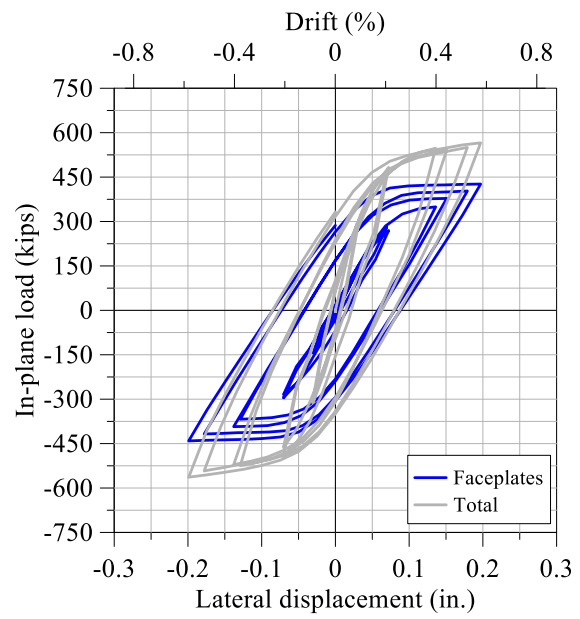
(a) Infill concrete            (b) Steel faceplates

Figure 3-41: LS-DYNA-predicted IP cyclic force-displacement relationships, CNSC3
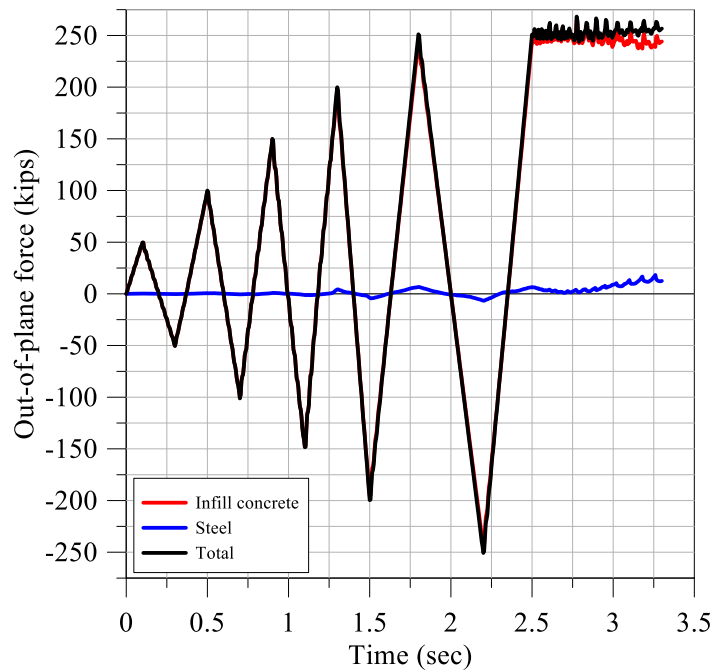


Figure 3-42: LS-DYNA-predicted components of the OOP cyclic force history, CNSC3
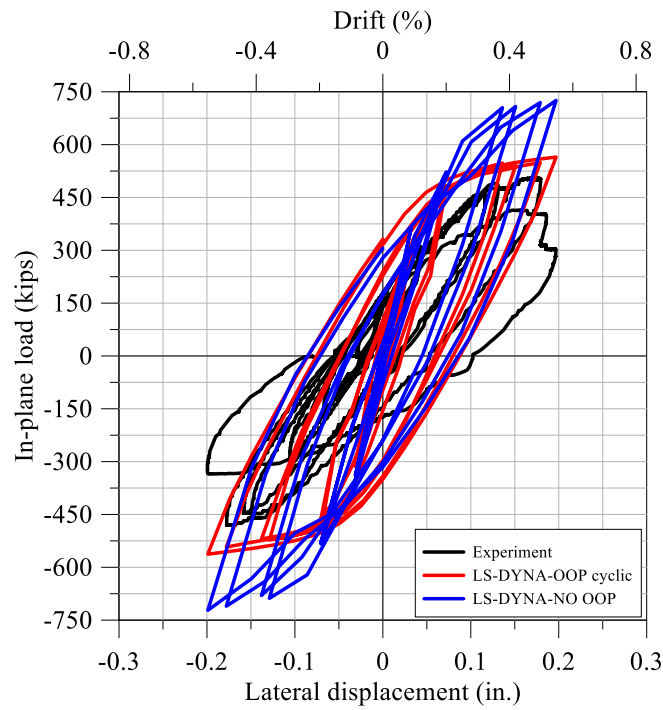
Figure 3-43: IP force displacement relationships, CNSC3
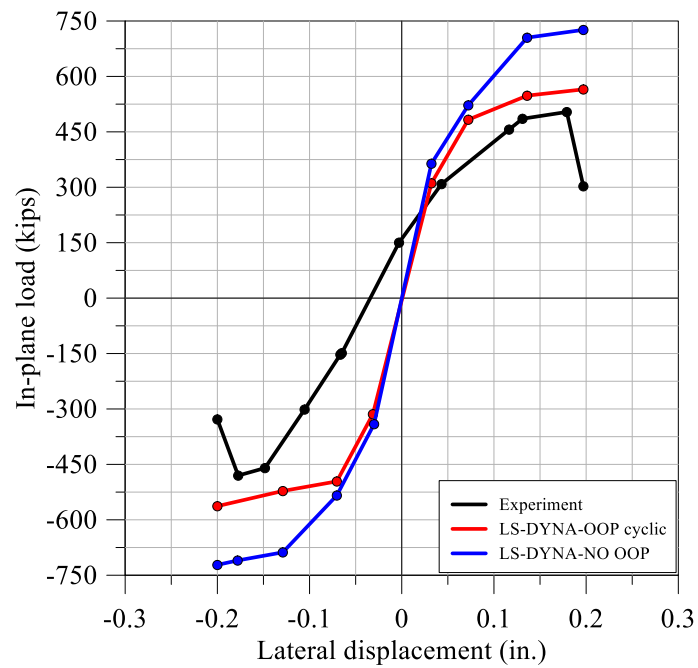


Figure 3-44: Backbone curves, CNSC3

### 3.3.4  Summary and Conclusions

The physical tests of CNSC1, CNSC2, and CNSC3 described in Section 2 were simulated using the general-purpose finite element program LS-DYNA. Numerical models developed by Epackachi et al. (2014b; 2015) that were validated for the prediction of the IP response of SC wall piers were utilized as a starting point for this study. Predictions of the numerical models were compared with the measurements from experiments at both global and local levels, including cyclic force-displacement relationships (in-plane and out-of-plane), equivalent viscous damping ratios, vertical stresses in the steel faceplates induced by OOP load, and observed damage (e.g., cracking of the infill concrete and buckling of steel faceplates).

The numerical predictions for CNSC1 and CNSC2 agreed reasonably well with measurements from the experiments. The predicted IP stiffness of CNSC1 and CNSC2 were both significantly greater than those observed in the experiment because the foundation (and its flexibility) was not considered in the numerical models; the predicted values of OOP stiffness agreed reasonably well with those measured in the experiments. The predicted distributions of vertical stress on the tension faceplate (under OOP loading) at different levels of OOP load were similar to those measured in the experiments. The predictions of peak IP shear resistance, post-peak strength reduction, and rate of reloading/unloading stiffness for peak and post-peak IP strength cycles agreed reasonably well with the experimental results, with the best results for CNSC1, for which the OOP loading (and average shear stress) were the smallest of the three tests. The predicted values of *EVD* for IP response were greater than those calculated from the experimental data because the numerically predicted hysteresis loops were wider (more energy dissipated per cycle). The damage predicted using the numerical models (i.e., cracking of infill concrete and buckling of steel faceplates) was in good agreement with that observed in the experiments. Crushing and spalling of concrete, indicated by large compressive strains in the numerical models, could not be captured explicitly because the Winfrith model assumes elastic-perfectly-plastic behavior in compression. Erosion, as a numerical workaround was not implemented. Load distribution between the steel faceplates and the infill concrete in the IP and OOP directions was also investigated using the numerical model; the steel faceplates and the infill concrete dominate the behavior of the SC wall in the IP and OOP directions, respectively.

The predicted response of CNSC3 overestimated the measured peak strength by approximately 12%. The numerical model did not recover the loss of post-peak strength and stiffness calculated from the experimental data, which was likely due to the inability of the Winfrith model, in the absence of a calibrated erosion strain, to simulate loss of material. Under IP loading, the steel faceplates dictate seismic performance. Under OOP loading, the infill concrete dictates seismic response. Because the Winfrith model is unable to directly address loss of material, physical damage to the concrete under OOP loading (e.g., spalling), which should affect the IP behavior, including loss of strength and stiffness, cannot be captured directly.

This limitation of the numerical model will be accommodated in the parametric study presented in Section 4 by investigating the IP behavior of SC wall piers subjected to OOP shear stresses less than a threshold limit taken equal to the shear strength of concrete per ACI 318-14 (ACI, 2014). If the applied OOP shear stress exceeds the shear strength of the concrete and a sufficient number of tie bars are not available to mitigate crack growth, the IP response predicted using LS-DYNA will not be reliable. Concrete erosion could be used as a numerical workaround, but the chosen value of erosion strain requires calibration for which the authors have no data bar that for CNSC3. An updated numerical model may be able to address this issue but the development of such a model is far beyond the scope of this project.

The parametric study presented in Section 4 will be used to develop a relationship between the level of applied OOP shear stress and the IP capacity of SC wall piers. The results of the parametric study, combined with the results of the CNSC experiments, are used to provide technical guidance on the analysis and design of SC wall piers subjected to combined IP and OOP loading.

# 4. DEVELOPING DESIGN GUIDANCE THROUGH PARAMETRIC STUDIES

## 4.1 Introduction

A parametric study was conducted using the numerical model of Section 3 to investigate the effect of OOP loading (magnitude and location) on the IP response of SC wall piers with different concrete compressive strength and tie bar spacing. Section 4.2 presents the parametric study and key results. Technical guidance for design of SC walls subjected to combined IP and OOP loading is presented in Section 4.3, and is based on the experiments of Section 2, the numerical simulations of Section 3, and the parametric study of Section 4.2.

## 4.2 Parametric Study

The simulations conducted in this parametric study are summarized in Table 4-1, where $f_c'$ is the compressive strength, $s$ is the tie bar spacing, $d$ is the depth of the cross section (=12 inches), and $a/d$ is the ratio of shear span to depth. Two values of compressive strength were considered in this study: 3500 and 5000 psi. Three values of $a/d$ were considered for each value of compressive strength: 0.5, 1.5, and 3. The ratio $a/d$ equal to 1.5 and 3 correspond to loading at the middle and top of the wall, respectively. For each value of $a/d$, three amplitudes of OOP shear stress were considered: $1\sqrt{f_c'}$, $2\sqrt{f_c'}$, and $3\sqrt{f_c'}$. All of these simulations were performed for two values of tie bar spacing: $d$ and $d/2$.

Given the limitations of the Winfrith model described in Section 3.3.4, the SC wall piers in this parametric study were subjected to OOP shear stresses less than the expected shear strength of plain concrete, which is strongly dependent on the ratio of shear span-to-depth of the loaded member. Per Figure 6-13 in Wight (2015), the shear stress (strength) of concrete with a longitudinal reinforcement ratio of 1.5% (assuming one steel faceplate acts as longitudinal reinforcement when the wall is subjected to an OOP bending moment), in the absence of shear reinforcement, is between $2\sqrt{f_c'}$ and $3\sqrt{f_c'}$. (The data in this figure are from tests of shallow beams with $a/d$ generally greater than or equal to 2.0. This range on maximum shear stress is for shallow (relatively thin) specimens, namely, 12 inches and smaller, and the design guidance presented later addresses the issue of wall thickness. Importantly, $a/d$ for the specimens tested as part of this research project was 1.5, for which a greater shear stress at failure is expected.) The lower end on this range of OOP shear stress, $2\sqrt{f_c'}$, is associated with good predictions of

IP response using LS-DYNA: the CNSC1 simulations in Section 3.3.1 for which the maximum OOP shear stress was $1.96\sqrt{f_c'}$. For CNSC2 (CNSC3), inclined cracking was observed at an OOP load corresponding to a shear stress of $4.33\sqrt{f_c'}$ ($4.92\sqrt{f_c'}$). The predictions of the cyclic IP response of CNSC2 and CNSC3 using LS-DYNA were reasonable but much poorer than for CNSC1. Accordingly, on the basis of these observations, the maximum shear stress associated with OOP loading was limited to $3\sqrt{f_c'}$ for the parametric studies in order to have confidence in the numerical predictions.

Figure 4-1a, Figure 4-2a and Figure 4-3a present the cyclic IP force-displacement relationships of SC walls subjected to OOP loads associated with shear stresses of $1\sqrt{f_c'}$, $2\sqrt{f_c'}$, and $3\sqrt{f_c'}$ with a tie bar spacing of $d$, for $a/d$ equal to 0.5, 1.5, and 3, respectively. The corresponding backbone curves for these simulations are presented in Figure 4-1b, Figure 4-2b and Figure 4-3b, respectively. The walls have a concrete compressive strength of 3500 psi and a tie bar spacing of 12 inches. The peak IP lateral loads of these nine SC walls are presented in Table 4-1: simulations 2 to 10. The peak lateral capacity of SC walls subjected to an OOP shear stress of $1\sqrt{f_c'}$, $2\sqrt{f_c'}$, and $3\sqrt{f_c'}$ for $a/d$ equal to 0.5 (1.5) [3] reduced by 1 (2) [4]%, 5 (8) [16]%, and 11 (17) [29]%, respectively, from the IP strength with no applied OOP shear stress (=729 kips). The results of the simulations show that the magnitude and location of the OOP load have a significant effect on the IP capacity of the SC walls. The reductions in IP strength become more evident as the magnitude of the OOP load and the height of its application above the foundation are increased, which leads to larger bending moments and higher longitudinal stresses in the faceplates. Since the IP behavior of the SC walls is governed by the steel faceplates, additional stresses induced by the OOP load, of the amplitude considered here, reduce the IP capacity of the wall pier. The OOP load, of the amplitude considered here, does not have a significant effect on the initial stiffness, pinching, and rate of reloading/unloading of SC walls, as observed in Figure 4-1a, Figure 4-2a and Figure 4-3a.

Table 4-1: Summary of LS-DYNA simulations

| Simulation | $f_c'$ (psi) | Tie bar spacing, $s$ (in.) | $a/d$ | OOP Load | OOP load (kips) | IP capacity (kips) | % reduction in IP capacity |
|---|---|---|---|---|---|---|---|
| 1 | 3500 | $d$ | - | 0 | - | 729 | - |
| 2 | 3500 | $d$ | 0.5 | $1\sqrt{f_c'}$ | 43 | 720 | 1 |
| 3 | 3500 | $d$ | 0.5 | $2\sqrt{f_c'}$ | 85 | 690 | 5 |
| 4 | 3500 | $d$ | 0.5 | $3\sqrt{f_c'}$ | 128 | 651 | 11 |
| 5 | 3500 | $d$ | 1.5 | $1\sqrt{f_c'}$ | 43 | 712 | 2 |
| 6 | 3500 | $d$ | 1.5 | $2\sqrt{f_c'}$ | 85 | 671 | 8 |
| 7 | 3500 | $d$ | 1.5 | $3\sqrt{f_c'}$ | 128 | 607 | 17 |
| 8 | 3500 | $d$ | 3 | $1\sqrt{f_c'}$ | 43 | 698 | 4 |
| 9 | 3500 | $d$ | 3 | $2\sqrt{f_c'}$ | 85 | 613 | 16 |
| 10 | 3500 | $d$ | 3 | $3\sqrt{f_c'}$ | 128 | 520 | 29 |
| 11 | 3500 | $d/2$ | - | 0 | - | 759 | - |
| 12 | 3500 | $d/2$ | 0.5 | $1\sqrt{f_c'}$ | 43 | 751 | 1 |
| 13 | 3500 | $d/2$ | 0.5 | $2\sqrt{f_c'}$ | 85 | 741 | 3 |
| 14 | 3500 | $d/2$ | 0.5 | $3\sqrt{f_c'}$ | 128 | 721 | 5 |
| 15 | 3500 | $d/2$ | 1.5 | $1\sqrt{f_c'}$ | 43 | 745 | 2 |
| 16 | 3500 | $d/2$ | 1.5 | $2\sqrt{f_c'}$ | 85 | 695 | 8 |
| 17 | 3500 | $d/2$ | 1.5 | $3\sqrt{f_c'}$ | 128 | 645 | 15 |
| 18 | 3500 | $d/2$ | 3 | $1\sqrt{f_c'}$ | 43 | 724 | 5 |
| 19 | 3500 | $d/2$ | 3 | $2\sqrt{f_c'}$ | 85 | 646 | 15 |
| 20 | 3500 | $d/2$ | 3 | $3\sqrt{f_c'}$ | 128 | 583 | 23 |
| 21 | 5000 | $d$ | - | 0 | - | 765 | - |
| 22 | 5000 | $d$ | 0.5 | $1\sqrt{f_c'}$ | 51 | 753 | 2 |
| 23 | 5000 | $d$ | 0.5 | $2\sqrt{f_c'}$ | 102 | 723 | 6 |
| 24 | 5000 | $d$ | 0.5 | $3\sqrt{f_c'}$ | 153 | 709 | 7 |
| 25 | 5000 | $d$ | 1.5 | $1\sqrt{f_c'}$ | 51 | 742 | 3 |
| 26 | 5000 | $d$ | 1.5 | $2\sqrt{f_c'}$ | 102 | 704 | 8 |
| 27 | 5000 | $d$ | 1.5 | $3\sqrt{f_c'}$ | 153 | 637 | 17 |

| 28 | 5000 | $d$ | 3 | $1\sqrt{f'_c}$ | 51 | 729 | 5 |
|----|------|-----|---|-----|-----|-----|-----|
| 29 | 5000 | $d$ | 3 | $2\sqrt{f'_c}$ | 102 | 649 | 15 |
| 30 | 5000 | $d$ | 3 | $3\sqrt{f'_c}$ | 153 | 577 | 25 |
| 31 | 5000 | $d/2$ | - | 0 | - | 793 | - |
| 32 | 5000 | $d/2$ | 0.5 | $1\sqrt{f'_c}$ | 51 | 789 | 0.5 |
| 33 | 5000 | $d/2$ | 0.5 | $2\sqrt{f'_c}$ | 102 | 770 | 3 |
| 34 | 5000 | $d/2$ | 0.5 | $3\sqrt{f'_c}$ | 153 | 763 | 4 |
| 35 | 5000 | $d/2$ | 1.5 | $1\sqrt{f'_c}$ | 51 | 785 | 1 |
| 36 | 5000 | $d/2$ | 1.5 | $2\sqrt{f'_c}$ | 102 | 744 | 6 |
| 37 | 5000 | $d/2$ | 1.5 | $3\sqrt{f'_c}$ | 153 | 697 | 12 |
| 38 | 5000 | $d/2$ | 3 | $1\sqrt{f'_c}$ | 51 | 763 | 4 |
| 39 | 5000 | $d/2$ | 3 | $2\sqrt{f'_c}$ | 102 | 700 | 12 |
| 40 | 5000 | $d/2$ | 3 | $3\sqrt{f'_c}$ | 153 | 637 | 20 |

To investigate the effect of OOP loading on the IP lateral capacity of SC walls with tie bar spacing smaller than $d$, the LS-DYNA models used in simulations 2 to 10 were revised with a tie bar spacing of $d/2$ (=6 inches). The IP force-displacement relationships for OOP shear stresses of $1\sqrt{f'_c}$, $2\sqrt{f'_c}$, and $3\sqrt{f'_c}$ for $a/d$ equal to 0.5, 1.5, and 3 are presented in Figure 4-4a, Figure 4-5a, and Figure 4-6a, respectively: the peak IP strengths are presented in Table 4-1 through simulations 12 to 20. The corresponding backbone curves for these simulations are shown in Figure 4-4b, Figure 4-5b, and Figure 4-6b, respectively. The IP capacity is reduced by 23% for an OOP shear stress of $3\sqrt{f'_c}$ and $a/d$ of 3 with respect to the IP strength with no OOP load (=759 kips); the reduction in IP capacity is slightly less than that observed for a tie bar spacing of $d$ and an OOP shear stress of $3\sqrt{f'_c}$ and $a/d$ of 3 (=29 %) (simulation 10).
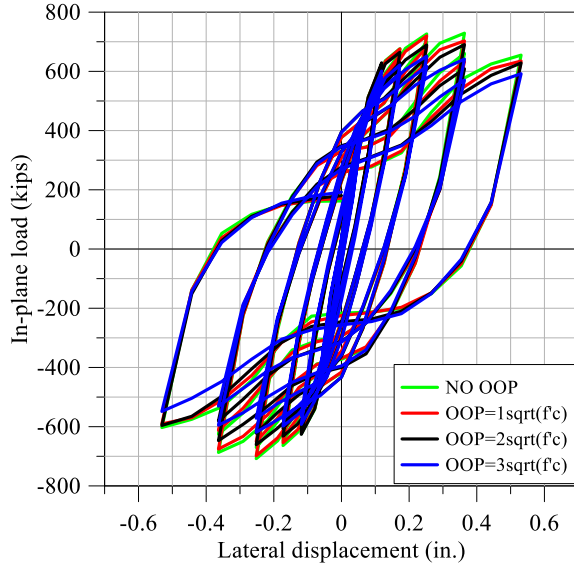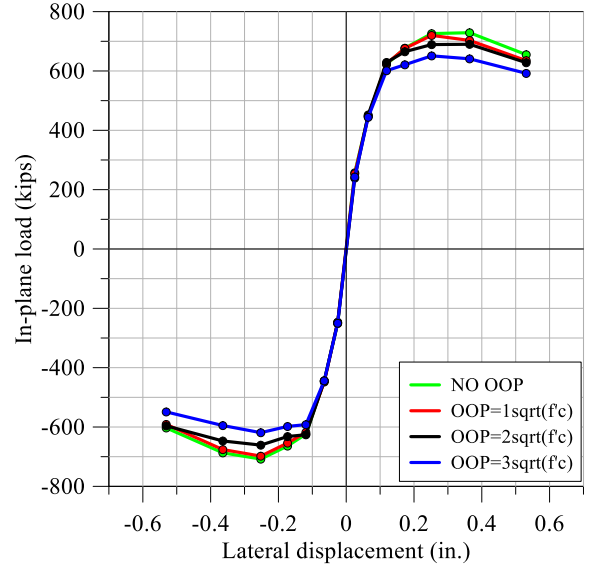
(a) IP force-displacement relationship　　　　(b) Backbone curves

Figure 4-1: IP behavior of SC walls, $a/d = 0.5$, $f'_c = 3,500$ psi, $s = d$



(a) IP force-displacement relationship　　　　(b) Backbone curves

Figure 4-2: IP behavior of SC walls, $a/d = 1.5$, $f'_c = 3,500$ psi, $s = d$

(a) IP force-displacement relationship

(b) Backbone curves

Figure 4-3: IP behavior of SC walls, $a/d = 3$, $f'_c = 3,500$ psi, $s = d$
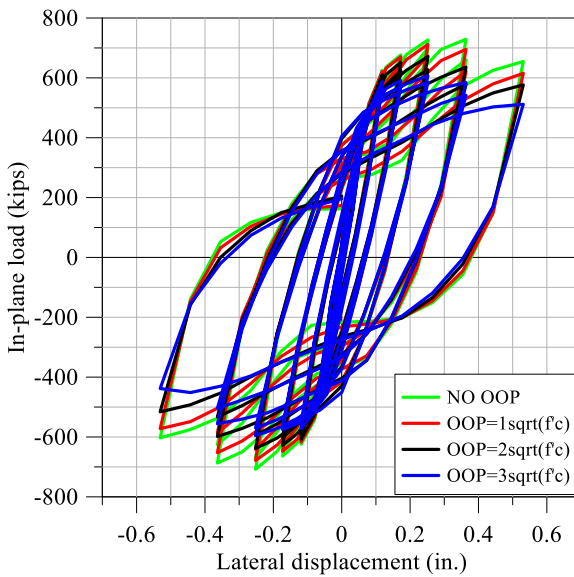


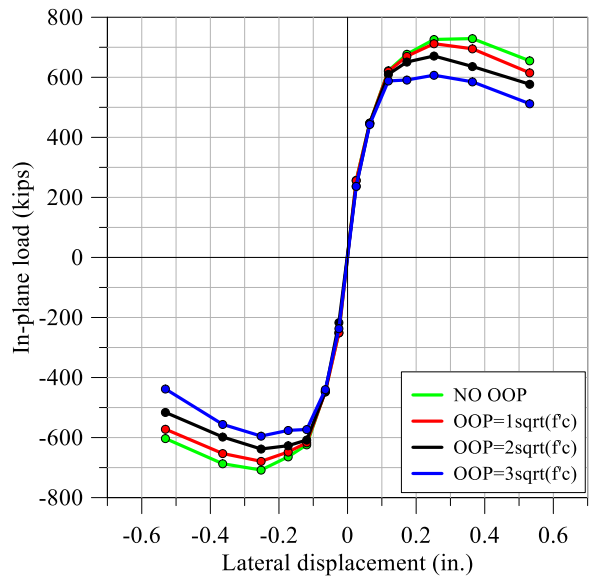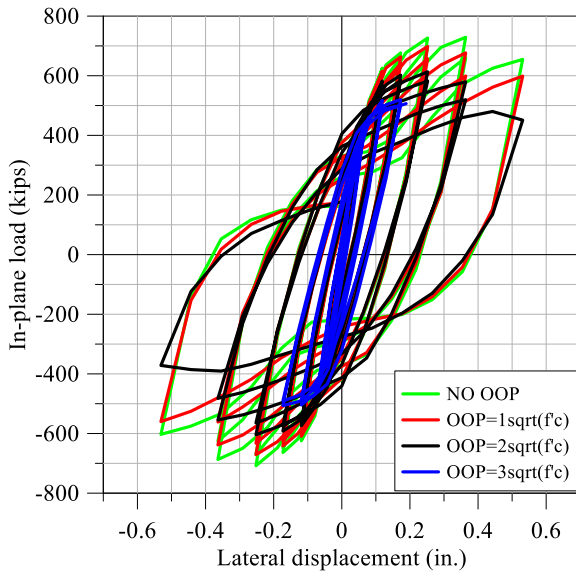(a) IP force-displacement relationship

(b) Backbone curves

Figure 4-4: IP behavior of SC walls, $a/d = 0.5$, $f'_c = 3,500$ psi, $s = d/2$
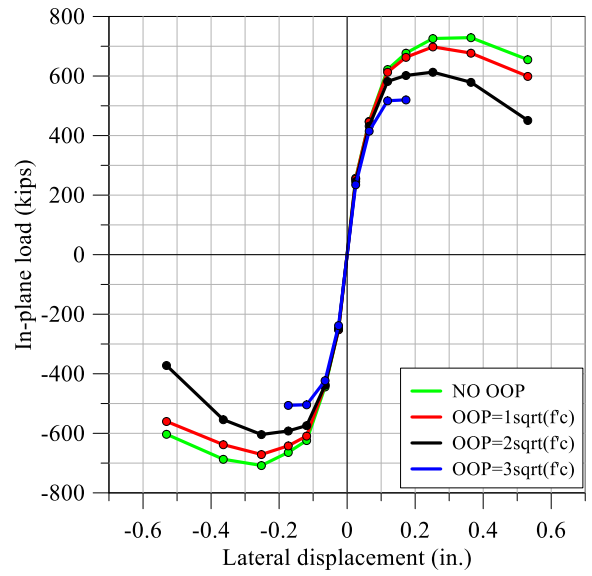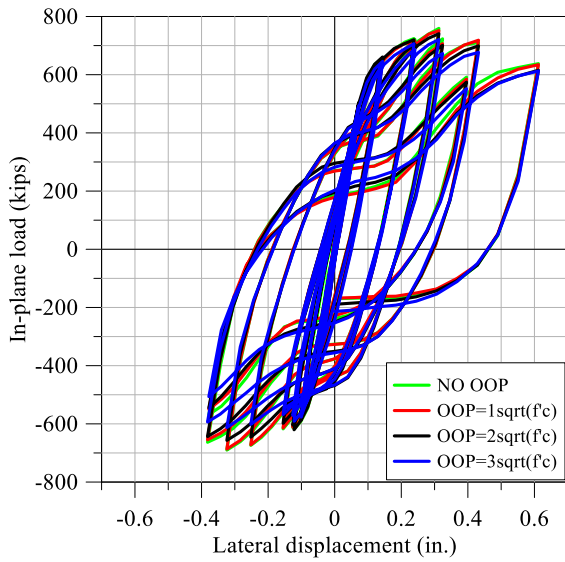
(a) IP force-displacement relationship    (b) Backbone curves

Figure 4-5: IP behavior of SC walls, $a/d = 1.5$, $f_c' = 3{,}500\,\text{psi}$, $s = d/2$



(a) IP force-displacement relationship    (b) Backbone curves

Figure 4-6: IP behavior of SC walls, $a/d = 3$, $f_c' = 3{,}500\,\text{psi}$, $s = d/2$

The LS-DYNA models used in simulations 2 to 10 were repeated with a higher concrete uniaxial compressive strength: 5000 psi. The increase from 3500 psi to 5000 psi increased the IP capacity, in the absence of OOP load, by 5%. The percentage increase in IP strength was expected to be small because the IP behavior is dominated by the steel faceplates.

82

Figure 4-7a, Figure 4-8a, and Figure 4-9a present the cyclic IP force-displacement relationships of SC walls subjected to OOP shear stresses of $1\sqrt{f_c'}$, $2\sqrt{f_c'}$, and $3\sqrt{f_c'}$ for $a/d$ equal to 0.5, 1.5, and 3, respectively. Figure 4-7b, Figure 4-8b, and Figure 4-9b present the corresponding backbone curves for these simulations, respectively, for $a/d$ of 0.5, 1.5, and 3. The peak IP lateral loads of these nine SC walls are presented in Table 4-1 through simulations 22 to 30. The peak lateral capacity of SC walls subjected to an OOP shear stress of $1\sqrt{f_c'}$, $2\sqrt{f_c'}$, and $3\sqrt{f_c'}$ for $a/d$ equal to 0.5 (1.5) [3] reduced by 2 (3) [5]%, 6 (8) [15]%, and 7 (17) [25]%, respectively, from the IP strength with no OOP load (=765 kips). The percentage reductions in IP capacity are similar to those obtained for 3500 psi concrete (simulations 2 to 10).

Simulations 22 to 30 were repeated with a tie bar spacing of $d/2$. The IP force-displacement relationships for OOP shear stresses of $1\sqrt{f_c'}$, $2\sqrt{f_c'}$, and $3\sqrt{f_c'}$ for $a/d$ equal to 0.5, 1.5, and 3 are presented in Figure 4-10a, Figure 4-11a, Figure 4-12a, respectively. Results are summarized in Table 4-1: simulations 31 to 40. The corresponding backbone curves for $a/d$ values of 0.5, 1.5, and 3 are presented in Figure 4-10b, Figure 4-11b, Figure 4-12b, respectively. The IP capacity was reduced by 20% for an OOP shear stress of $3\sqrt{f_c'}$ and $a/d$ of 3 (simulation 40) with respect to the IP strength with no OOP load (=793 kips); the reduction in IP capacity is slightly less than that observed for a tie bar spacing of $d$ and an OOP load of $3\sqrt{f_c'}$ and $a/d$ of 3 (simulation 30). As the magnitude and height of application of the OOP load are increased, the reductions in IP capacity are slightly less for a tie bar spacing of $d/2$ compared to that of a tie bar spacing of $d$; the same trends are observed for concrete compressive strengths of 3500 and 5000 psi.

(a) IP force-displacement relationship  (b) Backbone curves

Figure 4-7: IP behavior of SC walls, $a/d = 0.5$, $f'_c = 5,000$ psi, $s = d$
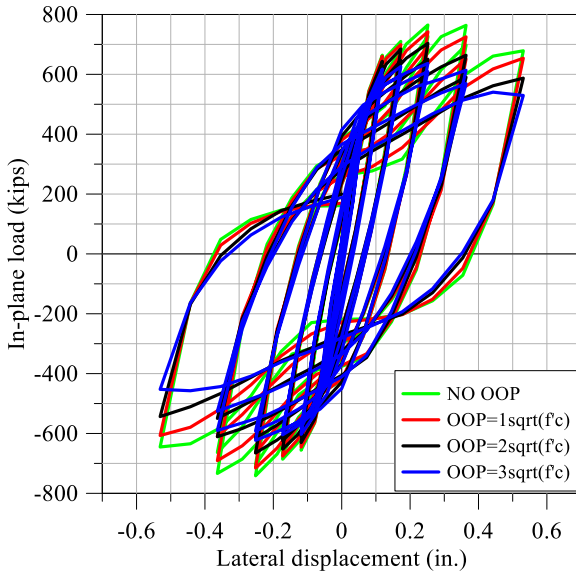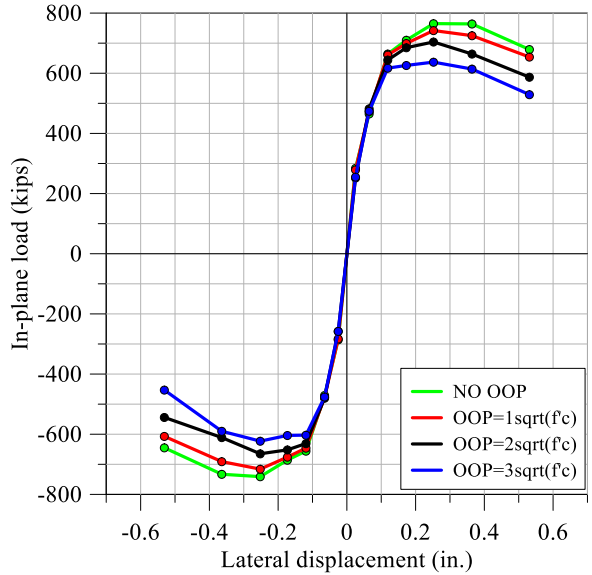


(a) IP force-displacement relationship  (b) Backbone curves

Figure 4-8: IP behavior of SC walls, $a/d = 1.5$, $f'_c = 5,000$ psi, $s = d$
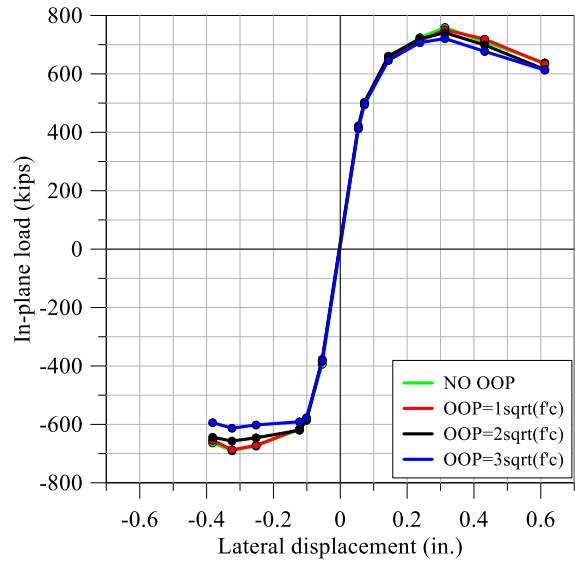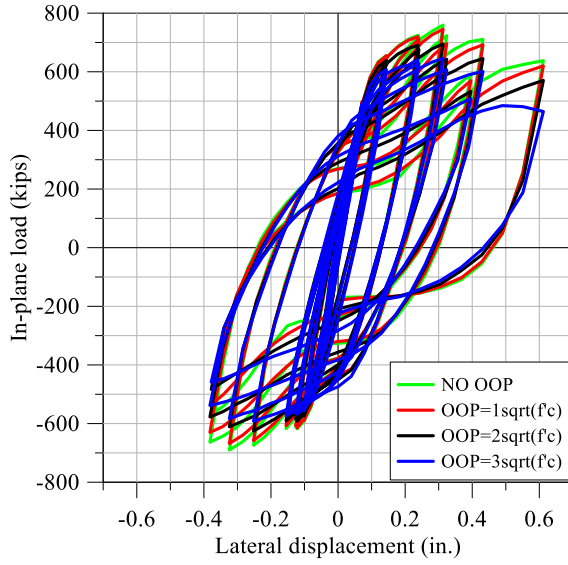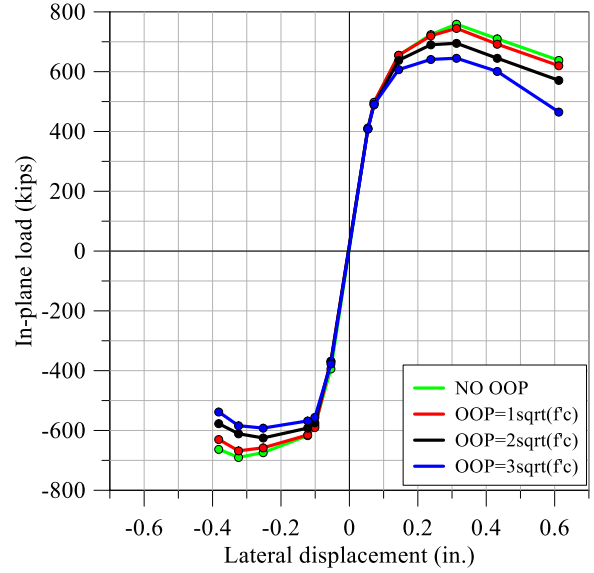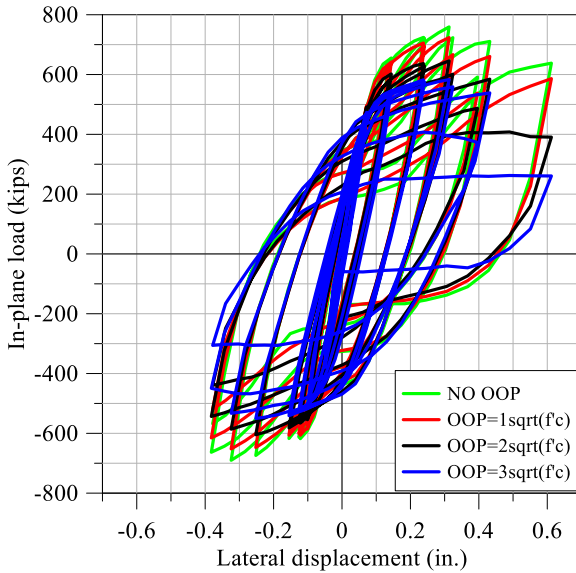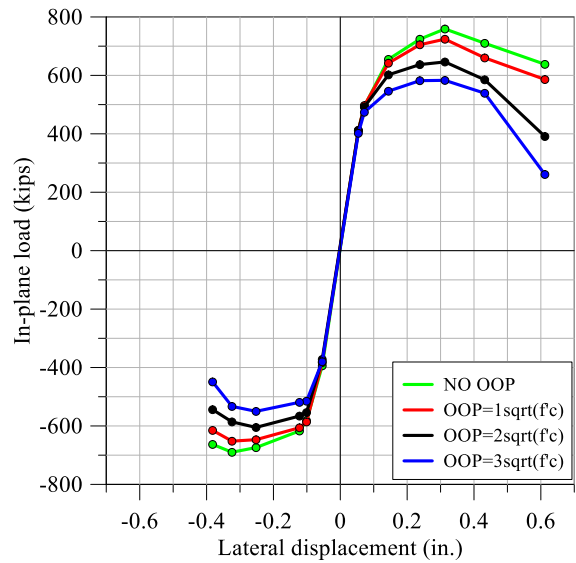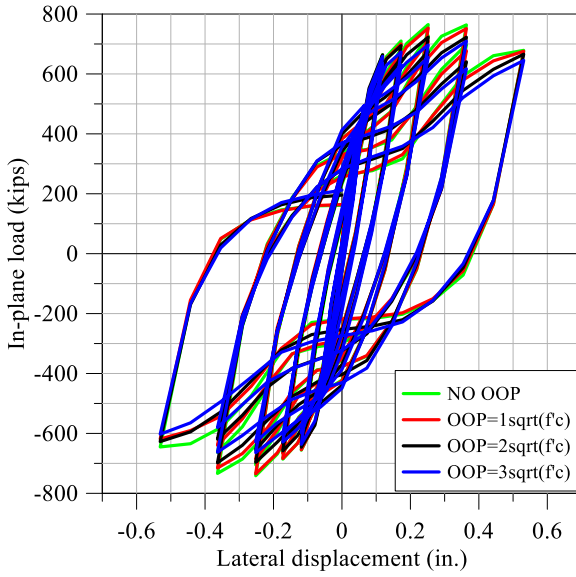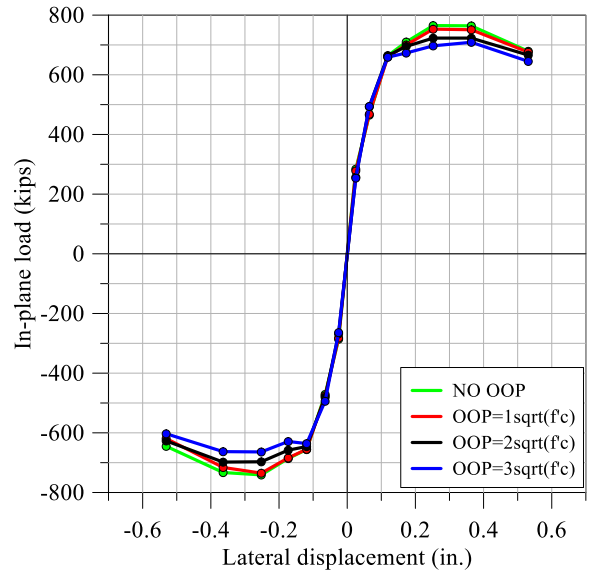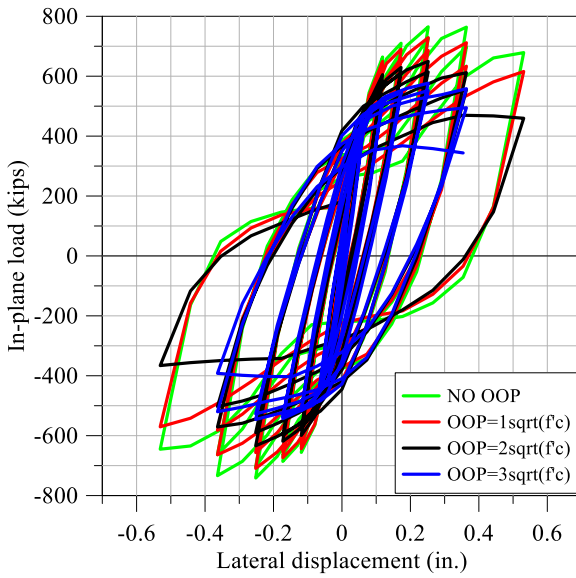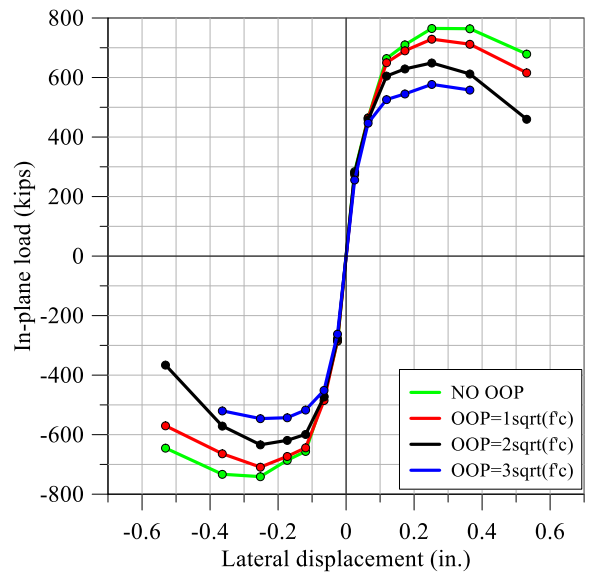
(a) IP force-displacement relationship          (b) Backbone curves

Figure 4-9: IP behavior of SC walls, $a/d=3$, $f'_c=5{,}000$ psi, $s=d$
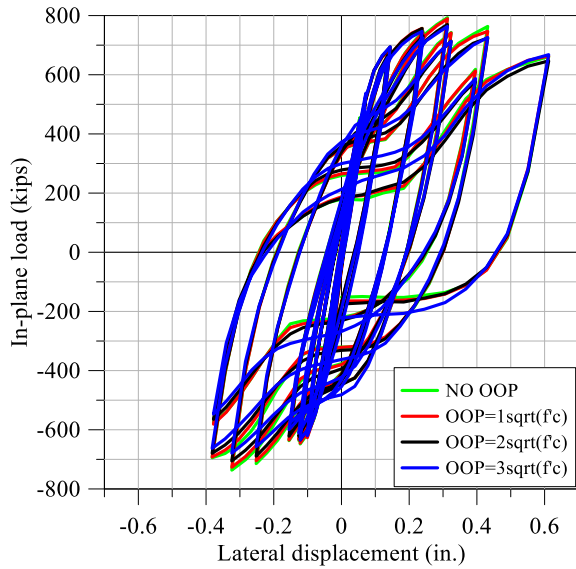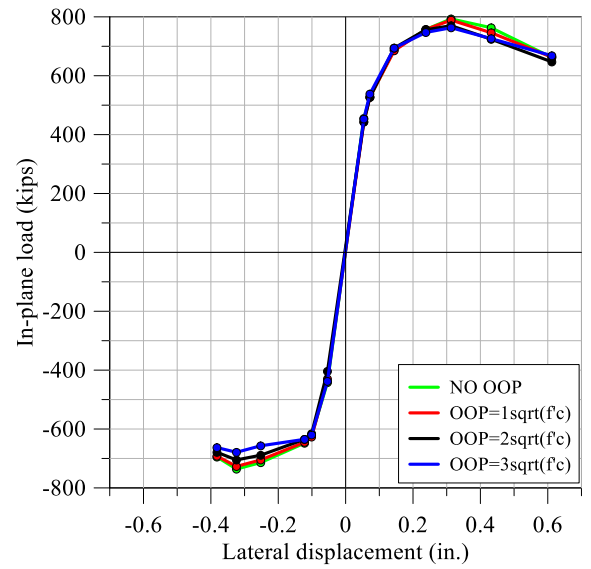


(a) IP force-displacement relationship          (b) Backbone curves

Figure 4-10: IP behavior of SC walls, $a/d=0.5$, $f'_c=5{,}000$ psi, $s=d/2$
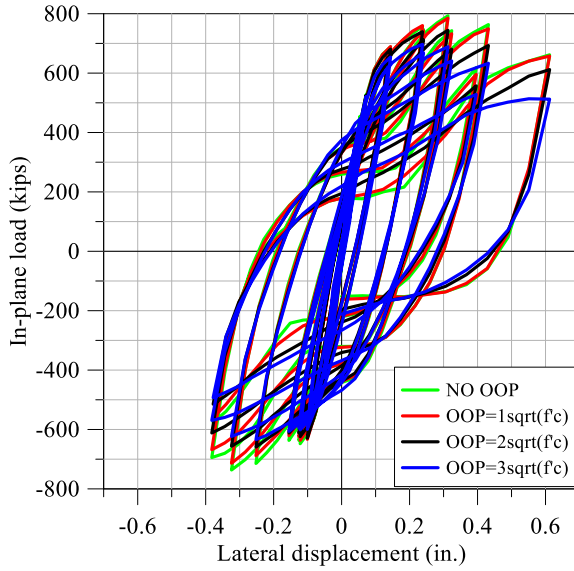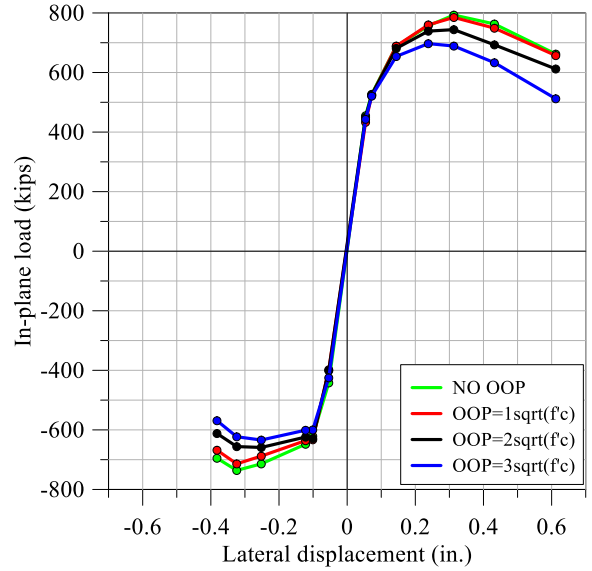
(a) IP force-displacement relationship　　　　(b) Backbone curves

Figure 4-11: IP behavior of SC walls, $a/d = 1.5$, $f_c' = 5,000$ psi, $s = d/2$
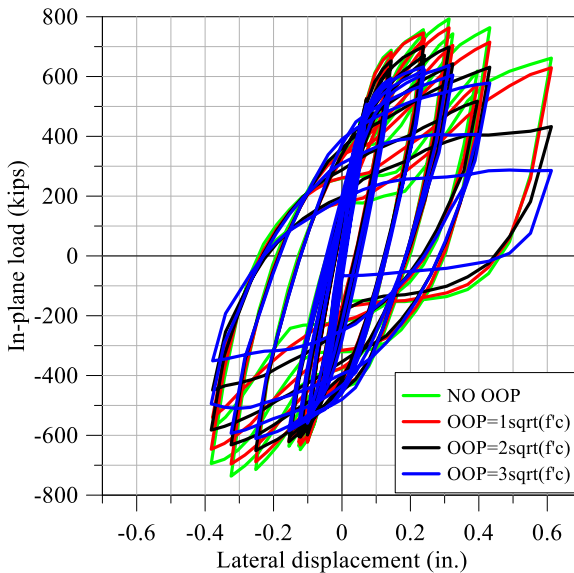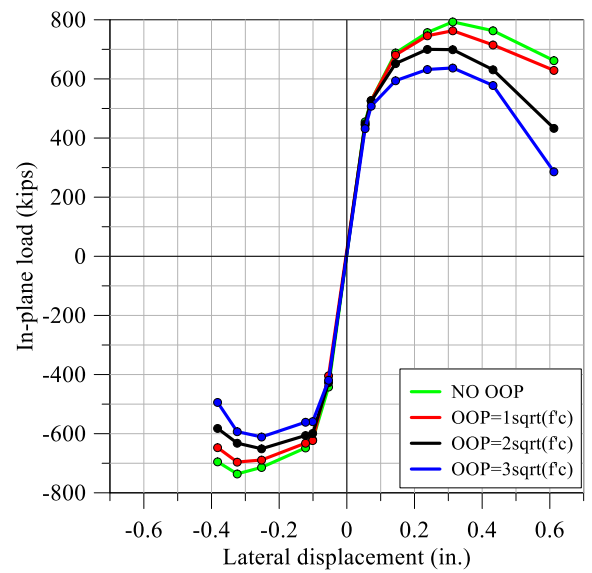


(a) IP force-displacement relationship　　　　(b) Backbone curves

Figure 4-12: IP behavior of SC walls, $a/d = 3$, $f_c' = 5,000$ psi, $s = d/2$

## 4.3 Technical Guidance

Technical guidance for design of SC walls subjected to combined IP and OOP loading will be the focus of this section and is based on the experiments of Section 2, the numerical simulations of Section 3, and the parametric study of Section 4.2. The results of the experiments were used to

validate the numerical models and provide technical guidance on the displacement ductility capacity of SC wall piers. The parametric studies were used to provide technical guidance on the effects of OOP loading (height and location) on IP capacity.

Figure 4-13 presents the IP force-displacement backbone curves for experiments CNSC1, CNSC2, and CNSC3, normalized by their respective IP capacities, $IP_c$. The backbone curves for CNSC2 and CNSC3 were shifted to the origin to allow for a direct comparison of their IP performance with that of CNSC1.

With the exception of tie bar spacing and concrete uniaxial compressive strength, the construction of the CNSC specimens was identical. Epackachi et al. (2014a) showed that connector (studs and tie rods) spacing had little effect on IP stiffness at levels of lateral load smaller than the peak value. The uniaxial compressive strengths of the concrete in CNSC1, CNSC2 and CNSC3, on the first day of testing, were 7700 psi, 5300 psi, and 5300 psi, respectively. Based on these concrete strengths, the initial stiffness of CNSC1 should have been greater than that of both CNSC2 and CNSC3. Per Figure 4-13, the initial stiffness of CNSC1 is greater than that of CNSC2 in both the first and third quadrants: the expected result; but not greater than that of CNSC3: an unexpected result, especially given that CNSC3 was damaged under OOP loading prior to IP loading and CNSC1 was not.

On the basis of the normalized backbone curves of Figure 4-13, it is evident that a) identical wall piers with low OOP shear stress (e.g., CNSC1) are more deformable (ductile) than those with high OOP shear stress (CNSC3), b) the installation of cross ties at spacing $d/2$, where $d$ is the thickness of the wall, results in a more deformable (ductile) SC wall than if the ties are spaced at distance $d$, and c) high OOP shear stress (and coexisting moment) in an SC wall pier may lead to non-ductile response IP, namely, no IP deformation capacity beyond the displacement associated with peak strength.

Displacement ductility has been a traditional seismic measure of component and system performance. For the three walls tested as part of this project, and assuming a maximum displacement equal to the displacement at which the resistance drops below 80% of the peak value, the maximum ductility of CNSC1 (CNSC2) [CNSC3] is approximately 3 (2) [1].
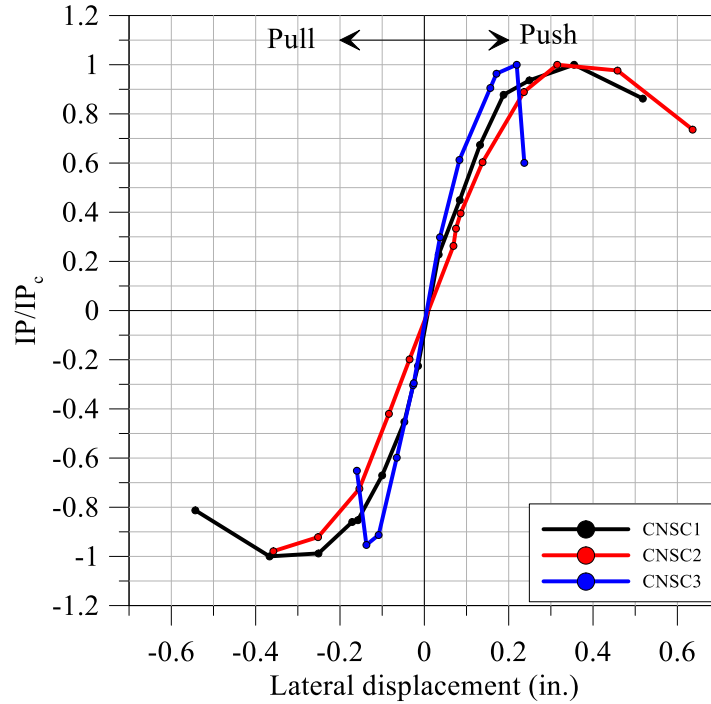
Figure 4-13: Normalized backbone curves, CNSC experiments

The peak resistances of CNSC1, CNSC2 and CNSC3 were 735 kips, 629 kips, and 504 kips, respectively. The greater strength of CNSC1 can be attributed in part to a) higher compressive strength (7700 psi versus 5300 psi) for the infill concrete, and b) a relatively low OOP shear stress. A comparison of the peak resistance of CNSC2 and CNSC3 makes clear the importance to IP strength of limiting damage due to OOP shear forces, which can be accomplished in part by the provision of closely spaced cross ties. The only meaningful difference between CNSC2 and CNSC3 was tie bar spacing because the compressive strength of the infill concrete was the same in both specimens and the maximum OOP shear stress was very similar: $4.73\sqrt{f_c'}$ for CNSC2 and $4.92\sqrt{f_c'}$ for CNSC3. In this instance, the provision of closely spaced tie bars (at $d/2$) enabled a much greater peak IP resistance (629 versus 504 kips).

Results from the parametric studies were mined to develop draft guidance for when to consider co-existing OOP shearing forces for IP design of SC wall piers. The relationships between applied OOP shear stress (normalized by $\sqrt{f_c'}$) and the peak IP capacity, IP$_{OOP}$ (normalized by the IP capacity with no applied OOP load, IP$_{NO\ OOP}$) for a uniaxial concrete compressive strength of 3,500 psi and a tie bar spacing of 12 inches are presented in Figure 4-14. The curves are shown for $a/d$ equal to 0.5, 1.5, and 3. A similar plot is shown in Figure 4-15 for a tie bar

spacing of 6 inches. As the magnitude of OOP shear stress and the ratio of shear span-to-depth increase, larger longitudinal stresses develop in the steel faceplates, reducing IP capacity. The reduction in tie bar spacing from $d$ to $d/2$, slightly improved the IP capacity performance of the SC walls for the larger magnitudes of OOP shear stress and ratios of shear span-to-depth considered in this parametric study; the benefits of reduced tie bar spacing are expected to increase as the magnitude of the OOP shear stress exceeds the inclined cracking load of the concrete.
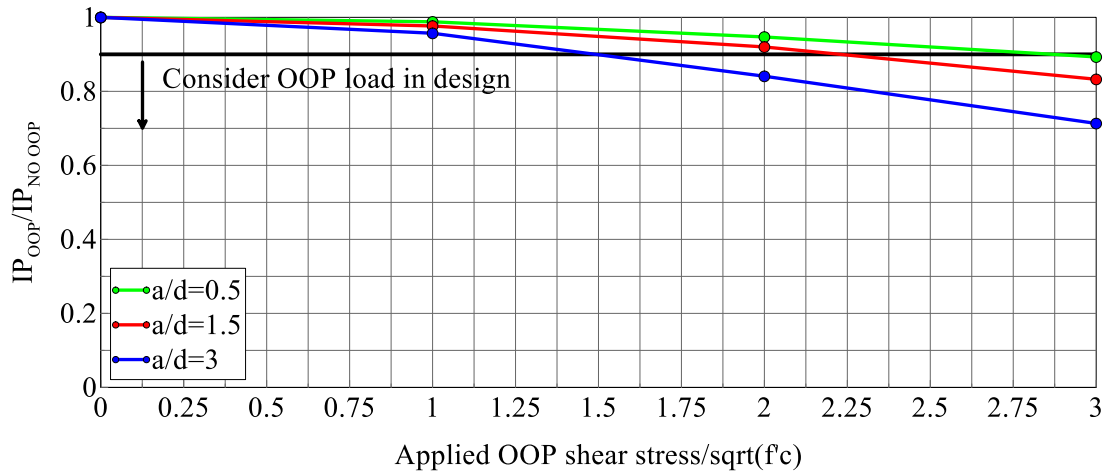


Figure 4-14: IP capacity vs. applied OOP shear stress, $f'_c = 3,500\,\text{psi}$, $s = d$
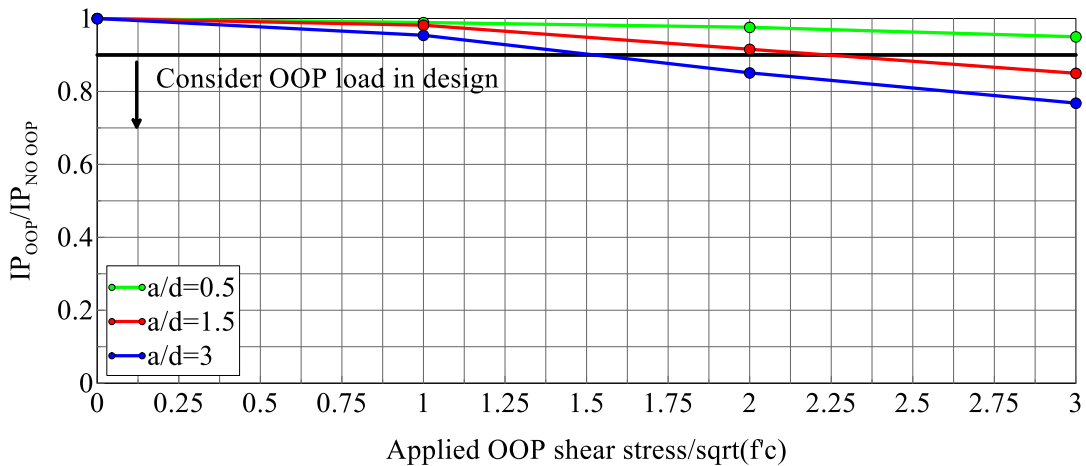


Figure 4-15: IP capacity vs. applied OOP shear stress, $f'_c = 3,500\,\text{psi}$, $s = d/2$

Figure 4-16 and Figure 4-17 present the information of Figure 4-14 and Figure 4-15, but for a uniaxial concrete compressive strength of 5,000 psi. The trends are identical to those described in the previous paragraph.
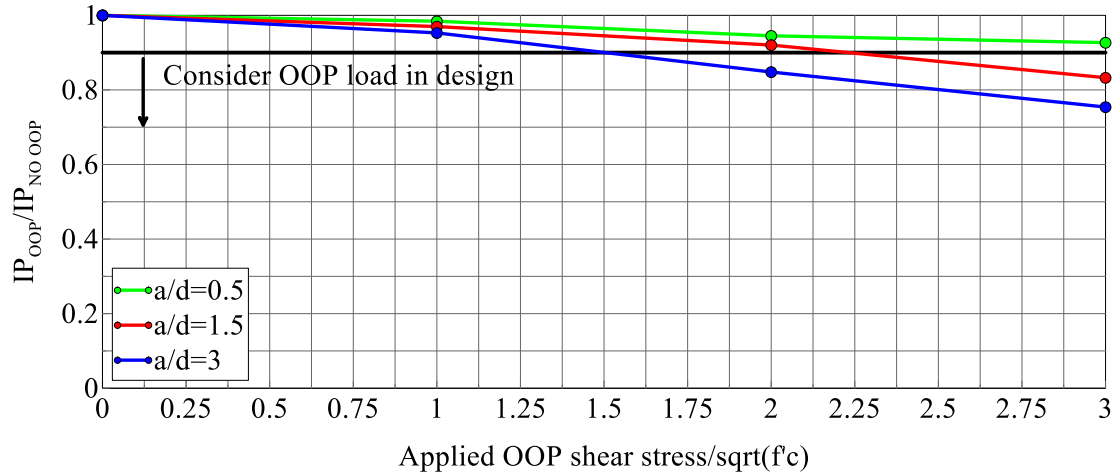


Figure 4-16: IP capacity vs. applied OOP shear stress, $f'_c = 5,000$ psi, $s = d$
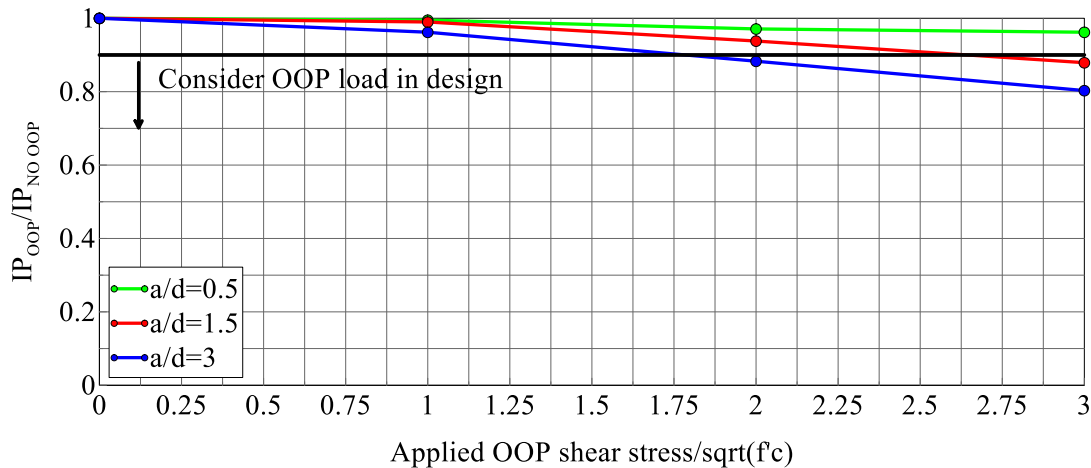


Figure 4-17: IP capacity vs. applied OOP shear stress, $f'_c = 5,000$ psi, $s = d / 2$

The discussions above address the effect of OOP loading on IP capacity. Two issues that ought be addressed in a future study, which will likely be specific to Canadian nuclear practice, are a) the strength reduction factors to be used for IP shear capacity calculations, b) strength reduction factors for OOP shear capacity calculations, c) strength reduction factors for combined IP and OOP loading. ASCE 43-05 (ASCE, 2005) provides guidance on how these factors should be calculated, which depend on whether the actions are ductile or non-ductile. A goal with

predictive equations for design strength (strength reduction factor multiplied by a nominal strength) is to achieve an exceedance probability of 98%.

The walls tested as part of this project had a thickness of 12 inches. It is well established that the shear strength of plain reinforced concrete elements is negatively affected by section depth, namely, an increase in depth (thickness for walls) will lead to a decrease in the average shear stress at failure. A ballot measure to address this issue has passed review by the ASCE Dynamic Analysis of Nuclear Structures Committee, which reduces nominal shear stress with depth, to a minimum value of approximately $1\sqrt{f_c'}$ to achieve the component-level target probability goals of ASCE 43.

Based on the physical testing of SC wall piers CNSC1, CNSC2, and CNSC3 and the observed trends in the parametric studies, the following design guidance is proposed for the construction of SC wall piers subjected to combined IP and OOP loadings

- OOP shear forces and bending moments can damage both infill concrete (shear force) and the steel faceplates (bending moment). Damage to the infill concrete will depend on a) the ratio of shear span to wall thickness, and b) the amplitude of the OOP loading. Damage to the steel faceplates will also depend on these two parameters.
- The effects of OOP loading should be addressed explicitly for design basis calculations. Damage to the infill concrete under IP loading will degrade OOP shear capacity, which is essentially a function of the capacity of the infill concrete only. The steel faceplates should not yield significantly (sufficient to buckle inelastically) under combined IP and OOP design basis loadings, with an appropriate margin (through a strength reduction factor) to achieve a 98% exceedance probability.
- The OOP shear strength of the infill concrete should address the effect of wall thickness on maximum average shear stress.
- A tie bar spacing of no greater than $d/2$ is recommended for SC wall piers subjected to OOP loads that exceed the design shear strength of plain concrete, accounting for depth effects, and calculated using a strength reduction factor suitable to achieve an exceedance probability of 98% per ASCE 43 (see above).
- Tie bars should be used instead of shear studs near the base of an SC wall in zones where concrete crushing and spalling is possible, to preserve the integrity of the cross section

and provide point restraint to the faceplates to delay their inelastic buckling.

- Figure 4-14, Figure 4-15, Figure 4-16, and Figure 4-17 could be used to help identify magnitudes of OOP shear stress and ratios of shear span-to-depth (wall thickness) beyond which OOP loadings ought be considered for design basis calculations of IP strength. The threshold shown in the figures is a 10% reduction in peak strength. Importantly, the negative impact of significant member thickness (as described above) is not addressed here.

Although not part of the scope of this project, it is important to consider the effects of beyond design basis loadings on the seismic performance of SC walls and wall piers. In the United States, one path to demonstrating adequate performance in shaking more intense than design basis is to ensure that the resulting design will perform its intended function with 95% confidence of a probability of failure of 5% or less for shaking equal to 167% design basis. For many components this requires the risk analyst to utilize deformation capacity beyond yield (or ductility) to justify adequate performance. On the basis of the tests of CNSC3 (and to a lesser degree CNSC2), this risk-oriented performance target may require that design basis strength of SC walls under OOP loading be limited to shear stress of less than $1\sqrt{f'_c}$, or even less if the wall has a thickness greater than 12 inches.

# 5. SUMMARY AND DESIGN GUIDANCE

## 5.1 Summary

A study was undertaken to investigate the effects of OOP loading on the IP behavior of SC composite wall piers, with a focus on the magnitude of the OOP load and the effect of tie bar spacing. Numerical simulations and physical testing were performed to develop draft guidance for consideration by CNSC.

Three large-scale rectangular SC wall specimens were built and tested under force-controlled monotonic OOP loading and displacement-control cyclic IP loading at the Bowen Laboratory at Purdue University. The results of the experiments indicate that the OOP load has a significant effect on the IP behavior of SC composite shear walls, in particular, the deformation capacity and peak resistance; the effects become very significant as the applied OOP load develops an average shear stress that is greater than the inclined cracking load of the concrete.

The three experiments were simulated using the general-purpose finite element program LS-DYNA. The numerical model was based on a validated model for IP loading that was developed by Epackachi et al. (2014a, 2015) for a prior project. The model was evaluated for OOP loading using data from tests of plain reinforced concrete beams (i.e., no shear reinforcement) and reasonable comparisons were obtained. The predictions of the numerical models of the tested wall piers were compared with global and local measurements made in the experiments, including cyclic force-displacement relationships (IP and OOP), equivalent viscous damping ratios, vertical stresses in the steel faceplates induced by OOP loading, and observed damage (i.e., cracking of the infill concrete and buckling of the steel faceplates). The predictions of response for CNSC1 (low OOP shear stress) were very good, reasonable for CNSC2 (high OOP shear stress but tie bars at spacing $d/2$) and somewhat poor for CNSC3 (high OOP shear stress and tie bars at spacing $d$). One reason for the poorer predictions for CNSC2 and CNSC3 can be traced to the use of the Winfrith model, which assumes elastic perfectly plastic behavior in compression.

A parametric study was conducted using the numerical model described above to investigate the effect of OOP loading (magnitude and location) on the IP response of SC wall piers. Different concrete compressive strengths and tie bar spacing were considered. Results of the parametric

studies showed that OOP load (or shear stress) has a significant effect on the IP capacity of SC wall piers, and that the effects become very significant as the ratio of shear span-to-depth and the magnitude of the OOP load are increased.

## 5.2 Design Guidance

An important objective of this project was to formulate design guidance for SC walls subjected to combined IP and OOP loading. The following guidance is offered for consideration of CNSC:

1.  The effects of OOP loading should be addressed explicitly for design basis calculations. The steel faceplates should not yield significantly (sufficient to buckle inelastically) under combined IP and OOP design basis loadings, with an appropriate margin (through a strength reduction factor) to achieve a 98% exceedance probability per ASCE 43-05.

2.  The OOP shear strength of the infill concrete should address the effect of wall thickness on maximum average shear stress. The balloted code change provision in ASCE 43-** could be used for this purpose.

3.  A maximum tie bar spacing of $d/2$ is recommended for SC walls subjected to OOP loads that exceed the nominal design strength of plain concrete, reduced as appropriate for wall thickness, and calculated using a strength reduction factor suitable to achieve a 98% exceedance probability per ASCE 43-05.

4.  Tie bars should be used instead of shear studs near the base of an SC wall in zones where concrete crushing and spalling is possible, to preserve the integrity of the cross section and provide point restraint to the faceplates to delay their inelastic buckling.

5.  Limits on IP and OOP design basis strength of SC walls should recognize the need for capacity in the event of beyond design basis shaking.

A numerical model has been developed in LS-DYNA, which is capable of predicting the IP cyclic response of SC wall piers, and the combined IP and OOP cyclic response of SC walls provided the OOP shear stresses are relatively low, of the order of $2\sqrt{f_c'}$ for shallow (relatively thin) walls. The model is described in detail in Sections 3 and 4 of this report.

Charts have been developed, and presented in Section 4, to identify what combinations of OOP

shear stress and ratios of shear span to depth (wall thickness) may result in significant reductions in IP shear capacity. These charts could be used for preliminary design of SC wall piers.

# 6. REFERENCES

American Concrete Institute (ACI). (2014). "Building code requirements for structural concrete and commentary," Farmington Hills, Michigan.

American Institute of Steel Construction (AISC). (2015). "Specification for safety-related steel structures for nuclear facilities including supplement no. 1 (ANSI/AISC N690s1-15)" Chicago, Illinois.

American Society of Civil Engineers (ASCE). (2005). "Seismic design criteria for structures, systems and components in nuclear facilities," *ASCE/SEI Standard 43-05*, Reston, VA.

Bresler, B., and Scordelis, A. C. (1963). "Shear strength of reinforced concrete beams," ACI Journal Proceedings, 60: 51-74.

Chopra, A. (2011). *Dynamics of Structures*, Fourth Edition, Prentice-Hall.

Comite Euro-international du Beton (CEB/FIP). (1990). "CEB-FIP model code 1990," Thomas Telford, London, England.

Epackachi, S., Nguyen, N., Kurt, E., Whittaker, A. and Varma, A. H. (2014a). "In-plane behavior of rectangular steel-plate composite shear walls," *Journal of Structural Engineering*, 141(7), 04014176.

Epackachi, S., Nguyen, N., Kurt, E., Whittaker, A., and Varma, A. H. (2014b) "Numerical and experimental investigation of the in-plane behavior of rectangular steel-plate composite walls," *Proc., ASCE Structures Congress*, Portland, OR, April.

Epackachi, S., Whittaker, A., Varma, A. H., and Kurt, E. (2015). "Finite element modeling of steel-plate concrete composite wall piers," *Engineering Structures*, 100: 369-384.

Kurt, E., Varma, A. H., Epackachi, S., and Whittaker, A. (2015) "Rectangular SC wall piers: summary of seismic behavior and design," *Proc., ASCE Structures Congress*, Portland, OR, April.

Livermore Software Technology Corporation (LSTC). (2013). "LS-DYNA keyword user's

manual - version R 7.0." Livermore, CA.

Mphonde, A. G., and Frantz, G. C. (1985). "Shear tests of high- and low-strength concrete beams without stirrups," ACI Journal Proceedings, 81: 350-357.

Wight, J. (2015). *Reinforced Concrete, Mechanics and Design*, Seventh Edition, Pearson.

Wittmann, F. H., Rokugo, K., Bruehwiler, E., Mihashi, H., and Simonin, P. (1988). "Fracture energy and strain softening of concrete as determined by means of compact tension specimens," *Materials and Structures*, 21: 21-32.